Generation and Propagation of Microseismic Signals from Footsteps

Army Engineer Waterways Experiment Station

September 1973

BEST SELLERS

FROM
NATIONAL
TECHNICAL
INFORMATION
SERVICE

Comparison of Energy Consumption Between West Germany and the United States
PB-245 652/ PAT 112 p. PC$5.50/MF$3.00

A Comprehensive Policy to Ameliorate Adverse Impacts of Transportation Facilities
PB-247 823/ PAT 138 p. PC$6.00/MF$3.00

A Comprehensive Policy to Ameliorate Adverse Impacts of Transporation Facilities, Appendix
PB-247 824/ PAT 310 p. PC$9.75/MF$3.00

Demand for Coal for Electricity Generation 1975–1984
PB-245 216/ PAT 40 p. PC$4.00/MF$3.00

A National Study of Adolescent Drinking Behavior, Attitudes and Correlates
PB-246 002/ PAT 405 p. PC$11.00/MF$3.00

Energy from Coal: Guidelines for the Preparation of Environmental Impact Statements
PB-242 960/ PAT 258 p. PC$9.00/MF$3.00

Energy Versus the Environment: The Issues
PB-246 382/ PAT 35 p. PC$4.00/MF$3.00

Improving the Dissemination of Scientific and Technical Information: A Practitioner's Guide to Innovation
PB-247 057/ PAT 203 p. PC$7.75/MF$3.00

Investigation and Evaluation of Cracking in Austenitic Stainless Steel Piping of Boiling Water Reactor Plants
PB-246 645/ PAT 123 p. PC$5.50/MF$3.00

Pipeline Industry's Practices Using Plastic Pipe in Gas Pipeline Facilities and the Resulting Safety Factors
PB-247 301/ PAT 436 p. PC$11.75/MF$3.00

NOx Combustion Control Methods and Costs for Stationary Sources. Summary Study.
PB-246 750/ PAT 117 p. PC$5.50/MF$3.00

Reactor Safety Study: An Assessment of Accident Risks in U.S. Commercial Nuclear Power Plants
PB-248 200/SET/ PAT 2,504 p. 8 Volumes PC$61.00

Report on Sulfur Oxide Control Technology
PB-246 667/ PAT 89 p. PC$5.00/MF$3.00

Research Evaluation of a System of Natural Air Conditioning
PB-243 498/ PAT 364 p. PC$10.50/MF$3.00

Retrofitting a Residence for Solar Heating and Cooling: The Design and Construction of the System
PB-247 482/ PAT 101 p. PC$5.50/MF$3.00

Saudi Arabia Five-Year Plan, 1975–1980
PB-246 572/ PAT 683 p. PC$16.25/MF$3.00

Shotcrete Practice in Underground Construction
PB-248 765/ PAT 501 p. PC$12.75/MF$3.00

Short-Term Coal Forecast, 1975–1980
PB-247 073/ PAT 120 p. PC$5.50/MF$3.00

State Energy Information Systems: A Survey
PB-247 457/ PAT 64 p. PC$4.50/MF$3.00

A Study of Fixed Capital Requirements of the U.S. Business Economy
PB-248 690/ PAT 84 p. PC$5.00/MF$3.00

Sulfates and the Environment—A Review
PB-248 122/ PAT 155 p. PC$6.75/MF$3.00

HOW TO ORDER

When you indicate the method of payment, please note if a purchase order is not accompanied by payment, you will be billed an addition $5.00 *ship and bill* charge. And please include the card expiration date when using American Express.

Normal delivery time takes three to five weeks. It is vital that you order by number or your order will be manually filled, insuring a delay. You can opt for *airmail delivery* for a $2.00 charge per item. Just check the *Airmail Service* box. If you're really pressed for time, call the NTIS Rush Order Service. (703) 557-4700. For a $10.00 charge per item, your order will be airmailed within 48 hours. Or, you can pick up your order in the Washington Information Center & Bookstore or at our Springfield Operations Center within 24 hours for a $6.00 per item charge.

You may also place your order by telephone or TELEX. The order desk number is (703) 557-4650 and the TELEX number is 89-9405.

Whenever a foreign sales price is NOT specified in the listings, all foreign buyers must add the following charges to each order: $2.50 for each paper copy; $1.50 for each microfiche; and $10.00 for each Published Search.

Thank you for your interest in NTIS. We appreciate your order.

METHOD OF PAYMENT

☐ Charge my NTIS deposit account no._____

☐ Purchase order no._____

☐ Check enclosed for $_____

☐ Charge to my American Express Card account number

Card expiration date_____

Signature_____

☐ Airmail Services requested

NAME_____

ADDRESS_____

CITY, STATE, ZIP_____

Item Number	Quantity		Unit Price*	Total Price
	Paper Copy (PC)	Microfiche (MF)		
			Sub Total	
			Additional Charge	
			Enter Grand Total	

All Prices Subject to Change
8/76

Clip and mail to:

NTIS

National Technical Information Service
U.S. DEPARTMENT OF COMMERCE
Springfield, Va. 22161
(703) 557-4650 TELEX 89-9405

AD A029350

Unclassified
Security Classification

DOCUMENT CONTROL DATA - R & D

(Security classification of title, body of abstract and indexing annotation must be entered when the overall report is classified)

1. ORIGINATING ACTIVITY *(Corporate author)*
U. S. Army Engineer Waterways Experiment Station
Vicksburg, Miss.

2a. REPORT SECURITY CLASSIFICATION
Unclassified

2b. GROUP

3. REPORT TITLE
GENERATION AND PROPAGATION OF MICROSEISMIC SIGNALS FROM FOOTSTEPS

4. DESCRIPTIVE NOTES *(Type of report and inclusive dates)*
Final report

5. AUTHOR(S) *(First name, middle initial, last name)*
Jerry R. Lundien
Bob O. Benn

6. REPORT DATE	7a. TOTAL NO. OF PAGES	7b. NO. OF REFS
September 1973	95	7

8a. CONTRACT OR GRANT NO.	9a. ORIGINATOR'S REPORT NUMBER(S)
b. PROJECT NO 1X663719DK73	Miscellaneous Paper M-73-12
c.	9b. OTHER REPORT NO(S) *(Any other numbers that may be assigned this report)*
d.	

10. DISTRIBUTION STATEMENT
Approved for public release; distribution unlimited.

11. SUPPLEMENTARY NOTES	12. SPONSORING MILITARY ACTIVITY
	Project Manager, Remotely Monitored Battlefield Surveillance System U. S. Army Materiel Command, Fort Monmouth, New Jersey

13 ABSTRACT

A study was conducted to investigate the generation and propagation of microseismic signals from man-walking targets. To illustrate the relation between terrain parameters and Rayleigh wave generation and propagation, the problem was divided into four parts, which were then studied graphically. These parts were: (a) the target-ground interaction, (b) energy coupling to the substrate, (c) Rayleigh wave propagation from the source, and (d) transmission of Rayleigh waves over surface macrogeometry features. Parameters that are included in the terrain model are: (a) surface rigidity in terms of nonlinear surface spring constants and (b) subsurface rigidity in terms of seismic properties (wave velocities and bulk density) and layer thickness. The terrain combinations include a wide variation in site conditions and have realism in terms of environments found in nature. Sample problems are included to demonstrate the signal construction techniques and are analyzed to show the effect of the various terrain parameters on the generation and propagation of the Rayleigh waves.

DD FORM 1 NOV 68 1473 REPLACES DD FORM 1473, 1 JAN 64, WHICH IS OBSOLETE FOR ARMY USE.

Unclassified
Security Classification

Unclassified

Security Classification

14. KEY WORDS	LINK A		LINK B		LINK C	
	ROLE	WT	ROLE	WT	ROLE	WT
Footsteps						
Microseismic waves						
Rayleigh waves						
Terrain factors						
Terrain models						
Wave propagation						

Unclassified

Security Classification

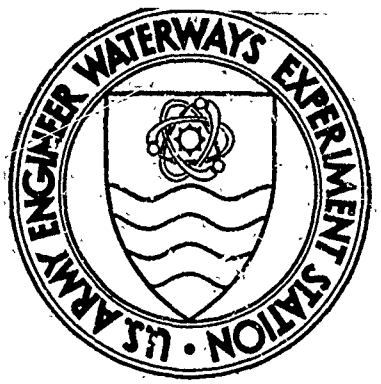

MISCELLANEOUS PAPER M-73-12

GENERATION AND PROPAGATION OF MICROSEISMIC SIGNALS FROM FOOTSTEPS

by

J. R. Lundien, B. O. Benn

September 1973

Sponsored by Project Manager, Remotely Monitored Battlefield Surveillance System
U. S. Army Materiel Command, Fort Monmouth, New Jersey

Conducted by U. S. Army Engineer Waterways Experiment Station
Mobility and Environmental Systems Laboratory
Vicksburg, Mississippi

MISCELLANEOUS PAPER M-73-12

GENERATION AND PROPAGATION OF MICROSEISMIC SIGNALS FROM FOOTSTEPS

by

J. R. Lundien, B. O. Benn

September 1973

Sponsored by Project Manager, Remotely Monitored Battlefield Surveillance System
U. S. Army Materiel Command, Fort Monmouth, New Jersey
Project No. 1X663719DK73

Conducted by U. S. Army Engineer Waterways Experiment Station
Mobility and Environmental Systems Laboratory
Vicksburg, Mississippi

ARMY-MRC VICKSBURG, MISS

11a

Foreword

This study is a part of a seismic research program conducted by the U. S. Army Engineer Waterways Experiment Station (WES) and sponsored by the Project Manager, Remotely Monitored Battlefield Surveillance System, U. S. Army Materiel Command, Fort Monmouth, New Jersey, under Project No. 1X663719DK73 entitled "Terrain Penetration and Parameter Study."

The study was under the general supervision of Messrs. W. G. Shockley, Chief, MESL, and W. E. Grabau, Chief, Environmental Systems Division, MESL, and under the direct supervision of Mr. Bob O. Benn, Chief, Environmental Research Branch (ERB), MESL. The computer programs used for this report were prepared by Mr. E. A. Baylot, Mrs. K. S. Long, and Mr. J. R. Lundien, ERB. This report was prepared by Messrs. Lundien and Benn.

Directors of WES during this study and preparation of the report were BG Ernest D. Peixotto, CE, and COL G. H. Hilt, CE. Technical Director was Mr. F. R. Brown.

Contents

Summary

A study was conducted to investigate the generation and propagation of microseismic signals from man-walking targets. To illustrate the relation between terrain parameters and Rayleigh wave generation and propagation, the problem was divided into four parts, which were then studied graphically. These parts were: (a) the target-ground interaction, (b) energy coupling to the substrate, (c) Rayleigh wave propagation from the source, and (d) transmission of Rayleigh waves over surface macrogeometry features.

Parameters that are included in the terrain model are: (a) surface rigidity in terms of nonlinear surface spring constants and (b) subsurface rigidity in terms of seismic properties (wave velocities and bulk density) and layer thickness. The terrain combinations include a wide variation in site conditions and have realism in terms of environments found in nature. Sample problems are included to demonstrate the signal construction techniques and are analyzed to show the effect of the various terrain parameters on the generation and propagation of the Rayleigh waves.

GENERATION AND PROPAGATION OF MICROSEISMIC SIGNALS FROM FOOTSTEPS

Introduction

1. The vertical component of a Rayleigh wave is commonly used as the energy vehicle to activate modern, seismic, unattended ground sensors (UGS). The amount of energy generated by a target of military interest (in this study the target is restricted to one man walking) is site dependent, and the effect of terrain on Rayleigh wave generation and propagation is known to be substantial. Unfortunately, very little is known quantitatively about the relative effects of specific terrain parameters on the phenomena. For this reason, generalizations or design "theorems" spanning a wide range of terrain variations cannot be specified with confidence. In an attempt to develop techniques to study the relations between terrain parameters and Rayleigh wave generation and propagation the U. S. Army Engineer Waterways Experiment Station (WES) has divided the problem of Rayleigh wave generation and propagation into four facets that are amenable to mathematical simulation: (a) the target-ground interaction; (b) energy coupling to the substrate; (c) Rayleigh wave propagation from the source; and (d) transmission of Rayleigh waves over surface macrogeometry features.

2. A series of mathematical models that can be used to predict microseismic signals in terrain materials have been developed at the WES.[1] Computer codes have been written to implement the model on a Honeywell 440 series digital computer. Predictions can thus be made rapidly and efficiently with the computer and can be used to evaluate the complex interactions of the four facets of signal generation and propagation identified above. The model can be used to study the effects of specific terrain parameters on the individual facets of the Rayleigh wave generation and propagation phenomena, thereby providing quantitative relations from which the most sensitive parameters can be identified. Further, the effect of the sum of two or more facets can be

derived. This flexible tool provides an effective means for incorporating consideration of terrain and its effects in UGS design and deployment.

Purpose and Scope

3. The purpose of this study was to utilize the WES computer model to study the effects of terrain, i.e. soil strength, density, compression and shear wave velocity, and thickness of soil layers, on the propagation of a Rayleigh wave generated by a man-walking target. The desired product was a series of relations of terrain parameters and coefficients that define the effect of each facet of Rayleigh wave generation and propagation identified in paragraph 1 on the total analog wave train. It was desired that these relations be designed such that a graphic solution (i.e. one that would predict the amplitude versus frequency) could be generated for a man walking over various combinations of terrain conditions at any range from the source.

4. In this report, the theoretical mathematical models used to generate the terrain-Rayleigh wave propagation relations are described. The terrain combinations studied include a wide variation in site conditions and have realism in terms of environments found in nature. The graphic techniques developed are presented and demonstrated on some sample problems. In addition, some computer predictions are compared with graphic solutions. Also included are several computer-predicted time-domain signals that correspond to the computer- and graphic-predicted seismic signal spectrum curves. Further, some generalizations concerning the effect of the terrain parameters on each facet studied are presented.

The Microseismic Propagation Model

5. The considerations in the generation and propagation of microseismic waves are shown in fig. 1. The medium in which the microseismic waves propagates is assumed to be composed of layers of homogeneous,

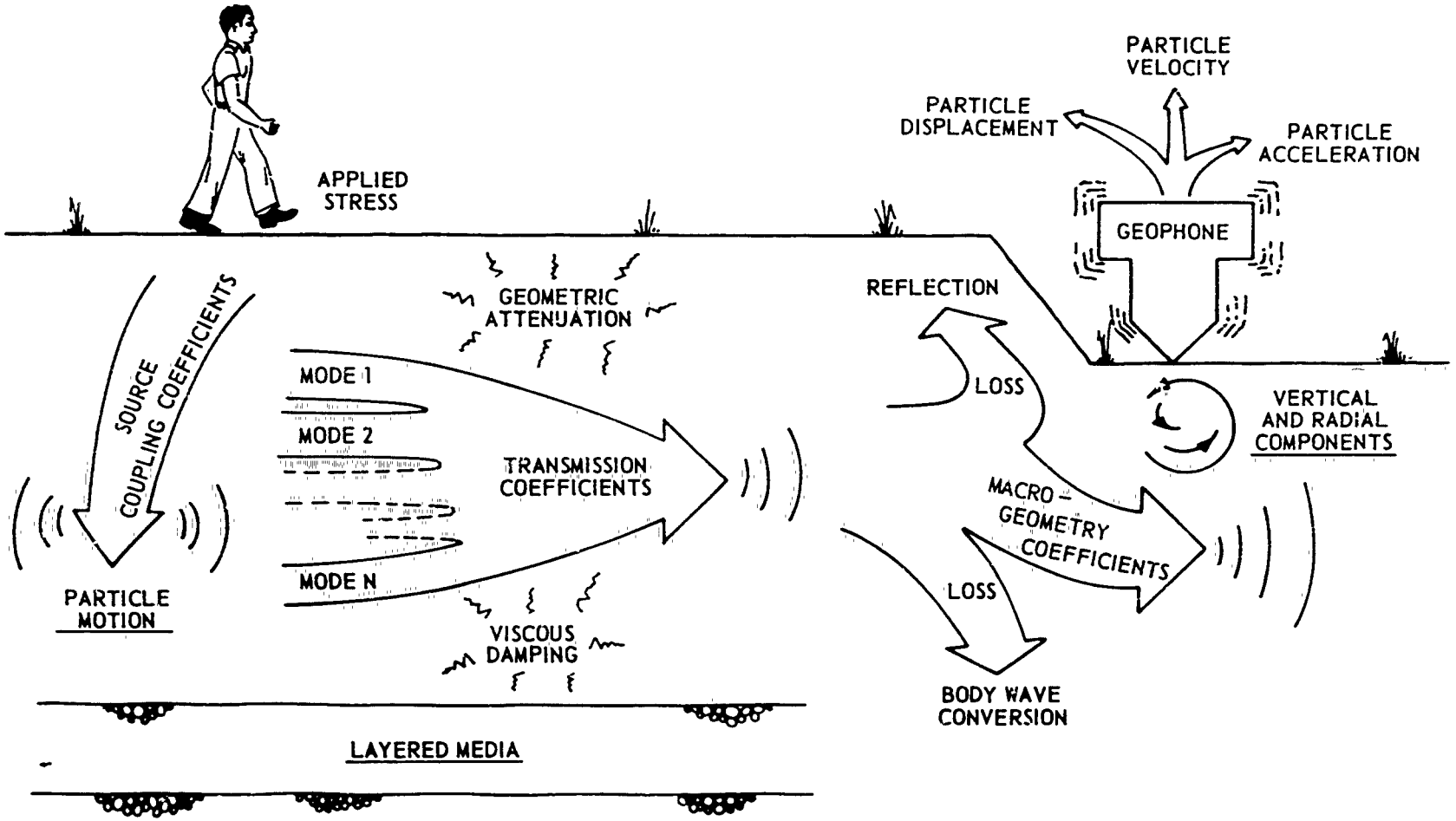

Fig. 1. Considerations in the generation and propagation of microseismic waves

viscoelastic material. The source of the seismic energy is a force (or stress) applied to the surface of the medium, which causes a corresponding motion in the medium as computed with the source coupling coefficients. The source is not restricted to any one form as long as a stress signal is available. In practical applications it can be a footstep, a vehicle (wheeled or tracked), acoustic noise (e.g. aircraft sound waves), or background noise (e.g. a pinecone dropping to the ground). Once the energy is coupled into the medium, it propagates away from the source in various modes. These modes can be interpreted as shear waves, compression waves, or the multiple modes of Rayleigh waves. In most cases for intrusion detection devices, the shear, compression, and higher-order Rayleigh wave modes are small with respect to amplitude in comparison with the fundamental Rayleigh wave and can be neglected. However, when these other modes are not negligible, their effect must be added, in turn, for a wave prediction. As the waves propagate away from the source, their amplitudes decrease as computed with the transmission coefficients. The decrease in amplitude is caused by geometric attenuation (i.e. the energy is spread over an expanding area as the signal phase fronts advance over greater distances) and viscous damping (i.e. losses due to radiation and friction between soil particles). If any topographic feature is included in the propagation path, its effect can be estimated with macrogeometry coefficients. Losses from topographic features are due to energy refraction, reflection, and wave conversion (e.g. a Rayleigh wave encountering a discontinuity can become a source of new Rayleigh waves and body waves with different transmission coefficients). At the desired range, the vertical and radial components of particle motion (i.e. displacement, velocity, and acceleration) can be predicted.

6. The prediction equation for particle motion as a function of range and time is shown below. A block diagram of the calculation procedures is shown in fig. 2.

$$A_{\ell p}(r,t) = \sum_{n=-a}^{n=a} \left(\omega_n e^{i\frac{\pi}{2}}\right)^{p-1} D_n e^{i\omega_n t} \sum_{m=1}^{m=b} S_{m,n} B_{m,n\ell} H^{(1)}_{(\ell-1)}(\kappa_{m,n} \cdot r) \qquad (1)$$

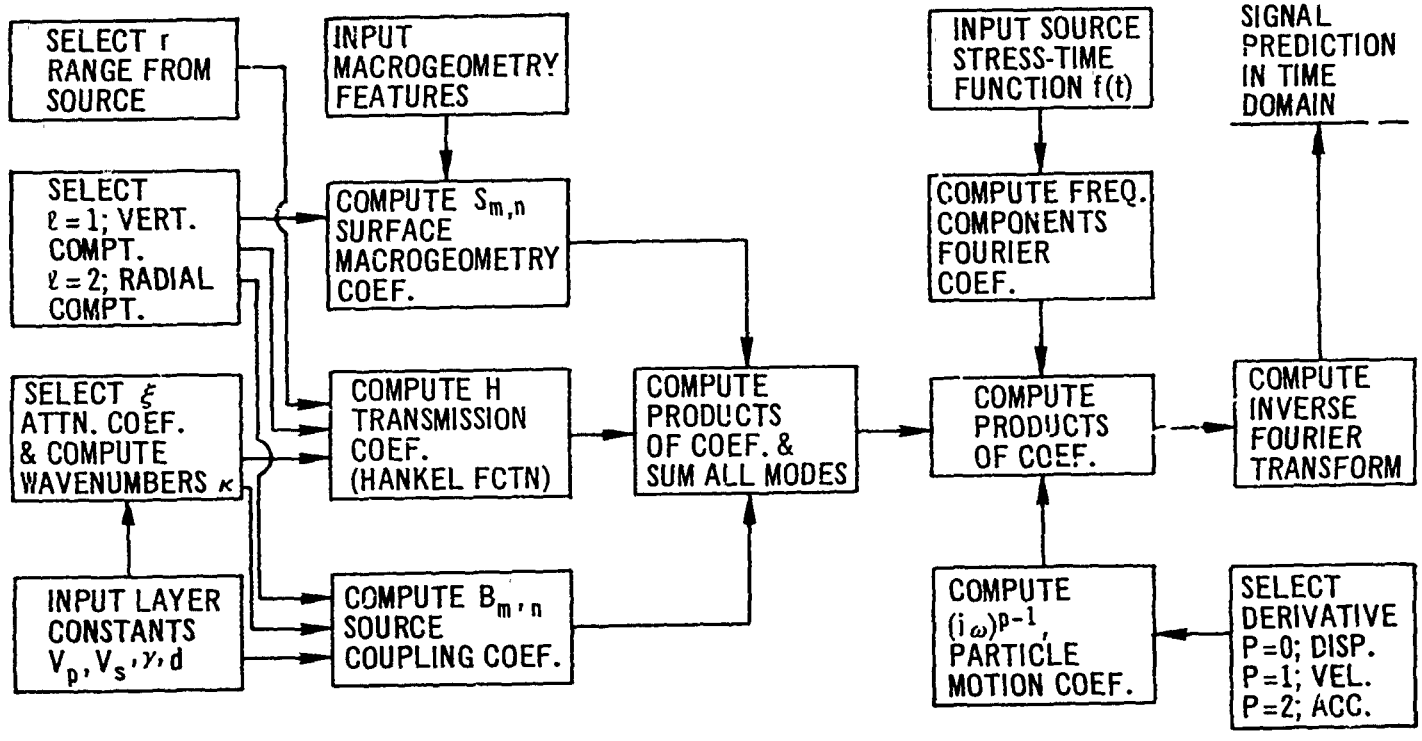

Fig. 2. Block diagram for prediction of seismic signals

where

A = particle motion

ℓ = signal component

p = particle motion number

r = range

t = time

n = frequency number

ω = circular frequency

D = Fourier coefficients for source signal

m = mode number

S = surface macrogeometry coefficients

B = source coupling coefficients

H = transmission coefficients

κ = wave number

7. Compression wave velocity, shear wave velocity, mass density, and layer thickness are used in the computation of the wave numbers and source coupling coefficients for Rayleigh waves. The computations are all made in the frequency domain, and the signal prediction is converted to the time domain via an inverse Fourier transform.

8. The source coupling coefficients and the transmission coefficients can be combined to form the site transfer function as shown in fig. 3. Source coupling coefficients have low values at low frequencies and high values at high frequencies. This frequency response is similar to that of a high-pass electronic filter. The transmission coefficients at any given range have high values at low frequencies and low values at high frequencies. This frequency response varies with range and is similar to that of a low-pass electronic filter. The site transfer function is the product (or if the coefficients are logarithmic values, the sum) of the source coupling coefficient and the transmission coefficient at each frequency. The site transfer function has a peaked response similar to that of a band-pass electronic filter. The frequency at which the peak is located is the predominant frequency of the site and it varies with range. Any source of input signals with a component at or near this predominant frequency will be greatly enhanced over the

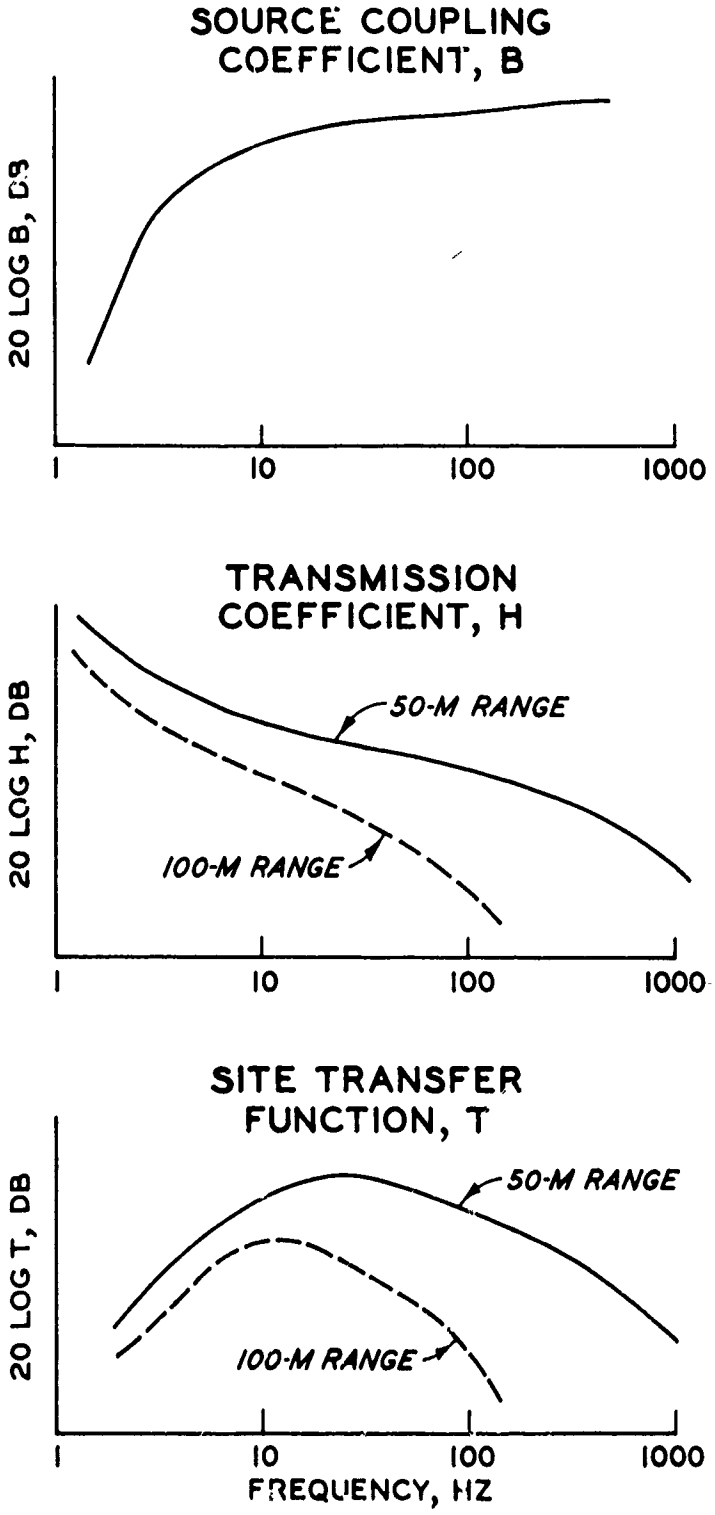

Fig. 3. Derivation of the site transfer function

other components. This observation has been made many times on field-measured data from various sources.

Graphic Modeling Technique

9. The graphic modeling technique, illustrated in fig. 4, allows a prediction of predominant frequency of a site or a prediction of the microseismic signal spectrum resulting from a footstep as a function of range. Other source signals can be substituted for the footstep signal if the stress spectrum is known. Families of relations (fig. 4) are derived using the comprehensive microseismic propagation model discussed in paragraphs 5-8 over a range of site properties. The relations consist of the amount of attenuation of the source signal in terms of 20 log of the variable in db ,* as a function of frequency resulting from (a) coupling of target-induced energy to the ground, (b) propagation of the signal at a given range, and (c) macrogeometry effects (decrease in signal amplitude due to refraction and reflection). The amount of energy transferred from the target to the ground surface is a complex function of the target loading rate and surface site conditions. This frequency-dependent function is derived by a separate computer program based on a spring-dashpot analog of the target-ground interaction and is formulated such that the nonlinear loading and unloading of the ground can be simulated.

10. The graphic technique requires the user to select a series of curves that correspond to site conditions for which a prediction is desired, i.e. a selection of (a) the source stress signal, (b) the site coupling coefficients, (c) the transmission coefficients, and (d) the surface macrogeometry coefficients. The sum of these four curves (fig. 4) (if curves are of logarithmic values where sums are

* In the strictest sense, the term db is reserved for the ratio of two power levels, P_1 and P_2, as $10 \log_{10} P_1/P_2$. However, for the case of scalar values, the form $20 \log_{10}$ is used with the assumption that the scalar value has been normalized with a value of unity. Thus, an approximate power spectrum is available in db, which can be converted to absolute scalar magnitude by dividing by 20 and taking the antilogarithm.

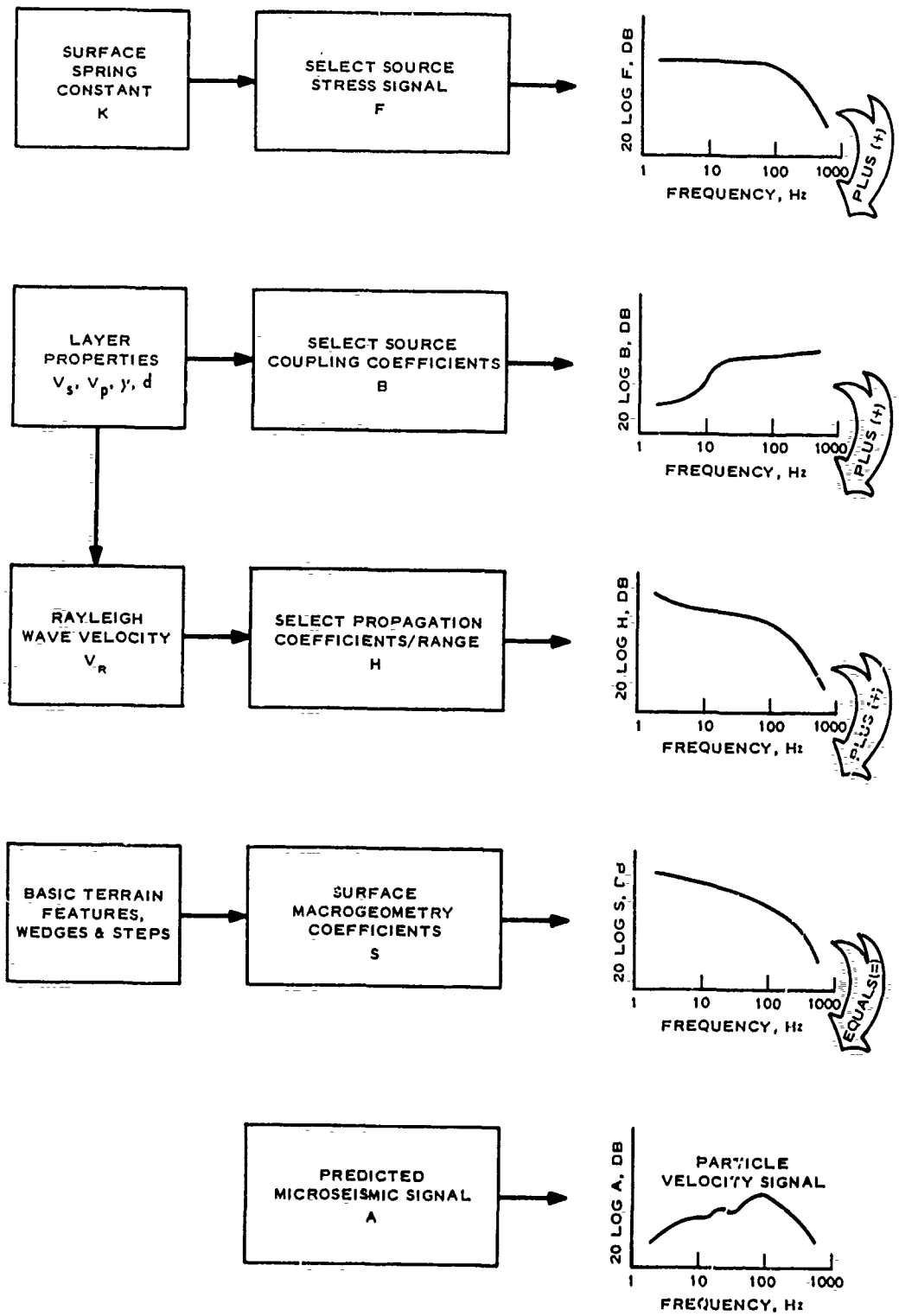

Fig. 4. Flow diagram for the graphic modeling technique

equivalent to products in the actual values) produces the spectrum of the microseismic signal (particle velocity versus frequency). The selection of each of the four separate curves requires some prior knowledge of the site properties or ranges of values over which predictions are to be made. Details are given below.

Source stress signals

11. At the present state of development, explicit detailed guidance cannot be given for selecting (or interpolating within the family of curves) the proper stress-time function for a footstep. It is believed, however, that the proper function can be reasonably inferred if the user carefully considers (in a qualitative sense) the mechanism of the target-ground interaction in the light of how the curves were derived.

12. The source stress signals generated for this study are for footsteps on material whose properties at the surface may be different from those in the substrate. Rather distinct superficial stratification exists for most natural soils where the surface is exposed to the environment (rain, freezing temperatures, drying conditions, etc.) or supports the growth of vegetation. When stressed, the surface materials react nonlinearly, even when subjected to relatively low stress levels such as might be generated by a man or a vehicle. The equation[2] used to compute these footstep signals is written for the mass of a man supported by a nonlinear spring (due to the ground surface) and dashpot (for friction and radiation damping), as follows:

$$M_e\ddot{y} + C_s\dot{y} + \phi(y) = F \qquad (2)$$

where

M_e = effective mass of man and soil

y = vertical displacement

C_s = damping constant

$\phi(y)$ = spring force exerted by ground surface

F = applied force from man's weight

13. The ground nearly always shows two spring forces $\phi(y)$:

that of the spring force exerted on a load under compression conditions, and that of the spring force that acts on a decreasing load during rebound conditions. Normally the rebound spring constant (i.e. shape of the force-deflection curve) is much higher than the compression spring constant (the compression spring constant is often referred to as the coefficient of subgrade reaction, k_s, in the literature dealing with pavement design[3]). The compression spring constant can have one of several shapes: (a) it can be linear, (b) it can increase as the vertical deflection, y, increases (compaction or strain-hardened condition), or (c) it can decrease as the vertical deflection, y, increases (fluidization or plastic condition). These cases are illustrated in a highly generalized form in fig. 5.

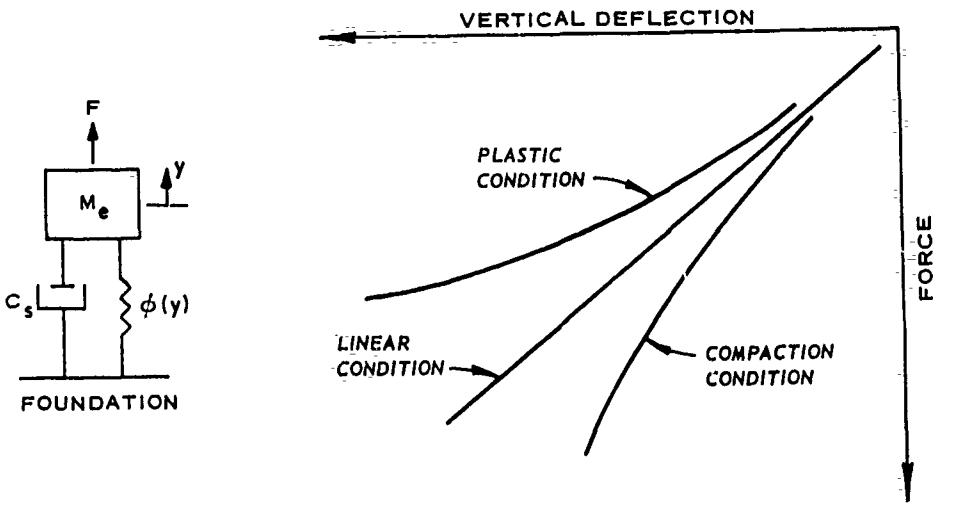

Fig. 5. Force-deflection characteristics for nonlinear spring $\phi(y)$

14. Force-deflection relations. Only limited information is available in the literature on force-deflection relations for surficial materials; nevertheless, these data indicate that the shape of the force-deflection curve is strongly related to soil strength. Considerable data are available on the strength of surface soils, especially in terms of cone index (which is used extensively in vehicle locomotion studies). It is believed that the shape of the force-deflection curve can be correctly inferred from cone index-depth relations. To

illustrate, each class of force-deflection relations, i.e. linear, compaction, and plastic, will be discussed in terms of cone index profiles found in nature.

15. The linear class is seldom found in natural surface soils; however, both the plastic and compaction conditions approach the linear condition at stress levels that are low compared with the shear strength of the material. For the linear condition to apply for a man-walking target, the top surface layer (i.e. less than 0.5 cm) has to exhibit considerable cohesion, and the surface cone index values have to be high (i.e. greater than 50). Further, the cone index has to remain high to a considerable depth (5 to 15 cm).

16. The compaction condition is the most common one found in nature. Typically, soil strength and density increase with depth, and, therefore, a load applied to the surface will compact the surface against a firmer foundation material. Thus, at some degree of compaction, the material can sustain quite large loads without further deflection. For footstep loading, the low surface strength values that either abruptly or gradually increase with depth are of interest. For example, in most cultivated fields the tilled surface soil has low strength, but the plow pan that often develops as a result of the cultivation is quite firm. A man's foot will normally (if the soil is moist) rut the weaker surface soil, but the underlying firm soil will sustain the man's weight without deflection. Also, in many pasture areas where a good grass mat and/or root zone has developed, the compaction condition will apply. In this case the grass mat will deflect rapidly with load, the root zone will allow another rate of deflection, and the foundation material will yield yet another force-deflection relation.

17. The plastic condition will apply to those natural conditions that permit the soil material to "flow" from the loaded area. Typically, for man-walking targets these are areas where the cone index values are quite low on the surface (i.e. less than about 35) and remain constant or decrease with depth. Many areas in nature can be found that exhibit these characteristics, for example, peat areas overlain with a thin veneer of surface soil, mud flats found along many coasts and backswamp

areas, old inland lakes, and the frost-active zone in cold regions during intermittent freeze-thaw cycles.

18. Calculation of force-deflection curves. Seven cases, selected from previous WES investigations to span a wide range of variations, were run to predict the force applied to the foundation material through the surface layer. The following assumptions were made:

a. The weight of the man was 160 lb (equivalent to a mass of 72.5 kg).

b. The damping constant changed when the spring constant was changed. The system was critically damped under rebound (unloading) conditions and 0.03 critically damped under compression (loading) conditions.

c. The unloading spring constant, $k_{s,r}$, was 10 times larger than the linear (elastic) approximation of the loading spring, $k_{s,c}$.

d. The loading rate (i.e. the transfer rate in one footstep) was linear and such that the man's mass was transferred from one footstep to the next in 0.01 sec.

e. The equations for the spring forces, $\phi(y)$, were:

(1) For compaction conditions:

$$\phi(y) = \frac{k_{s,c}y}{1 - \frac{y^2}{z_{max}^2}} \tag{3}$$

(2) For plastic conditions:

$$\phi(y) = \frac{k_{s,c}y}{1 + \frac{y^2}{z_{max}^2}} \tag{4}$$

where

$k_{s,c}$ = spring constant for linear (elastic) approximation of loading spring

z_{max} = deflection at maximum bearing strength: for compaction condition, z_{max} is the deflection asymptote for y under high loads; for plastic condition, z_{max} is the deflection beyond which the material appears to collapse.

19. Plates 1-7 give (a) the force-deflection curves from which the loading and unloading spring constants were obtained, (b) the stress signal in the time domain, and (c) the stress signal in the frequency domain. Parts (a) and (b) are presented to aid in selection of the proper stress signal in the frequency domain, part (c), which is the curve needed for the prediction of microseismic signals. The seven cases are discussed briefly in the following paragraphs.

20. The soil conditions for cases 1 and 2 were characterized by high strength of the surface soil, i.e. cone index >150. For case 1 the strength decreased with depth, whereas for case 2 the strength increased with depth; i.e. cases 1 and 2 illustrate plastic and compaction conditions, respectively. The force-deflection curves for these cases are given in plates 1 and 2 (left-hand plots), respectively. The loading and unloading spring constants are 2.71×10^6 and 2.42×10^7 N/m, respectively. These spring constant values are compatible with those expected for a well-compacted, unimproved road. Comparison of the two plates shows that they are nearly identical, and that the response was nearly linear, indicating that both materials were behaving as if they were on the low end of the plastic and compaction curves. In both cases, the applied load left a rut only 0.04 cm deep. As would be expected (considering the force-deflection curves), the stress-time histories were nearly identical (see plots in part b, plates 1 and 2). Also, the force-frequency plots are very similar throughout the frequency range studied. The predominant energy was generated in a frequency band from 20 to 70 Hz.

21. The force-deflection curve for case 3 is characteristic of the plastic condition (see plate 3). The average cone index to the depth of rutting[4] was in the neighborhood of 25 and remained about the same or decreased below that depth. The amount of rutting in this case

was relatively small, i.e. 0.9 cm. The spring constants are 2.0×10^5 and 2.0×10^6 N/m for the loading and unloading situations, respectively. The resulting force-time history is lower in amplitude and has considerably more energy in the lower frequencies (less than 30 Hz) than was found in the first two cases.

22. The spring constants for case 4 (plate 4) are the same as those for case 3. The resulting rut depth was less (0.67 cm compared with 0.9 cm), because the surface soil strength was slightly higher and increased with depth, i.e. compaction condition. The force-deflection curve is almost linear in the force range studied, and, therefore, the response is on the low end of the force-deflection curve. It is expected that this case can be found frequently in untilled areas in nature. The stress-time signal for this case has a higher amplitude than for cases 1-3; however, the energy is contained in the frequencies from 0 to 30 Hz in about the same proportion as in case 3.

23. Case 5 represents a quite soft surface soil condition. The surface cone index was about 9 and remained constant or decreased with depth (i.e. plastic condition). A man walking over the surface generated a rut of 9 cm. The spring constants for this case are 2.0×10^4 and 2.0×10^5 N/m for the loading and unloading situations, respectively. The stress-time signal is relatively low in amplitude, and the predominant energy is contained in the frequency range from 0 to 7 Hz (see plate 5c).

24. The spring constants for case 6 are the same as for case 5; however, the force-deflection curve indicates rapid initial deflection under load, but the rate of deflection rapidly decreases with load, i.e. compaction condition (plate 6). This type of response would be expected if the surface soil strength was relatively low and increased rapidly with depth. For this example the rut depth was 2 cm, and the average cone index to depth of rutting was almost 20. The loading and response for case 6 generated a stress-time signal with a peak amplitude about three times greater than those of the first five cases. This stress-time signal generated considerably more energy in the frequency range from 5 to 50 Hz than did the signal in the other cases.

25. Case 7 has the same spring constants as cases 5 and 6; however, the soil strength profile increased less with depth, resulting in a nearly linear force-deflection curve (plate 7). This loading resulted in a rut depth of 5.8 cm. The cone index was about 15 at the surface, but gradually increased with depth. The stress-time signal generated by this target-ground interaction had a peak amplitude of about 145 megadynes, which is slightly less than in case 6 but greater than in cases 1-5. This stress-time signal had considerable energy from 0 to 4 Hz. For frequencies greater than 4 Hz, the energy content followed the same trends as those in cases 3, 4, and 5.

26. The pertinent data for each case discussed above are summarized below.

Plate No.	Spring Type	$k_{s,c}$ N/m	$k_{s,r}$ N/m	z_{max} m	Rut Depth cm	Approx CI
1	Low plastic	2.71×10^6	2.42×10^7	0.01	0.04	>150
2	Low compaction	2.71×10^6	2.42×10^7	0.01	0.04	>150
3	Plastic	2.0×10^5	2.0×10^6	0.01	0.09	25
4	Low compaction	2.0×10^5	2.0×10^6	0.1	0.67	30
5	Plastic	2.0×10^4	2.0×10^5	0.1	9.0	9
6	Compaction	2.0×10^4	2.0×10^5	0.04	2.0	20
7	Low compaction	2.0×10^4	2.0×10^5	0.2	5.8	14

27. As stated in paragraph 11, explicit guidance cannot yet be given for selecting the proper force-frequency curve to make a prediction by the graphic technique. However, it is hoped the discussion above and the summary tabulation will provide insight into making such a selection. Ideally, field-measured force-deflection curves should be used, but a reasonable selection can be made on the basis of soil type (soft, medium, or hard) and footprint depth, e.g. the spring constants can be estimated approximately by noting the depth of a footprint left by a man of average weight.

Source coupling coefficients

28. Although this study is restricted to man-walking targets,

the source coupling, transmission, and macrogeometry coefficients can be combined to derive a site transfer function (see paragraph 8) that will allow prediction of terrain effects on a seismic signal generated by any source of relatively low stress level, e.g. a man, a vehicle, a helicopter, etc.

29. The source coupling coefficient B was used to relate applied force in megadynes to particle velocity in centimeters per second. These relations were computed using the WES microseismic propagation model (equation 1) and are functions of material properties (compression wave velocity V_p, shear wave velocity V_s, and soil mass density γ) and layer thickness (if layers are present). Curves for the vertical and radial components of the source coupling coefficients were generated for (a) a homogeneous half-space, (b) a layer on top of a homogeneous half-space, and (c) two layers on top of a homogeneous half-space.

30. The seismic properties of materials used to calculate the source coupling coefficients are given in table 1. They encompass a wide range of variation. For example, the compression wave velocities span a range from 100 to 2000 m/sec. This range covers many terrain materials found in nature, as evidenced by the following tabulation.[5]

Soil or Rock Types	Estimated Compression Wave Velocity m/sec
Dry, loose topsoils and silts	180 to 365
Dry sands, loams, and slightly sandy or gravelly soft clays	300 to 485
Dry gravels; moist sandy and gravelly soils	450 to 910
Dry, heavy gravelly clays; moist heavy clays; cobbly materials with considerable sands and fines; soft shales; soft or weak sandstones	910 to 1450
Water; saturated silts or clays; wet gravels	1460 to 1524
Compacted moist clays; saturated sands and gravels; soils below the water table; dry, medium shales; moderately soft sandstones; weathered moist shales and schists	1460 to 1829

(Continued)

Soil or Rock Types	Estimated Compression Wave Velocity m/sec
Hardpan; cemented gravels; hard clays; boulder tills; compact cobbly and bouldery materials; medium to moderately hard shales and sandstones; partially decomposed granites; jointed and fractured hard rocks	1676 to 2438
Hard shales and sandstones; interbedded shales and sandstones; slightly fractured limestones and crystalline rocks	2438 to 3657
Unweathered limestones, granites, gneiss, and other dense rocks	3657 to 6100

31. The Rayleigh and shear wave velocities used are commensurate with the compression wave velocity. In many terrain materials Rayleigh wave velocity can be assumed to be equivalent to shear wave velocity and to be 40-50 percent of compression wave velocity. The mass density also spans the natural range of variation, i.e. values of mass density of 1.3-2.0 g/cm^3 cover most soil materials and values of 2.3 and 2.6 are typical of highly consolidated or rock material. Material G (table 1) was selected to represent a frozen medium.

32. The tabulation in paragraph 30 provides crude estimates of compression wave velocity as a function of material type. Compression wave velocities vary dramatically as a function of material type, and a closer approximation (for the selection of the proper coupling coefficient for a specific site) can be made if the empirical equations described in the following paragraphs are used.

33. Prediction equation for compression wave velocity. A multiple regression computer program was used to develop the following empirical equation for the prediction of compression wave velocity in soil materials as a function of basic soil parameters.*

* L. E. Link, "A System for Predicting Seismic Sensor Performance," Technical Report (in preparation), U. S. Army Engineer Waterways Experiment Station, CE, Vicksburg, Miss.

$$V_{pi} = 552.0 + 4.9H_i^{0.5}\, e^{\left[\frac{W_i \gamma d_i}{(1-\gamma d_i/2.65)} + 1\right]} - 79.6\, e^{\left[W_i + \gamma d_i (1+W_i)\right]} \qquad (5)$$

where

V_{pi} = compression wave velocity for i^{th} layer, m/sec
H_i = depth to bottom of i^{th} layer from surface, cm
W_i = average soil moisture content for i^{th} layer, percent
γd_i = average dry density for i^{th} layer, g/cm^3
e = base of natural logarithm

This equation was developed using selected field data collected in Panama and West Germany, and at Fort Huachuca and Yuma, Ariz., and Vicksburg, Miss. It provides a method for obtaining compression wave velocity whenever on-site wave velocity cannot be measured or estimates are desired for seasonal variations.

34. Surface soils are sometimes underlain by rock instead of a second soil layer, especially in mountainous regions; thus, an ability to predict compression wave velocity for rock materials is necessary. However, since compression wave velocity varies dramatically as a function of rock type and condition (weathering, fracturing, etc.), no attempt was made to develop a specific prediction capability for rock. Instead, it is recommended that the last three materials listed in the tabulation in paragraph 30 be used for estimating V_p values on the basis of rock type and condition. Although the tabulation allows only crude estimates of V_p to be made for rock materials, it is believed that these values will be adequate to provide a reasonable picture of the substrate because of the usually great contrast that will exist between V_p values for surface soils and those for most rock materials.

35. Prediction of shear wave velocity. A prediction equation for shear wave velocity V_s similar to that for predicting the compression wave velocity V_p of any soil with depth could not be

developed because of a lack of data. However, if Poisson's ratio σ is known, the ratio V_s/V_p can be determined with the following equation:

$$\frac{V_s}{V_p} = \sqrt{\frac{1 - 2\sigma}{2 - 2\sigma}} \tag{6}$$

Previous experiments have shown that Poisson's ratio for natural soils normally ranges between 0.30 and 0.49. By assuming that, in general, most soils can be described by a Poisson's ratio of 0.4, a value of 0.4 can be computed for V_s/V_p or

$$V_s = 0.4V_p \tag{7}$$

By using this equation and the empirical equation for predicting V_p, a technique is available for estimating shear wave velocity for any soil layer with depth.

36. In rock materials Poisson's ratio may vary from approximately 0.10 to 0.40 as a function of the rock type heterogeneities and rock weathering. If an average value of 0.25 is assumed, the ratio V_s/V_p then becomes 0.58, and the expression can be written

$$V_s = 0.58V_p \quad \text{(for hard rock)} \tag{8}$$

Since all types of rock and rock in every state of deterioration exist in the real world, it cannot be assumed that the expression $V_s = 0.58V_p$ will hold true in all cases. It will, however, provide a means for estimating V_s for rock from the estimates of V_p shown in paragraph 30.

37. Conditions studied. Various combinations of the materials described in table 1 were selected for study. As stated in paragraph 29, three types of soil models were used: (a) a homogeneous half-space, (b) one layer over a homogeneous half-space, and (c) two layers over a homogeneous half-space. Various layer thicknesses were used: 0.25, 0.75, 1.5, 3.0, and 6 m. The major portion of the study

was conducted on "normal" soil models, i.e. the density and rigidity of the material increased with depth. However, to determine the effects of a frozen layer over thawed material, a combination of material G over material B (see table 1) was studied. The various cases studied and the plates in which the results are plotted are tabulated below.

	Site Composition		Source Coupling Coefficients	
Case	Top Layer Material	Base Material	Radial Component Plate No.	Vertical Component Plate No.
1	A	Homogeneous	8	9
2	B	Homogeneous	8	9
3	C	Homogeneous	8	9
4	D	Homogeneous	8	9
5	E	Homogeneous	8	9
6	F	Homogeneous	8	9
7	G	Homogeneous	8	9
8	A	D (1 layer over base material)	10	19
9	A	E	11	20
10	A	F	12	21
11	B	D	13	22
12	B	E	14	23
13	B	F	15	24
14	C	E	16	25
15	C	F	17	26
16	G	B	18	27
17	B	C-F (2 layers over base material)	28	28
18	B	D-E	29	29

38. As seen from the tabulation above, plates 8 and 9 show the radial and vertical source coupling coefficients, respectively, for each material taken as a homogeneous half-space (cases 1-7). The combination shown in plates 18 and 27 of a high-velocity layer (material G) over a base (material B) is given as an example of a frozen site (case 16). The rest of the profiles are examples of unfrozen sites. Two examples (cases 17 and 18) are given for a site with two layers on top of a homogeneous half-space (see plates 28 and 29). Cases 8-16 are for sites that can be characterized by one layer over a half-space.

For many terrain situations this more simplified terrain model (i.e. one layer on top of a half-space) has been found adequate for calculations made over the frequency range used by the seismic intrusion sensors.

39. A comprehensive analysis of plates 9-29 to summarize trends as functions of the various combinations of materials has not been made; however, some tentative generalizations are presented in the following paragraphs.

Source coupling
coefficients-terrain relations

40. Homogeneous half-space. The source coupling coefficients B for a homogeneous half-space increase with frequency and are proportional to the square of frequency (see plates 8 and 9). The relative amplitude of the source coupling coefficients is set by the rigidity of the material. For example, a rigid material is characterized by a high shear modulus (a high shear wave velocity) and a low tendency to deform under an applied stress; a rigid material has small source coupling coefficients. Conversely, a less rigid material will deform to a greater extent under an applied stress and has larger source coupling coefficients. Over the range of variation presented in this report, the source coupling coefficients are approximately proportional to $(1/V_s)^3$. For homogeneous materials, the radial component of 20 log B is approximately 6 db less than the vertical component of 20 log B . (Compare plates 8 and 9.) This difference of 6 db means that the radial component of the source coupling coefficient is about 50 percent of the vertical component.

41. One layer over homogeneous half-space (normal soils). The value of 20 log B for one layer over a homogeneous half-space appears to exhibit asymptotic tendencies, i.e. the high-frequency asymptote has values approximately equal to the source coupling coefficients for a homogeneous half-space composed of the surface material, and the low-frequency asymptote has values approximately equal to the source coupling coefficients for the foundation material alone. The effect of layer thickness on the value of 20 log B is readily seen in plates 10-27; in

general, as the layer thickness decreases the coupling coefficients decrease. Also, as the layer thickness decreases, the transition band between the high- and low-frequency asymptotes shifts to higher frequency.

42. One layer over homogeneous half-space (frozen soil). The curves for 20 log B for a more rigid material (e.g. frozen layer) over a less rigid infinite half-space have an appearance much different from that for the unfrozen case. This appearance is primarily due to the position of the high- and low-frequency asymptotes, which are reversed from those of the unfrozen soil, as would be expected. The more rigid surface seems to be acting as a plate on a compressible half-space to give low coupling coefficient values.

43. Two layers over homogeneous half-space. The curves for 20 log B for two layers over a homogeneous half-space (plates 28 and 29) have high- and low-frequency asymptotes, as in the one-layer case. In both plates, the radial component is larger than the vertical component over a considerable frequency range and is characterized by a large resonance peak in the middle of the transition frequency band. The effect of differences in foundation material shows up in the values computed for 20 log B . For example, the situation illustrated in plate 28 is one that has 4.5 m of relatively low shear wave velocity (i.e. 120 and 200 m/sec, respectively, for each layer) material over a highly contrasting base material (shear wave velocity = 1000 m/sec). In the case illustrated in plate 29, there are 2.25 m of low shear wave velocity (120 and 200 m/sec, respectively) material over a base material with a shear wave velocity of 500 m/sec. This combination results in the vertical component of 20 log B being less for the situation shown in plate 28 than for the situation in plate 29 at low frequencies (less than about 14 Hz), and greater or approximately the same at higher frequencies. The radial component has grossly the same values in both situations, but the rapid change with frequencies apparent in the curves occurs at lower frequencies for the more highly contrasting materials.

Transmission coefficients

44. The transmission coefficients H are plotted in plates 30-32

in terms of 20 log H versus κR, where

$$\kappa R = \frac{2\pi f R}{V_R} \tag{9}$$

and

κ = wave number, m^{-1}

R = range from source, m

f = frequency, Hz

V_R = Rayleigh wave phase velocity, m/sec

The coefficients were generated under the assumption that the ground is underdamped with a value equal to 0.03 of critical damping (a value which is an acceptable compromise for many soil conditions). Plates 30-32 can be used to determine relations of the site transmission coefficients (in terms of 20 log H) versus frequency provided that the relations of Rayleigh wave phase velocity versus frequency (dispersion) for the site are known. V_R-frequency relations for specific site conditions can be obtained from plates 33-42, and these relations can be used to calculate values of κR over the frequencies of interest. Corresponding values of 20 log H can be read directly from plates 30-32.

45. Phase velocity was computed as a function of frequency for the same cases as were the source coupling coefficients (paragraph 37). The resulting relations are shown in table 1 and plates 33-42 as summarized below.

Case	Site Composition: Top Layer Material	Site Composition: Base Material	Rayleigh Wave Phase Velocity Versus Frequency Plate No.
1	A	Homogeneous	*
2	B	Homogeneous	*
3	C	Homogeneous	*
4	D	Homogeneous	*
5	E	Homogeneous	*
6	F	Homogeneous	*
7	G	Homogeneous	*

(Continued)

* Rayleigh wave phase velocity values are shown in table 1.

Case	Site Composition: Top Layer Material	Site Composition: Base Material	Rayleigh Wave Phase Velocity Versus Frequency Plate No.
8	A	D (1 layer over base material)	33
9	A	E	34
10	A	F	35
11	B	D	36
12	B	E	37
13	B	F	38
14	C	E	39
15	C	F	40
16	G	B	41
17	B	C-F (2 layers over base material)	42
18	B	D-E	42

46. It should be noted that for cases 1-7, i.e. homogeneous half-space, the values for Rayleigh wave phase velocity do not change with frequency, and the values listed in table 1 can be used directly to determine the transmission coefficients for a given set of site conditions.

47. As with the source coupling coefficients-terrain relations, a comprehensive analysis of plates 33-42 to summarize trends as a function of the various combinations of materials has not been made. However, layer thickness, as well as material properties, has a profound effect on the Rayleigh wave dispersion curve. Some of the tentative generalizations are presented in the following paragraphs.

Rayleigh wave phase velocity-terrain relations

48. Homogeneous half-space. The Rayleigh wave phase velocity V_R for a homogeneous half-space is fixed by the media seismic properties (i.e., V_s, V_p, and γ) and does not change with frequency (see table 1). The ratio V_R/V_s is generally in the order of 0.90 to 0.95 for most terrain materials.

49. One layer over homogeneous half-space (normal soils). (See plates 33-40.) The Rayleigh wave phase velocity V_R for one layer over

a homogeneous half-space changes with frequency. In the case of normal or unfrozen soils, i.e. where rigidity increases with depth, the value of the Rayleigh wave velocity is dependent on the material in which the majority of the wave is propagating. For example, if the wavelengths are long compared with the first-layer depth, the Rayleigh wave velocity approaches the Rayleigh wave phase velocity of the foundation material. As shown in plates 33-40 the contrast in the propagation velocities between the first layer and the half-space is reflected in the dispersion curves because the Rayleigh wave phase velocity must take on values that lie between these two values. Further, it can be seen that the relation between Rayleigh phase velocity and frequency is also a function of first-layer depth. In general, the high-frequency asymptote has values approximately equal to the Rayleigh wave phase velocity of a homogeneous half-space composed of the surface material, and the low-frequency asymptote has values approximately equal to the Rayleigh wave phase velocity of a homogeneous half-space composed of only the foundation material. The change from low to high velocity starts at a frequency f where the wavelength $\lambda(\lambda = V_R/f)$ is between 1.0 and 1.5 times the layer thickness. The width of the transition frequency band (i.e. the width of the band of frequencies over which the change occurs between asymptotes) measured in octaves appears to increase in a linear fashion with the top layer shear wave velocity. For example, the width of the transition frequency band is approximately 1-1/2 octaves for a top layer shear wave velocity of 40 m/sec (see plates 33-35) and 3 octaves for a shear wave velocity of 200 m/sec (see plates 39 and 40).

50. Some preliminary comparisons were made of the Rayleigh wave phase velocity relations with the relations of source coupling coefficients in an attempt to derive a means for collapsing the data to a simpler form. A gross relation for the vertical component evolved, i.e. $B = f^2/V_R^3$ (see paragraph 40); however, this equation does not adequately define the relation between the two functions, as evidenced by the fact that the effects of layering only approximately occur at the same frequency. For example, the Rayleigh wave phase velocity converges to form one curve at low frequencies; whereas most of the 20 log B

curves are shown to be separated at these frequencies. This inconsistency in the two relations is probably due to resonance effects (such as those caused by the surface layer acting on a half-space), and further study is needed before a general simple equation can be derived that defines the relations between the two functions.

51. One layer over homogeneous half-space (frozen soils). The Rayleigh wave phase velocity for one layer over a homogeneous half-space (plate 41) also changes with frequency for frozen soils (simulated by assuming a high-velocity layer over a lower-velocity foundation material) but in a manner just reversed from that of the unfrozen soils. The same generalizations appear to hold true for frozen soils as for unfrozen soils, if it is realized that the high-frequency asymptote will have values approximating the high Rayleigh wave phase velocity of the surface material, and the low-frequency asymptote will have values approximating the low Rayleigh wave velocity of the foundation material.

52. Two layers over homogeneous half-space. The Rayleigh wave phase velocity for two layers over a homogeneous half-space varies with frequency in a manner very similar to that for one layer over a homogeneous half-space. The high-frequency asymptote has values approximating the Rayleigh wave phase velocity of a homogeneous half-space composed of the top layer material, and the low-frequency asymptote has values approximating the Rayleigh wave phase velocity of a homogeneous half-space composed of the foundation material. The effect of the second layer is to cause the transition frequency band to increase over that shown for a one-layer system. If the second layer is thick enough, a second asymptote may appear midway between the high and low asymptotes, which is related to the second-layer shear wave velocity.

Surface macrogeometry coefficients

53. The surface macrogeometry coefficients S for wedges[6] are plotted in plate 43 as 20 log S versus wedge interior angle θ ; 20 log S for steps[7] are plotted in plate 44 versus $2\pi fH/V_s$, where f = frequency, Hz; H = step height, m; and V_s = shear wave velocity, m/sec. A wedge is defined by two plane surfaces that join to form a change in slope. A step is an abrupt change in elevation and is really formed by

two wedges at 90 deg, separated in distance by the height of the step. Normally, surface macrogeometry coefficients can be assumed to be unity (20 log S = 0) unless the terrain feature is large in comparison with a wavelength of the propagating wave, i.e. the feature is larger than, for example, a half wavelength, λ (in meters) where $\lambda = V_R/f$.

54. The wavelengths of propagating waves are a function of frequency and, for wide-band sources, would have wide ranges of values. Thus, it might be advisable to make a prediction for a site as though it were flat terrain to determine the site predominant frequency. If the wavelength of the predominant frequency were large compared with the macrogeometry feature, the effect would be relatively small; however, even small terrain features will have an effect on the high-frequency components. Thus, if accurate predictions are desired, complex terrain features must be described by using a combination of wedges and steps and summing the effects of each. For steps, the value of 20 log S can be determined (see plate 44) as a function of step height; for wedges, the distance over which the wedge is formed must be large with respect to a wavelength before the value of 20 log S need be applied, and the appropriate value can be selected from plate 43.

55. The macrogeometry coefficients for a wedge are functions of the wedge angle θ (measured as an angular deviation from the approaching plane surface) and Poisson's ratio σ . Poisson's ratio can be defined in terms of compression and shear wave velocities, V_p and V_s , as

$$\sigma = \frac{1 - 2(V_s/V_p)^2}{2 - 2(V_s/V_p)^2} \tag{10}$$

Waves propagated in either direction on a wedge have the same macrogeometry coefficients.

56. In contrast to the wedge coefficients, the step coefficients are functions of frequency; as frequency increases, the amplitude of the wave traversing a step is reduced by the coefficient. Also, two curves are shown for the step coefficients; one for the wave incident

to the elevated side, and one for the wave incident on the depressed side.

57. The macrogeometry coefficients are given for homogeneous half-space materials only. However, as a first approximation, the homogeneous half-space coefficients can be used for a layered site, using the material properties of the layer that carries most of the seismic energy.

Graphic Modeling Procedure

58. Three examples are given to illustrate the graphic modeling procedure. This procedure requires the user to select one curve each for the source stress signal, the source coupling coefficients, the transmission coefficients, and the macrogeometry coefficients. Values from each of the curves are selected at various frequencies and tabulated. The microseismic signal is then constructed by adding the values at each frequency and plotting the results versus frequency.

Site 1 results

59. Particle velocity signals were predicted for a man walking at a range of 10 m on a 0.75-m-thick layer of material B over an infinite half-space of material F. A source stress signal representing a footstep on a hard surface under a low compaction condition (plate 2) was selected to demonstrate signal propagation over a flat surface with approximately the same properties as the subsurface material. Table 2 summarizes the values read from the figures and plates identified at the bottom of the table at the frequencies indicated in the left-hand column. The graphic solution is shown in fig. 6 together with a digital computer solution of the same problem. Agreement between the two solutions is excellent at most frequencies, except near the lower bound where the digital computer solution gives somewhat larger values than the graphic solution. The digital computer time-domain prediction for particle velocity shown in fig. 7 is the inverse Fourier transform of the digital computer frequency-domain signal in fig. 6. This time-domain signal is shown here as a matter of interest

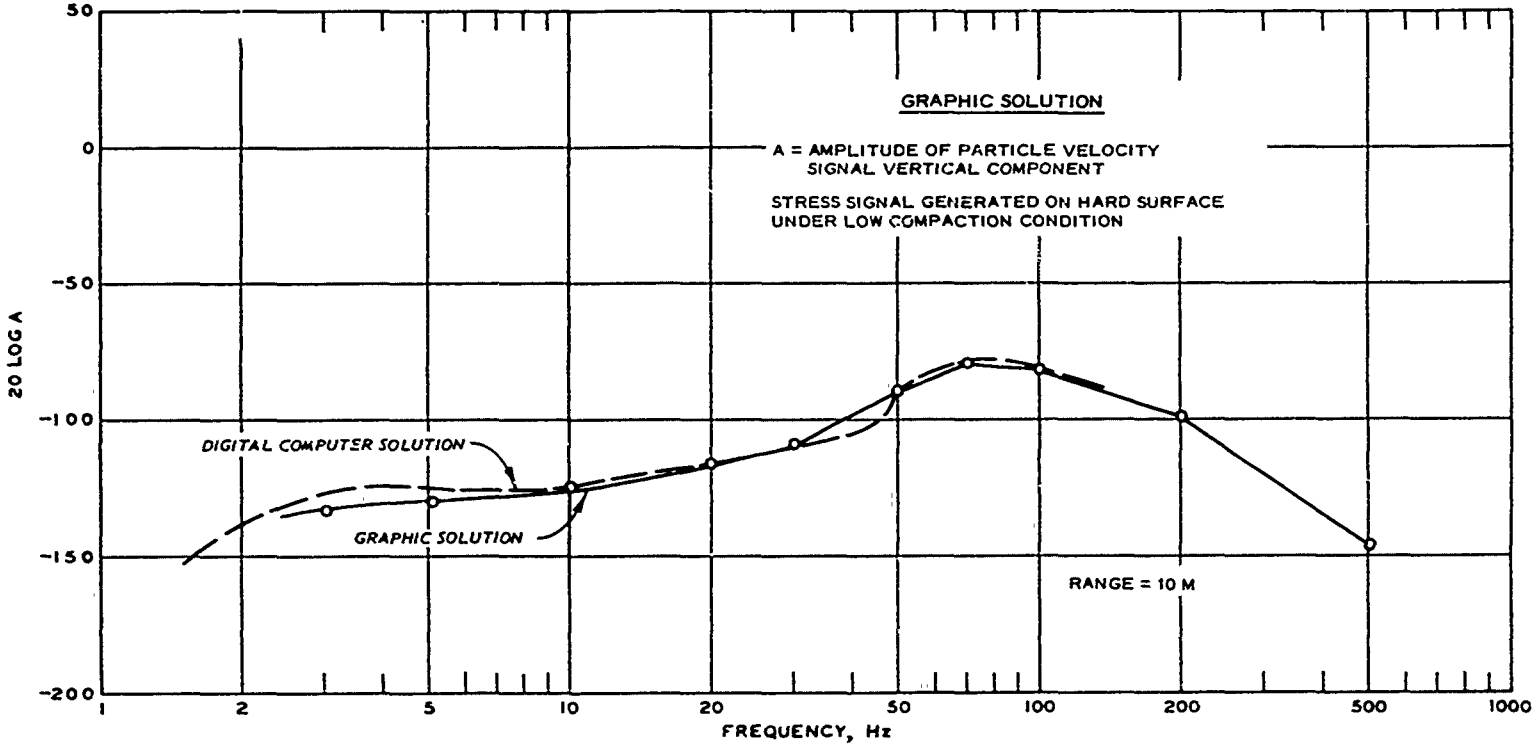

Fig. 6. Example site 1: frequency-domain signals over flat surface of a 0.75-m-thick layer of material B on an infinite half-space of material F; source stress signal from plate 2

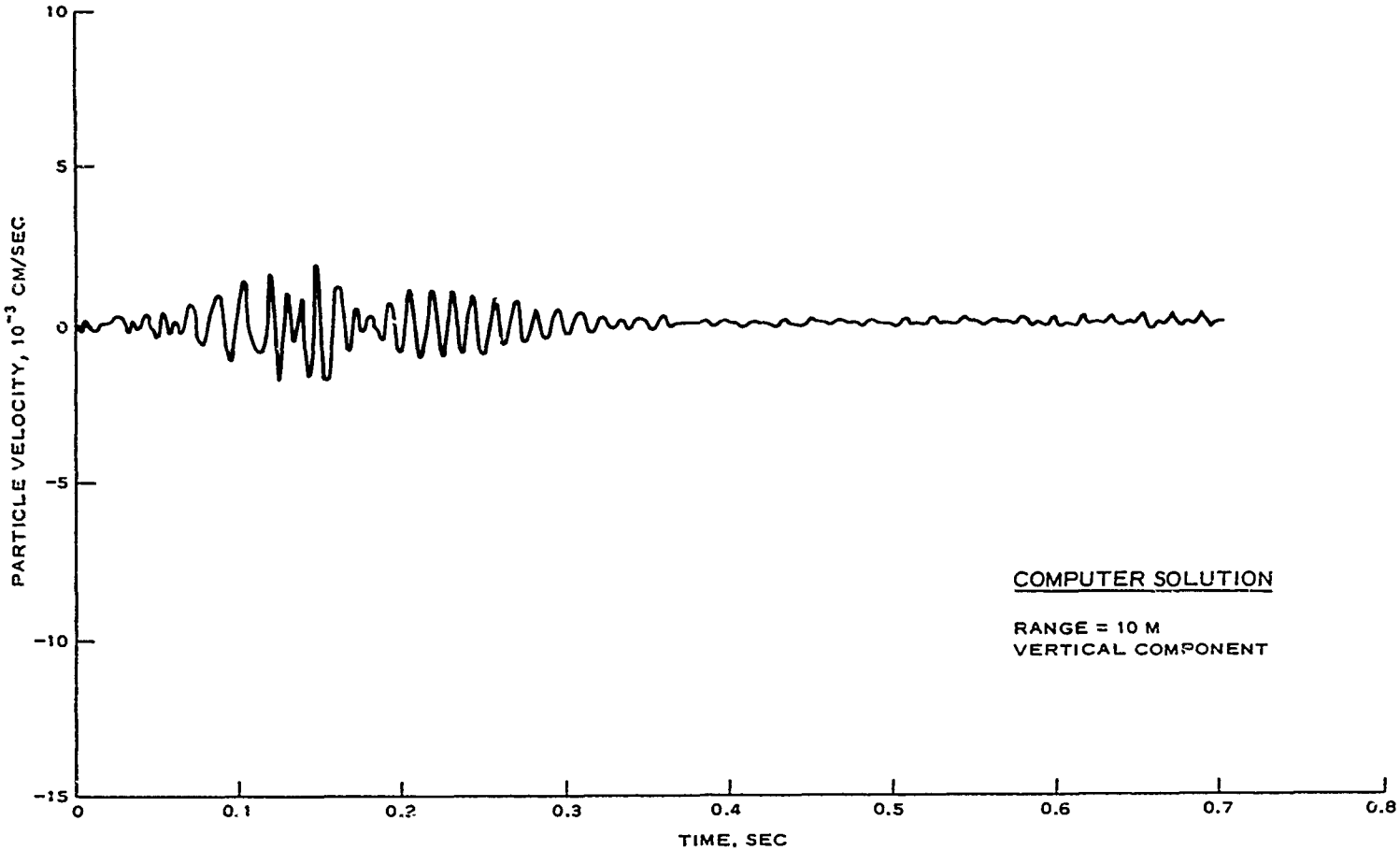

Fig. 7. Example site 1: time-domain signal over flat surface of a 0.75-m-thick layer of material B over an infinite half-space of material F; source stress signal from plate 2

(as are the rest of the time-domain signals shown in this section), since the graphic process results in a frequency-domain signal only.

Site 2 results

60. Particle velocity signals were predicted for a 3-m layer of material B over an infinite half-space F in the same manner as shown for site 1 in table 2. A source stress signal representing a footstep on a flat hard surface under a low compaction condition (plate 2) was selected as before. Note that except for the layer thickness (i.e. 3 m instead of 0.75 m), the conditions are the same as for the conditions at site 1. The graphic solution for ranges of 5, 10, 20, 30, and 40 m is shown in fig. 8. The digital computer time-domain predictions for particle velocity corresponding to the graphic predictions in the frequency domain are shown in fig. 9. When the 10-m-range graphic solutions of figs. 6 and 8 are compared, a broad peak with a predominant frequency of approximately 50 Hz is shown for the 3-m-thick-layer site; whereas the 0.75-m-thick-layer site has a slightly narrower peak with a predominant frequency of 80 Hz. In the time domain the 3-m-thick-layer site (fig. 9) has a high-amplitude short-duration signal, and the 0.75-m-thick-layer site (fig. 7) has a lower-amplitude long-duration signal. Also, as seen in fig. 8, as the range increases (i.e. from 5 to 40 m), the predominant frequency of the site shifts from 60 to 25 Hz, and the amplitude at the predominant frequency decreases with range.

Site 3 results

61. Site 3 is identical with site 2 in substrate conditions, i.e. they are both composed of a 3.0-m layer of material B over infinite half-space of material F. However, the surface material at site 3 is not as firm as that at site 2. The source stress signal for this "medium" surface under plastic conditions was selected from plate 3 (case 3). Also, site 3 exhibits an abrupt change in slope; whereas site 2 is flat. This change in slope is represented by a 50-deg wedge, and its effect on a propagating signal can be obtained from plate 43. In this example, a Poisson's ratio of 0.4 was used; therefore, the value 20 log S is 6.

62. Fig. 10 shows the computer-generated relations of particle velocity versus time for site 3 at a range of 10 m. These relations do

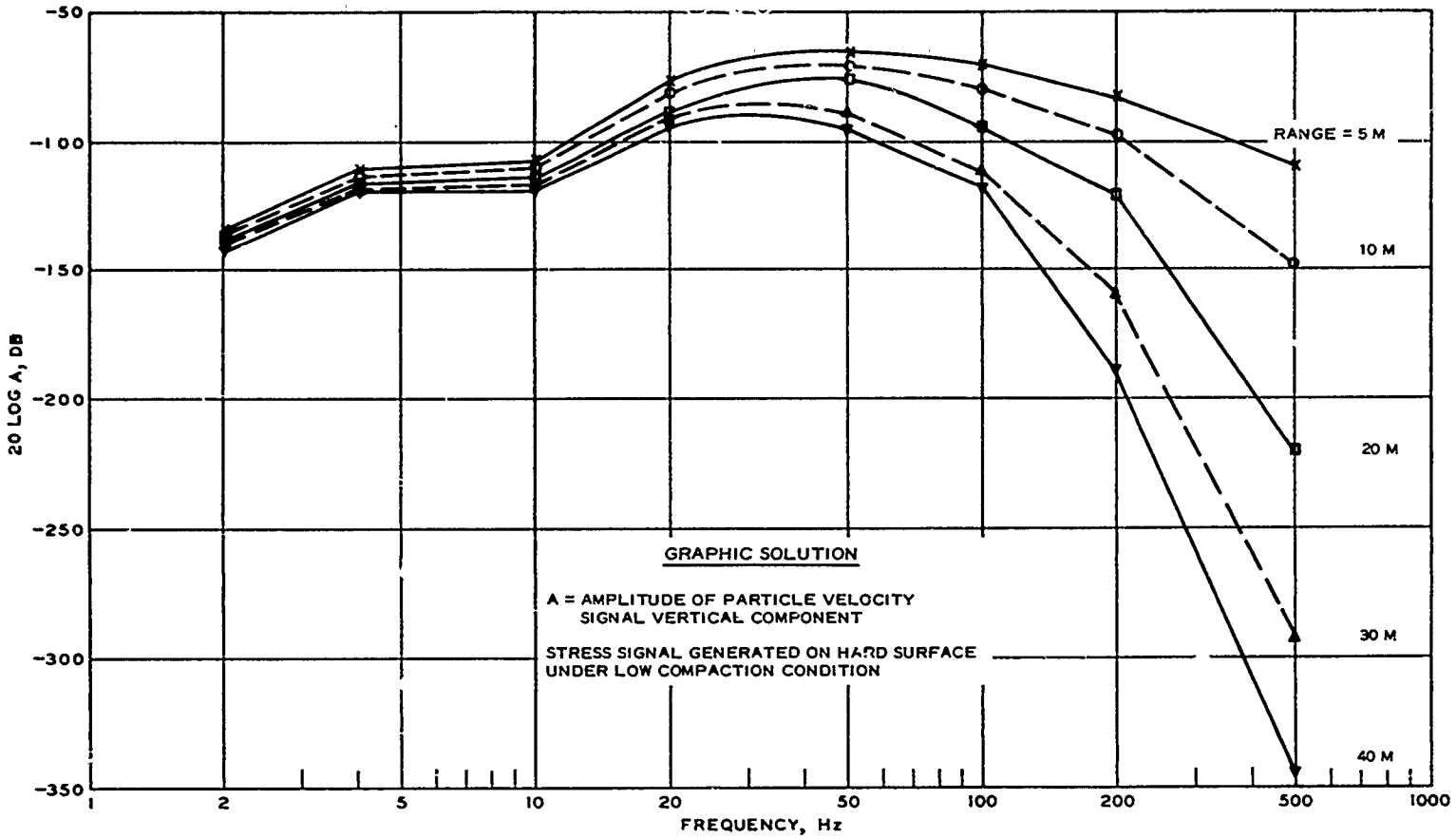

Fig. 8. Example site 2: frequency-domain signals over flat surface at various ranges, 3.0-m-thick layer of material B on infinite half-space of material F; source stress signal from plate 2

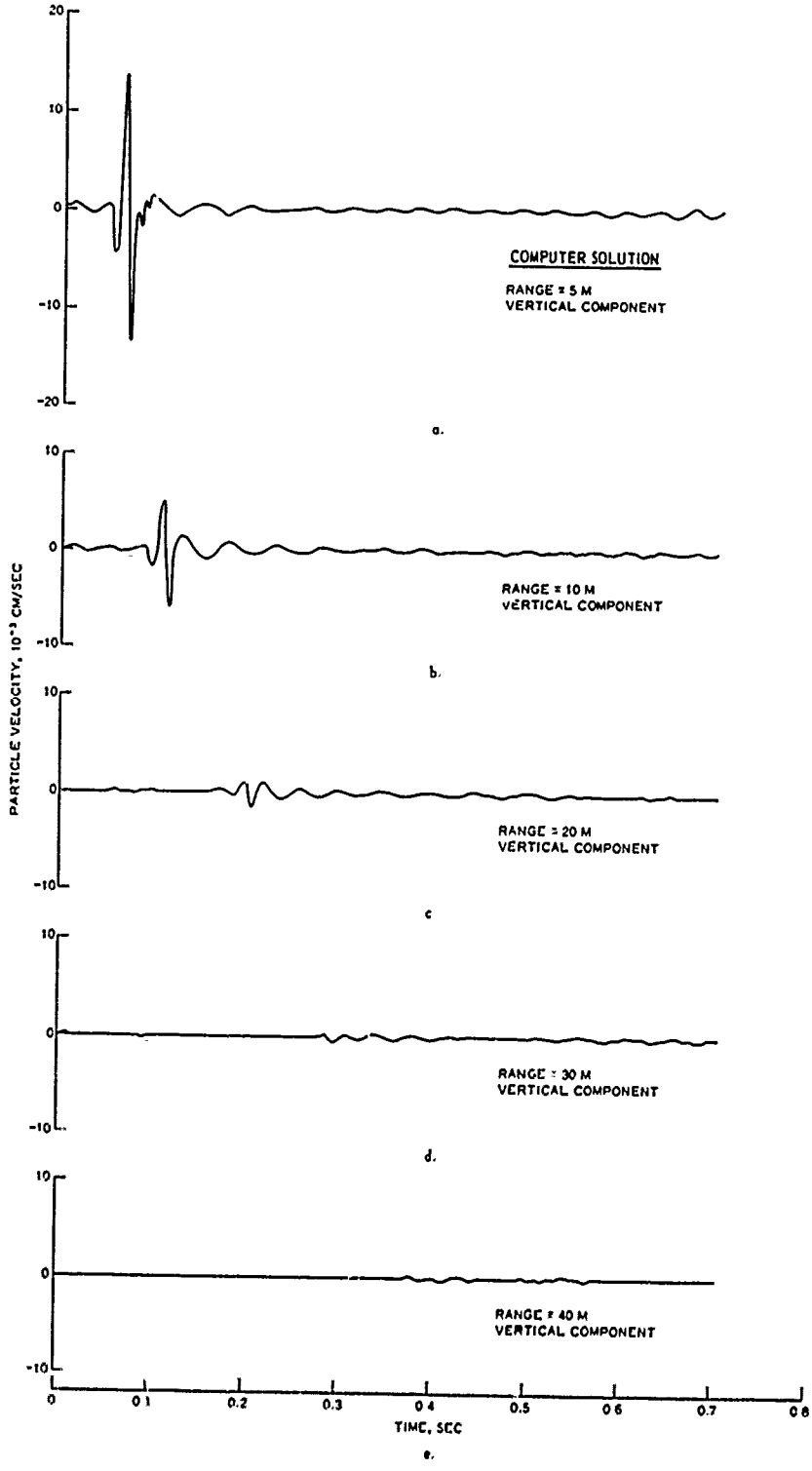

Fig. 9. Example site 2: time-domain signal over flat surface of 3-m-thick layer of material B over infinite half-space of material F; source stress signal from plate 2

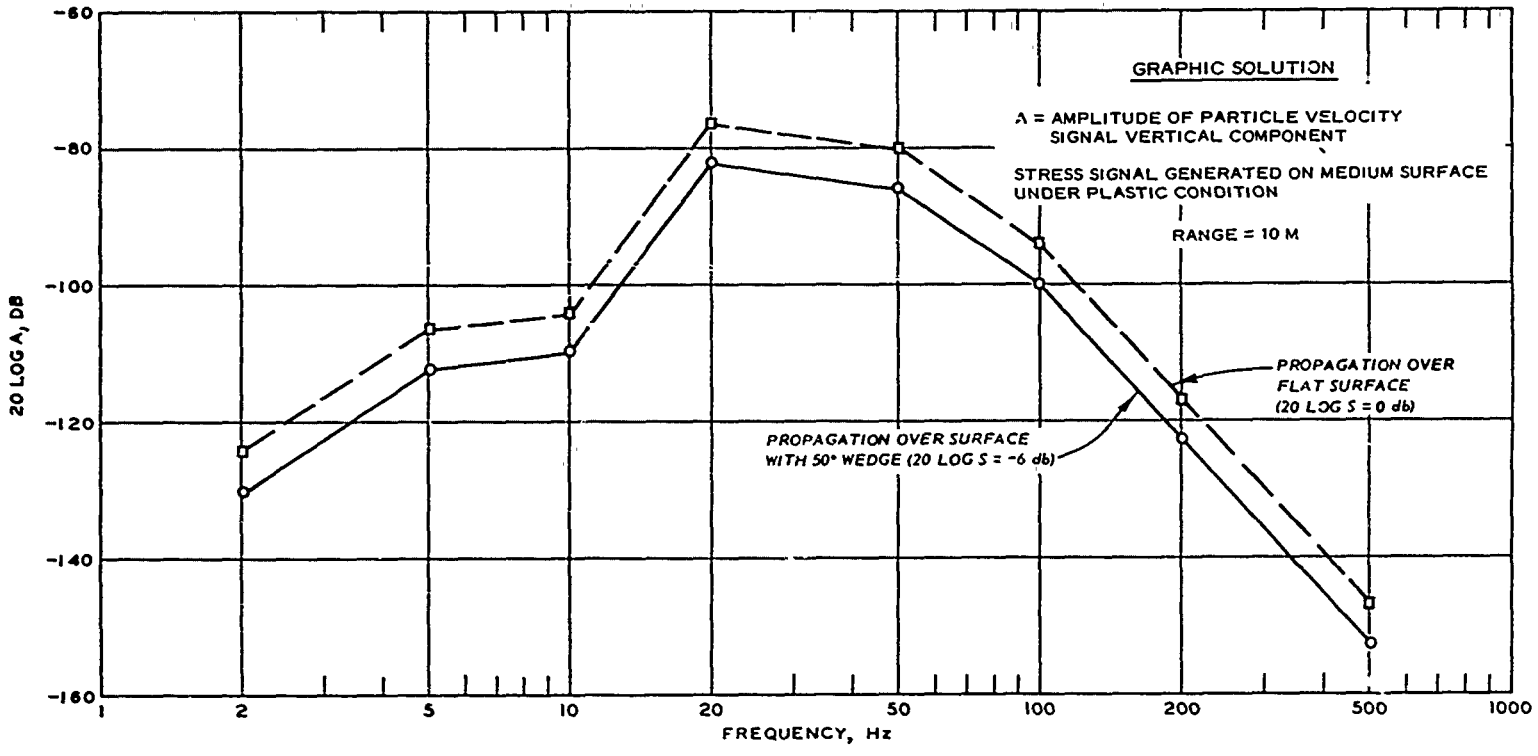

Fig. 10. Example site 3: frequency-dcmain signals over flat and sloped surfaces, 3-m-thick layer of material B on infinite half-space of material F; source stress signal from plate 3

not account for the effects of the surface macrogeometry feature, and, therefore, can be compared directly with those in plot b, fig. 9, to estimate the effect of changing the input stress signal (i.e. change from case 2 to case 3, see plates 2 and 3) on the particle velocity-time relations. The softer surface material resulted in a reduction in peak amplitude from 5 to 2.5 $\times 10^{-3}$ cm/sec and a signal of noticeably longer duration. Also, the predominant frequency for site 3 was less than that predicted for site 2 (i.e. about 20 compared with 50, see figs. 8 and 10). The effect of the signal propagating over the 50-deg wedge can also be seen in fig. 10. The result was obtained by subtracting 6 db from the prediction of propagation over the flat surface; 6 db is equivalent to a 50 percent reduction in the amplitude of the particle velocity-time relation shown in fig. 11.

Summary and Recommendations

63. The study has primarily dealt with the development and presentation of simple graphic procedures that can be used to predict seismic signal amplitudes and frequency characteristics. During this phase of the study, exhaustive analysis of the relations derived to develop the graphic procedures was not accomplished; nevertheless, the following generalizations can be advanced.

Summary

64. A simple but useful graphic solution to the wave generation and propagation phenomena for man-walking targets was developed. The solution is such that the terrain effects on (a) target-ground interaction, (b) energy source coupling, (c) transmission, and (d) surface macrogeometry can be isolated and studied, thereby permitting the user to determine quantitatively how the separate contributors (a-d above) interact synergistically. Generalizations based on the curves generated in this report must be made within the parameter ranges used to generate the curves. It is emphasized that whenever the generalizations are applied in situations outside the parameter ranges from which extractions were made, errors may arise. However, interpolations within the

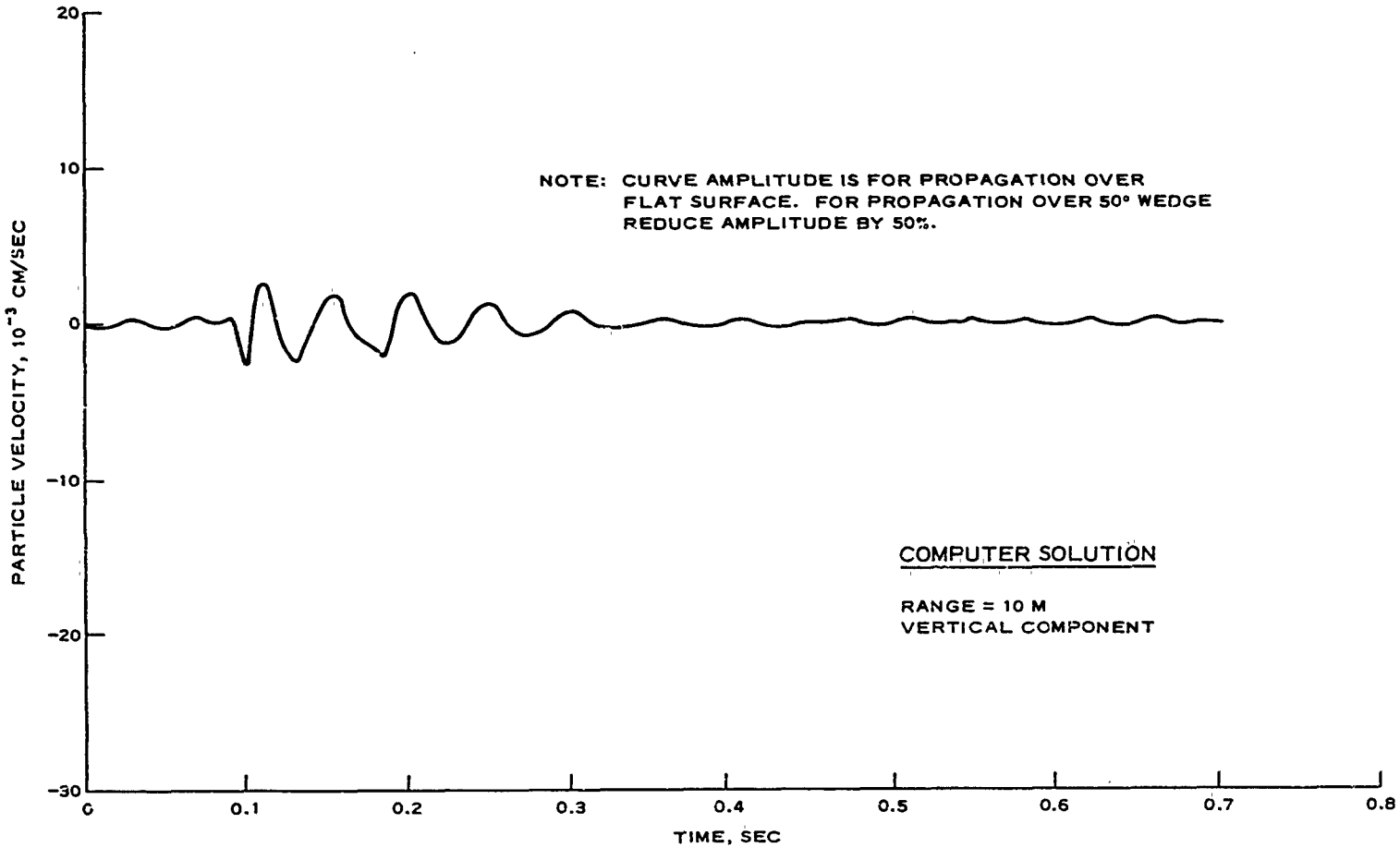

Fig. 11. Example site 3: time-domain signals over flat and sloped surfaces, 3-m-thick layer of material B over infinite half-space of material F; source stress signal from plate 3

parameter ranges studied can be made with confidence, and, therefore, generalizations concerning cases not actually studied in this report are possible (paragraphs 9 and 10).

65. To mathematically simulate the wave generation and propagation phenomena, a soil model consisting of at least the following factors is required (paragraphs 5-8):

a. Force-deflection (soil surface) relations.

b. Seismic properties of each propagating medium (V_s , V_p , γ , and layer thickness) to a depth approximately equal to a half wavelength of the lowest frequency of importance.

c. The range from signal source to sensor.

d. Generalized surface macrogeometry features, i.e. features described as combinations of steps and wedges.

e. Soil damping factor (in this study an average damping factor of 0.03 was used).

66. The results of this study show (paragraphs 40-43, 48-52, and 58-62) that site properties influence, to a large degree, the character of the signal from a footstep. The signal arriving at the sensor is affected by (a) target-ground interaction, (b) energy coupling to the substrate, (c) propagation from the source to the sensor, and (d) transmission of the wave over surface geometry features. The graphic solution developed as depicted in fig. 4 requires the summation of the effects enumerated above. Because of this summation process over the frequency range of interest it has been established that, if the source signal has certain frequency components that have extremely low amplitudes, these components will have large negative logarithmic values and will not contribute substantially to the total seismic signal. The only way these frequency components can form a part of the signal is by way of the uncontrollable background noise. In the same manner, if the source coupling or the site transfer function has low amplitude over parts of the frequency spectrum, these parts will be highly attenuated in the seismic signal that is generated.

Recommendations

67. Inasmuch as the analytical tools for studying the effects of

terrain on Rayleigh wave generation and propagation are just emerging from research, experience gained from use of the models is still quite limited. For this reason, generalizations or "theorems" useful to the design and deployment of UGS must be derived through deliberate application of the models. Therefore, it is recommended that results of the study reported herein be considered interim, and that the study of the terrain effects on generation and propagation of seismic signals from man-walking targets be continued. It is especially desirable that a more comprehensive set of signal-terrain relations be generated and studied with the objective of collapsing the myriad of curves to a simpler and more widely applicable graphic solution.

68. It is further recommended that the study be expanded to include multiple personnel and vehicle targets. It is particularly desirable that forcing functions (stress-time signals) be derived for a family of Warsaw Pact vehicles, and that these forcing functions be used in the sensitivity studies. It is believed that the work recommended above, in conjunction with data presented in this report, will be exceptionally useful to:

a. Fill in gaps in sensor design data base.

b. Identify target feature consistency (i.e. features insensitive to terrain variations).

c. Design sensor fields (i.e. calculate effective range of devices to determine layout and spacing for optimum protection).

d. Simplify site requirements for mapping criteria (i.e. the model can be used to identify site parameters that can be combined or inferred from other more easily identifiable site characteristics).

Literature Cited

1. Lundien, J. R. and Nikodem, H., "A Mathematical Model for Predicting Microseismic Signals in Terrain Materials," Technical Report M-73-4, Jun 1973, U. S. Army Engineer Waterways Experiment Station, CE, Vicksburg, Miss.
2. Van Deusen, B. D., "A Statistical Technique for the Dynamic Analysis of Vehicles Traversing Rough Yielding and Non-Yielding Surfaces," May 1966, Advanced Projects Organization, Chrysler Corporation, Detroit, Mich.
3. Hough, B. K., Basic Soils Engineering, 1st ed., Ronald Press, New York, 1957.
4. Rush, E. S. and Rula, A. A., "A Limited Study of Effects of Soil Strength on Walking Speed," Miscellaneous Paper No. 4-950, Dec 1967, U. S. Army Engineer Waterways Experiment Station, CE, Vicksburg, Miss.
5. Henbest, O. J., Erickes, D. C., and Hixson, D. H., "Seismic and Resistivity Methods of Geophysical Exploration," Technical Release No. 44, U. S. Department of Agriculture, Soil Conservation Service, Engineering Division, Washington, D. C.
6. Kane, J. and Spence, J., "Rayleigh Wave Transmission on Elastic Wedges," Geophysics, Vol 28, No. 5, Oct 1963, pp 715-723.
7. McGarr, A. and Alsop, L. E., "Transmission and Reflection of Rayleigh Waves at Vertical Boundaries," Journal of Geophysical Research, Vol 72, No. 8, Apr 1967, pp 2169-2180.

Table 1

Seismic Properties of Media

Material	Phase Velocities, m/sec: Shear Wave V_s	Compression Wave V_p	Rayleigh Wave* V_R	Density g/cm^3
A	40	100	38	1.3
B	120	300	113	1.6
C	200	500	189	1.9
D	200	500	189	2.0
E	500	1000	467	2.3
F	1000	2000	937	2.6
G	400	1000	377	1.55

* Rayleigh wave phase velocity refers to that for homogeneous half-space only; for layered half-space, refer to curves of V_R versus frequency.

Table 2

Site 1 Graphic Construction Process

Site 1: One layer over infinite half-space, flat surface

Top layer: Material B, 0.75 m thick

Half-space: Material F

Range: R = 10 m

Source: Stress signal generated on hard surface under low compaction condition.

Frequency, f Hz	V_R m/sec*	$2\pi fR/V_R$	20 log H**	20 log F†	20 log B††	20 log S‡	20 log A‡‡
3	920	0.205	8.5	-4.0	-138.0	0	-133.5
5	918	0.342	7.2	-5.0	-133.5	0	-131.3
10	920	0.683	3.6	-2.0	-126.0	0	-124.4
20	925	1.359	1.0	-1.0	-116.0	0	-116.0
30	910	2.071	-2.2	0.5	-107.0	0	-108.7
50	370	8.491	-13.0	2.0	-78.0	0	-89.0
70	242	18.170	-19.0	-2.0	-57.5	0	-78.5
100	130	48.332	-31.5	-8.0	-42.0	0	-81.5
200	120	104.720	-49.0	-21.0	-29.0	0	-99.0
500	115	273.182	-95.0	-37.5	-13.0	0	-145.5

* Rayleigh wave phase velocity V_R from plate 38.

** Transmission coefficient H from plates 30-32.

† Source stress signal F from plate 2.

†† Source coupling coefficients B from plate 24.

‡ Surface macrcgeometry coefficients S from plates 43 and 44.

‡‡ Predicted microseismic signal A: particle velocity, cm/sec (20 log A = 20 log H + 20 log F + 20 log B + 20 log S); see fig. 6.

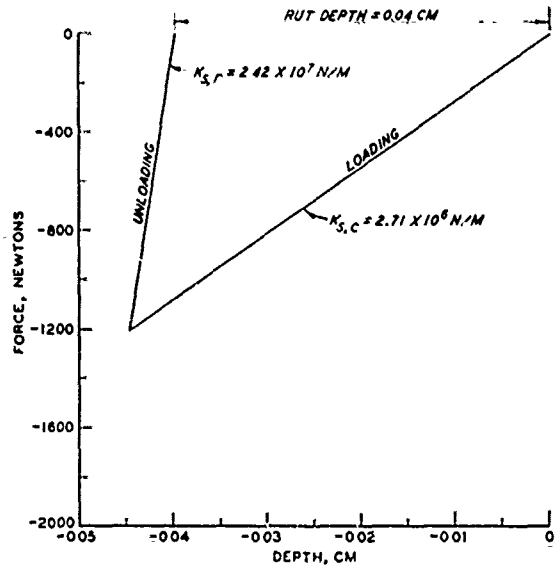

a. SURFACE SPRING FORCE VS DEPTH FOR ONE LOADING CYCLE

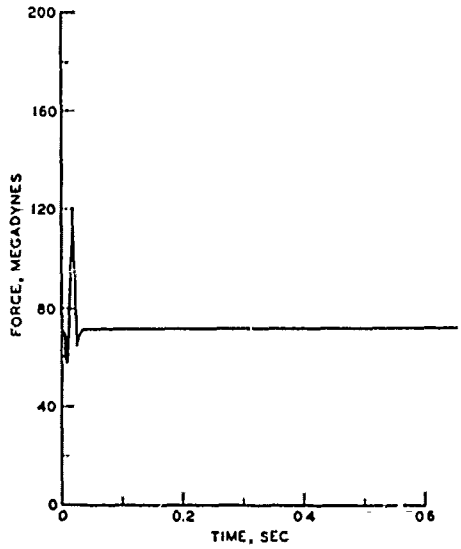

b STRESS SIGNAL · TIME DOMAIN

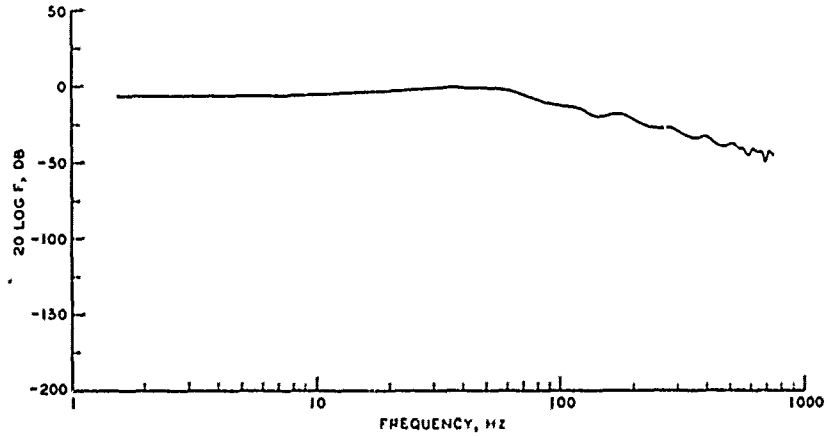

c. STRESS SIGNAL F - FREQUENCY DOMAIN

SURFACE RESPONSE CURVES
HARD SURFACE
LOW PLASTIC CONDITION
CASE I

PLATE 1

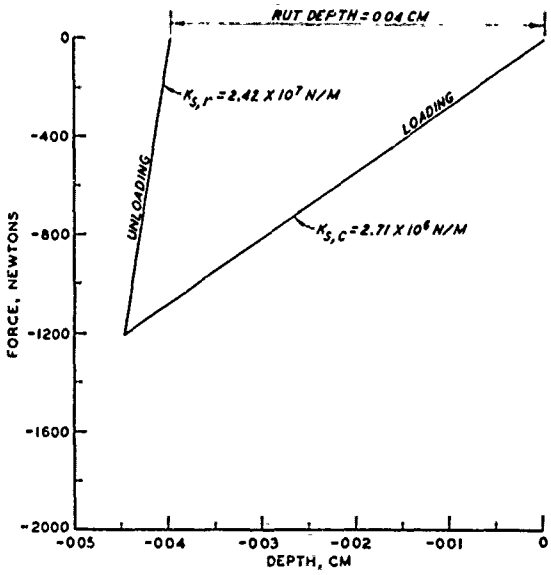

a. SURFACE SPRING FORCE VS DEPTH FOR ONE LOADING CYCLE

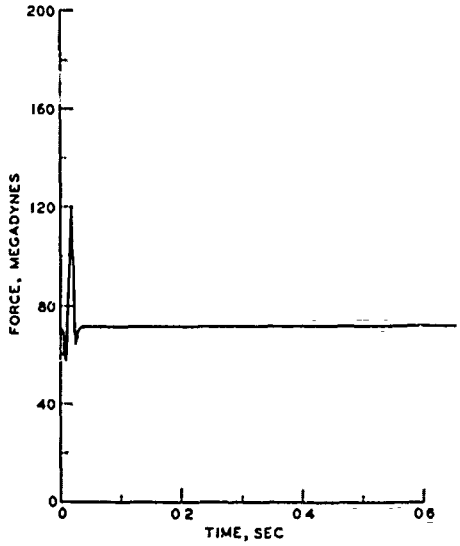

b STRESS SIGNAL - TIME DOMAIN

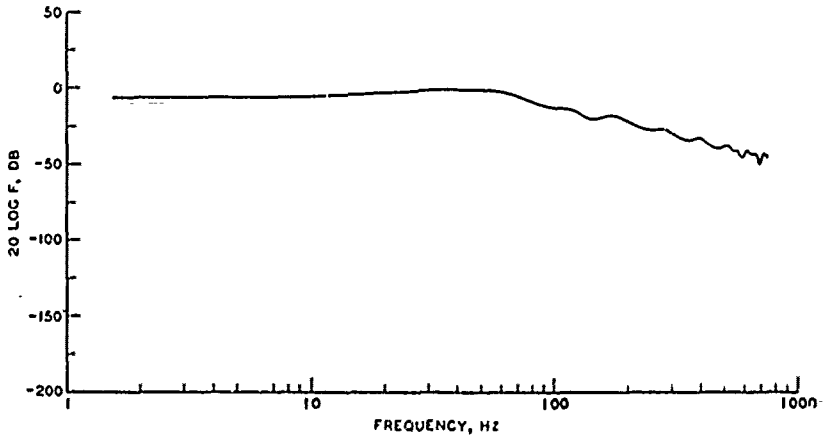

c. STRESS SIGNAL F - FREQUENCY DOMAIN

SURFACE RESPONSE CURVES
HARD SURFACE
LOW COMPACTION CONDITION
CASE 2

PLATE 2

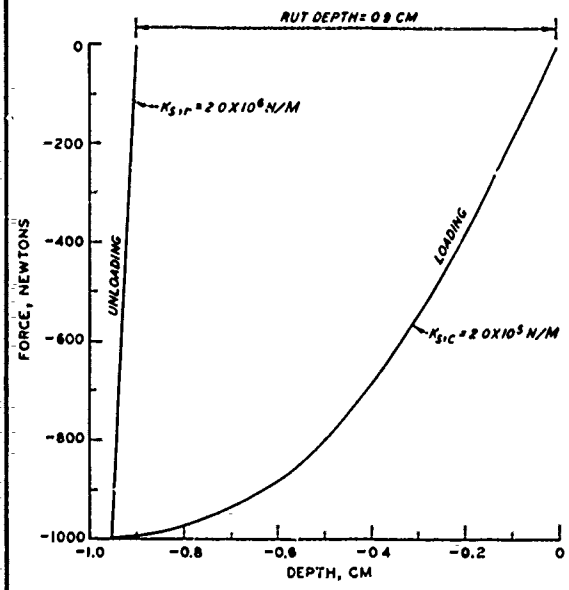

a. SURFACE SPRING FORCE VS DEPTH FOR ONE LOADING CYCLE

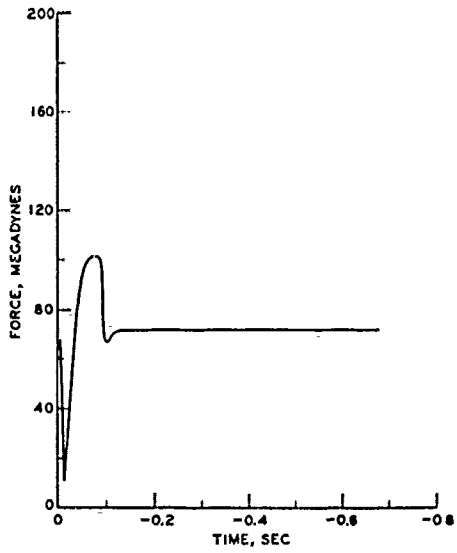

b. STRESS SIGNAL - TIME DOMAIN

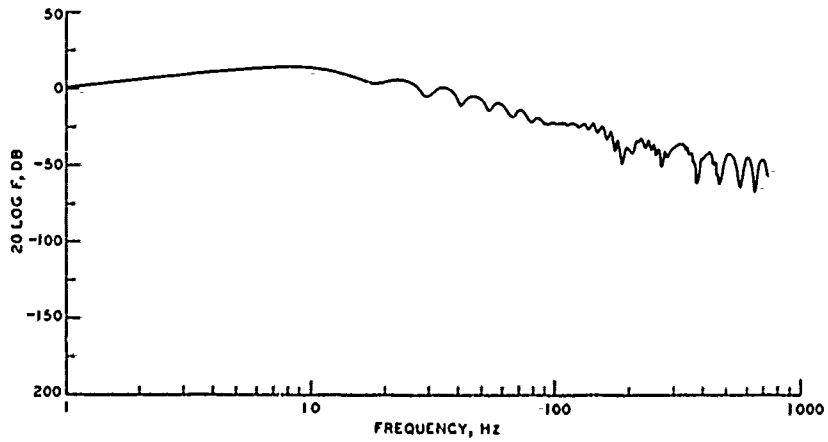

c. STRESS SIGNAL F - FREQUENCY DOMAIN

SURFACE RESPONSE CURVES
MEDIUM SURFACE
PLASTIC CONDITION
CASE 3

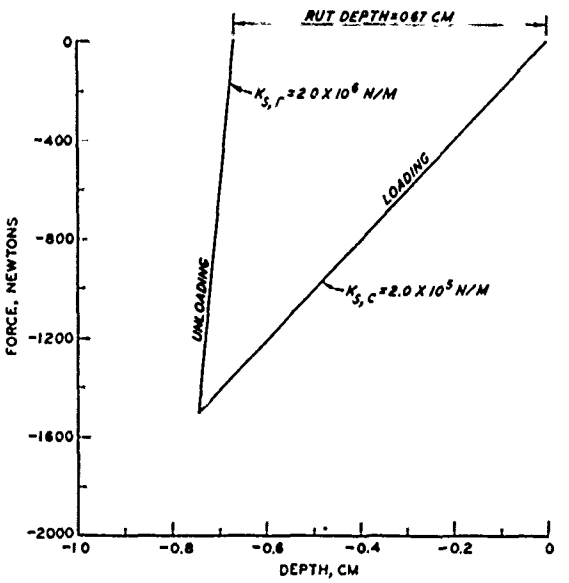

a. SURFACE SPRING FORCE VS DEPTH FOR ONE LOADING CYCLE

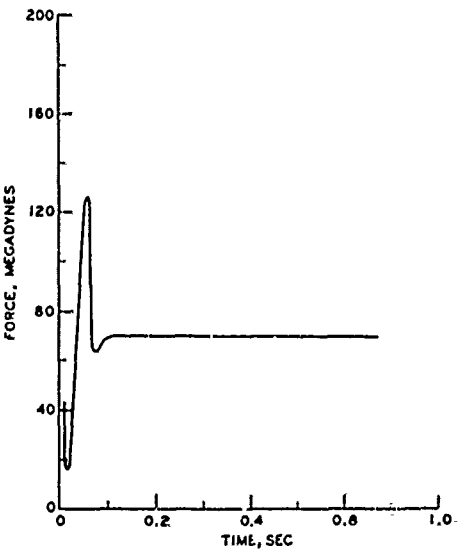

b. STRESS SIGNAL - TIME DOMAIN

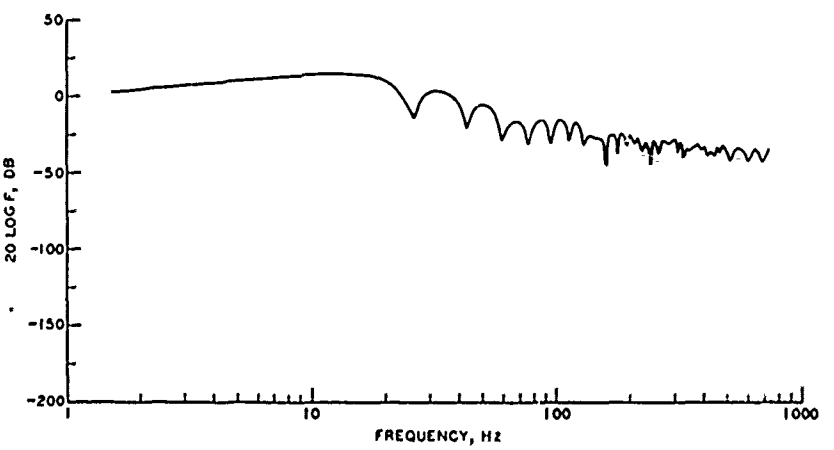

c. STRESS SIGNAL F - FREQUENCY DOMAIN

SURFACE RESPONSE CURVES
MEDIUM SURFACE
LOW COMPACTION CONDITION
CASE 4

PLATE 4

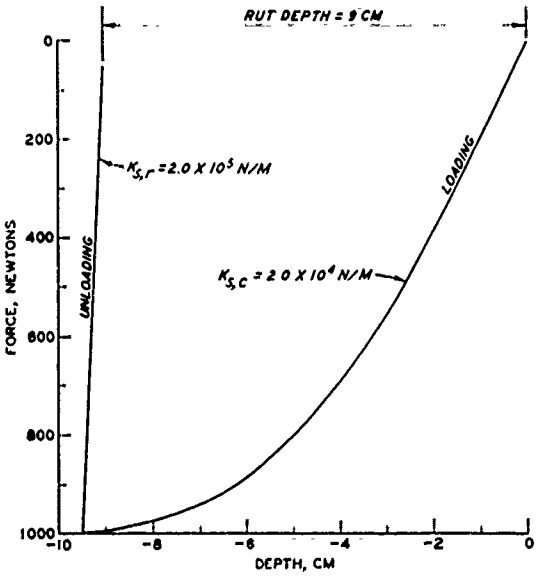

a. SURFACE SPRING FORCE VS DEPTH FOR ONE LOADING CYCLE

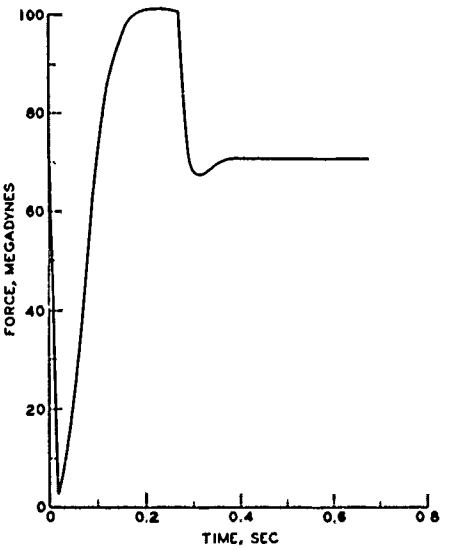

b STRESS SIGNAL - TIME DOMAIN

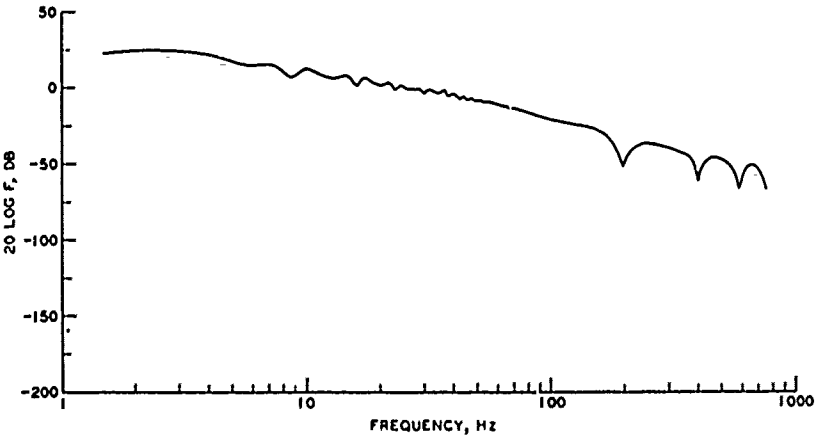

c. STRESS SIGNAL F - FREQUENCY DOMAIN

SURFACE RESPONSE CURVES
SOFT SURFACE
PLASTIC CONDITION
CASE 5

PLATE 5

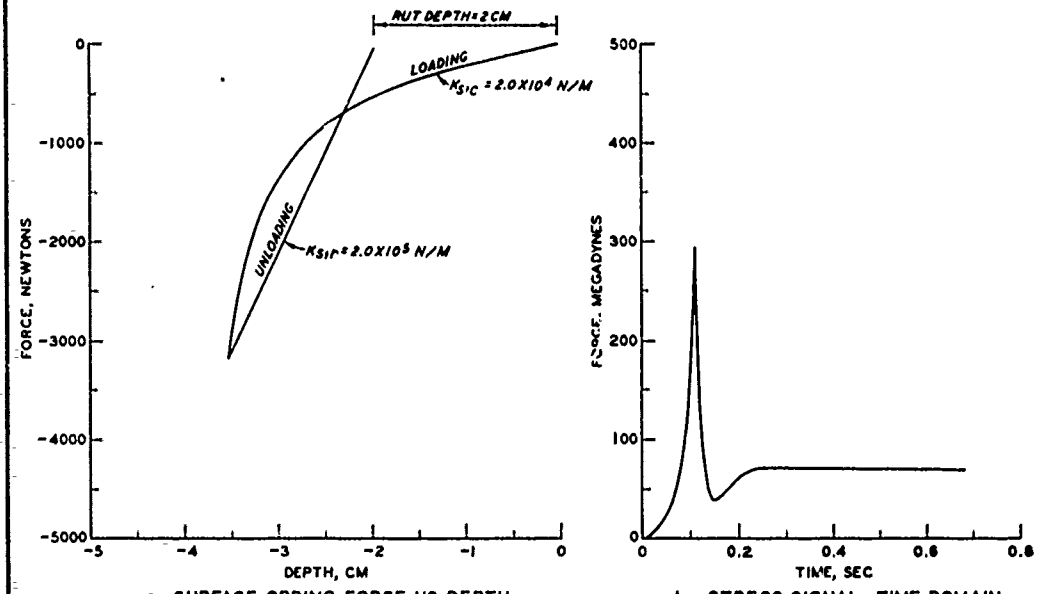

a. SURFACE SPRING FORCE VS DEPTH FOR ONE LOADING CYCLE

b. STRESS SIGNAL - TIME DOMAIN

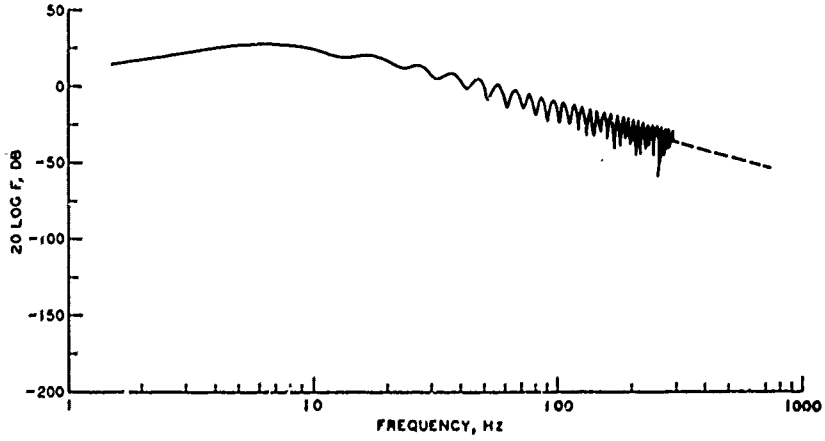

c. STRESS SIGNAL F - FREQUENCY DOMAIN

SURFACE RESPONSE CURVES
SOFT SURFACE
COMPACTION CONDITION
CASE 6

PLATE 6

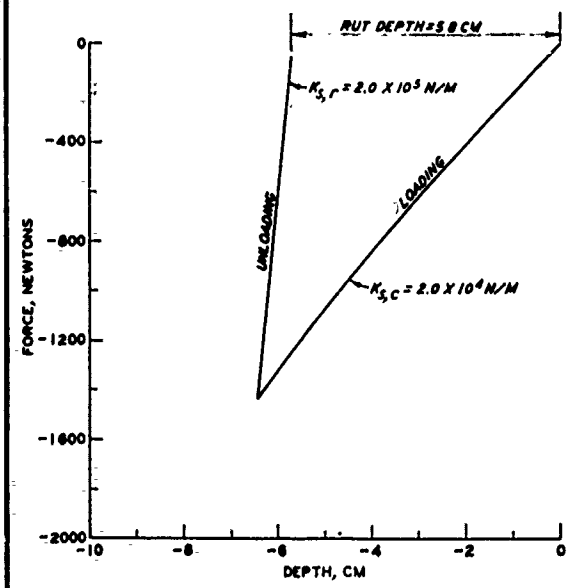

a. SURFACE SPRING FORCE VS DEPTH FOR ONE LOADING CYCLE

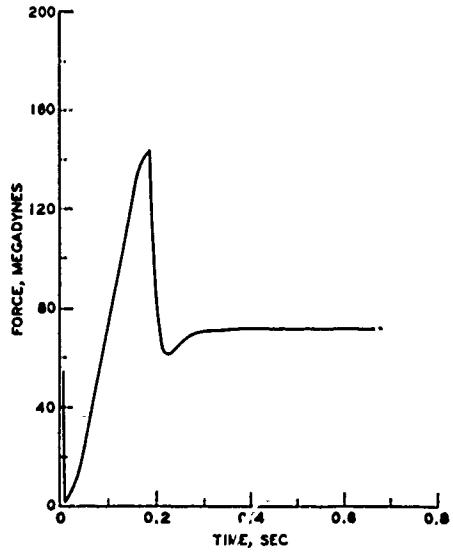

b. STRESS SIGNAL - TIME DOMAIN

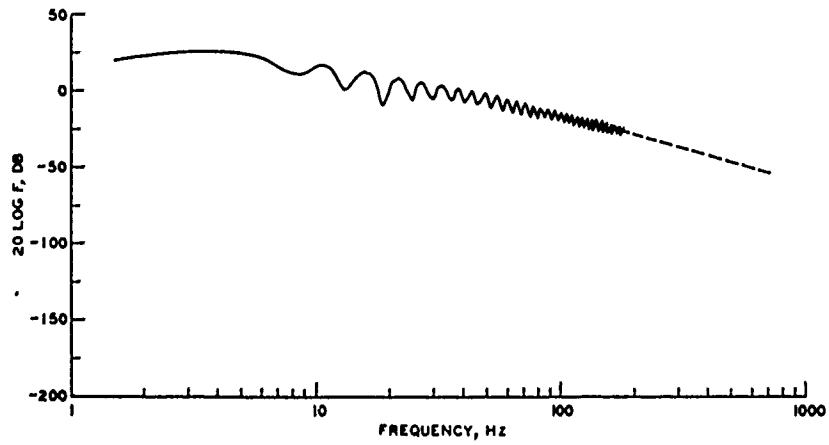

c. STRESS SIGNAL F - FREQUENCY DOMAIN

SURFACE RESPONSE CURVES
SOFT SURFACE
LOW COMPACTION CONDITION
CASE 7

PLATE 7

PLATE 8

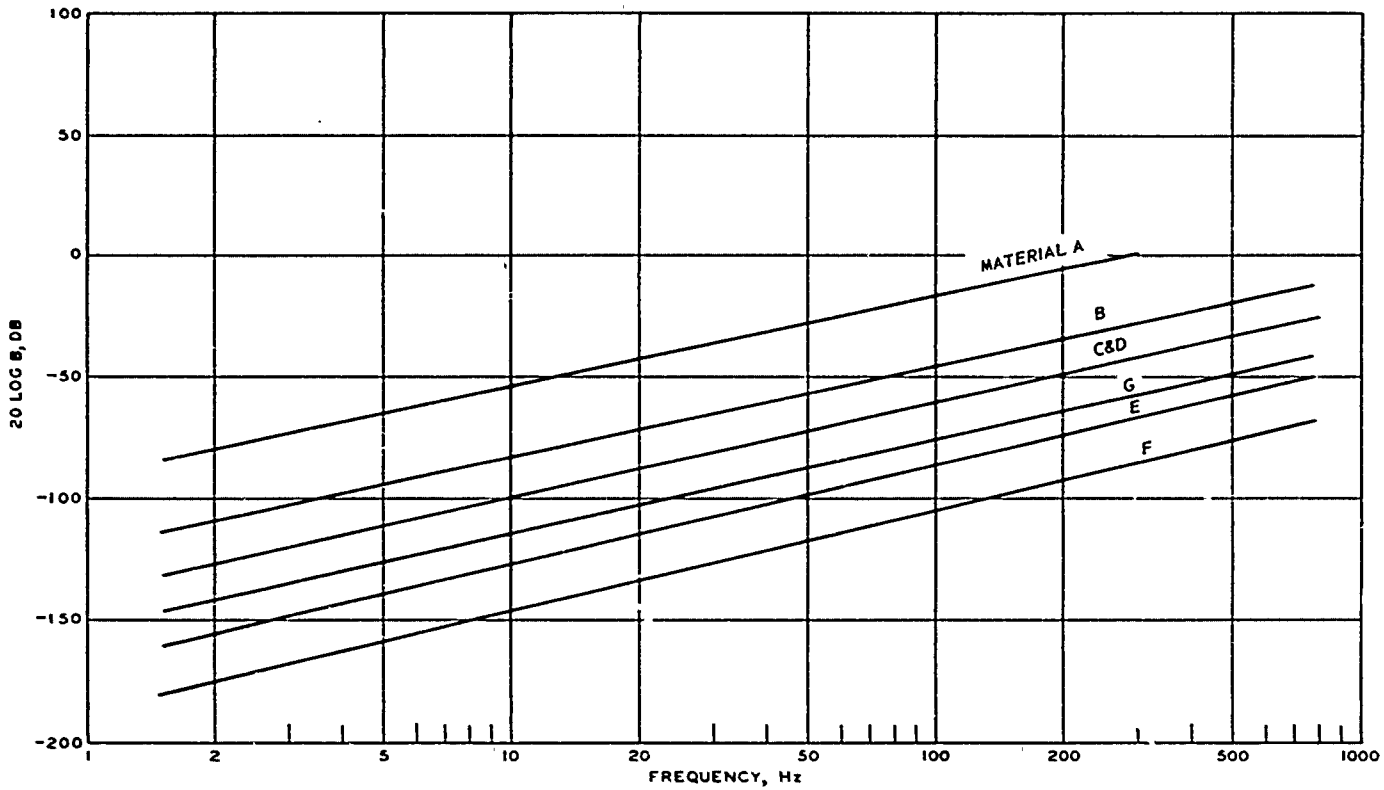

SOURCE COUPLING COEFFICIENT, B

RADIAL COMPONENT, ξ = 0.03

HOMOGENEOUS HALF-SPACE

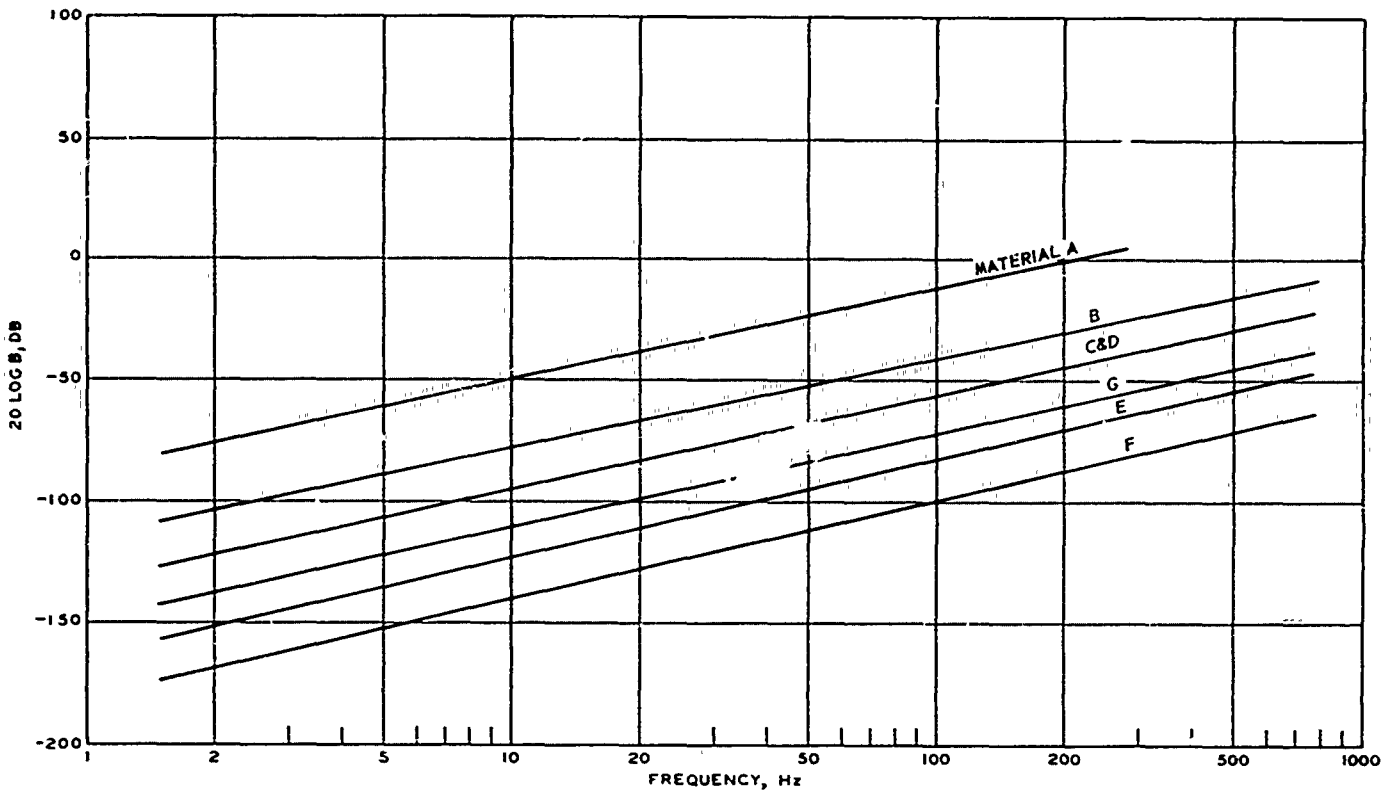

SOURCE COUPLING COEFFICIENT, B

VERTICAL COMPONENT, $\xi = 0.03$

HOMOGENEOUS HALF-SPACE

PLATE 9

SOURCE COUPLING COEFFICIENT, B
RADIAL COMPONENT ξ = 0.03
TOP LAYER MATERIAL - A
BASE MATERIAL - D
FIRST LAYER THICKNESS, M
0.25
0.75
1.5
3.0
6.0
FREQUENCY, Hz
20 LOG B, DB
400
300
200
100
0
-100
-200
1
2
5
10
20
50
100
200
500
1000

PLATE 10

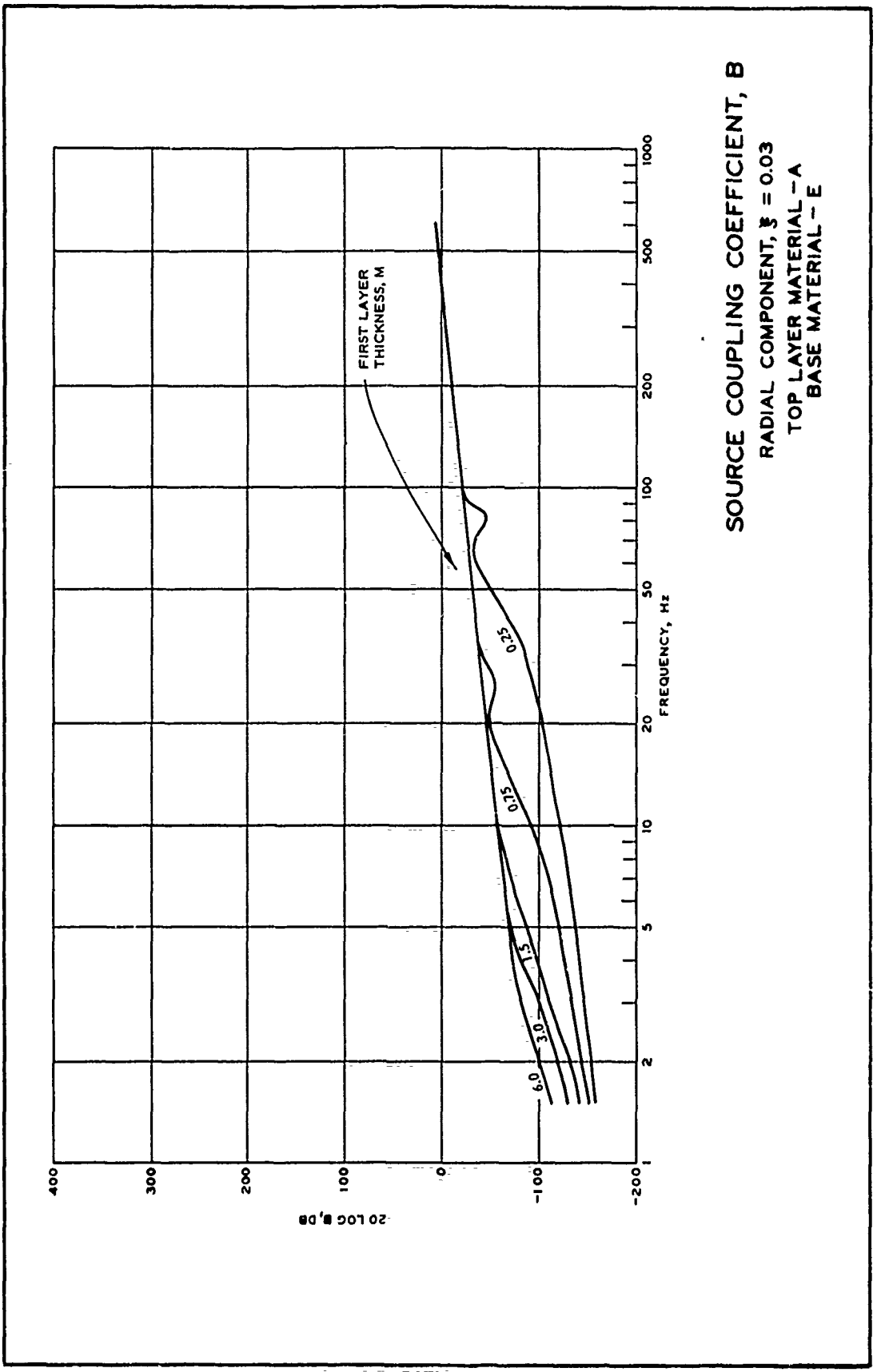
SOURCE COUPLING COEFFICIENT, B
RADIAL COMPONENT, ζ = 0.03
TOP LAYER MATERIAL – A
BASE MATERIAL – E
FIRST LAYER THICKNESS, M
0.25
0.75
1.5
3.0
6.0
FREQUENCY, Hz
1
2
5
10
20
50
100
200
500
1000
20 LOG B, DB
400
300
200
100
0
-100
-200

PLATE 11

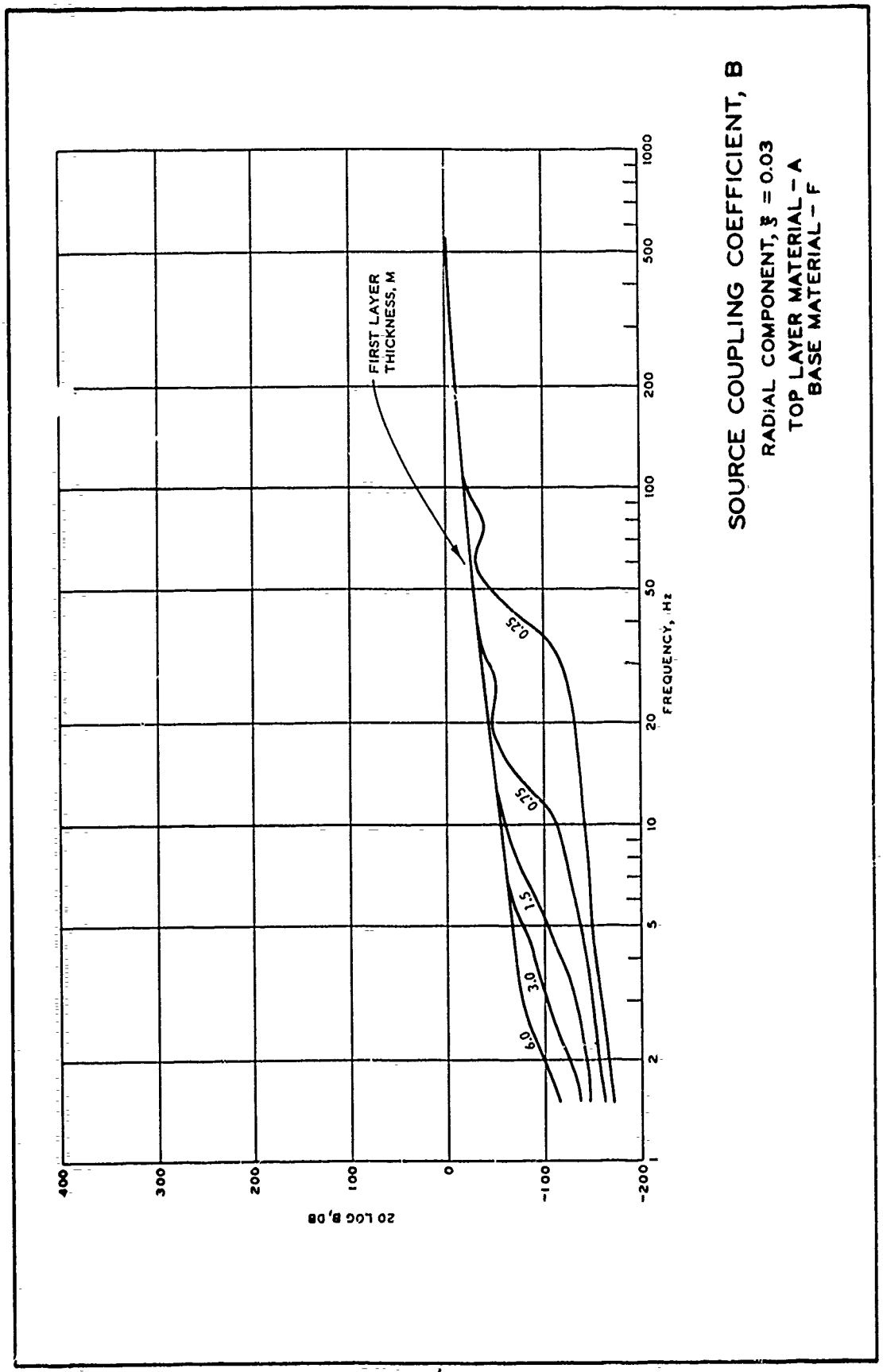
SOURCE COUPLING COEFFICIENT, B
RADIAL COMPONENT, ξ = 0.03
TOP LAYER MATERIAL – A
BASE MATERIAL – F
FIRST LAYER THICKNESS, M
0.25
0.75
1.5
3.0
6.0
FREQUENCY, Hz
1
2
5
10
20
50
100
200
500
1000
20 LOG B, DB
400
300
200
100
0
-100
-200

PLATE 12

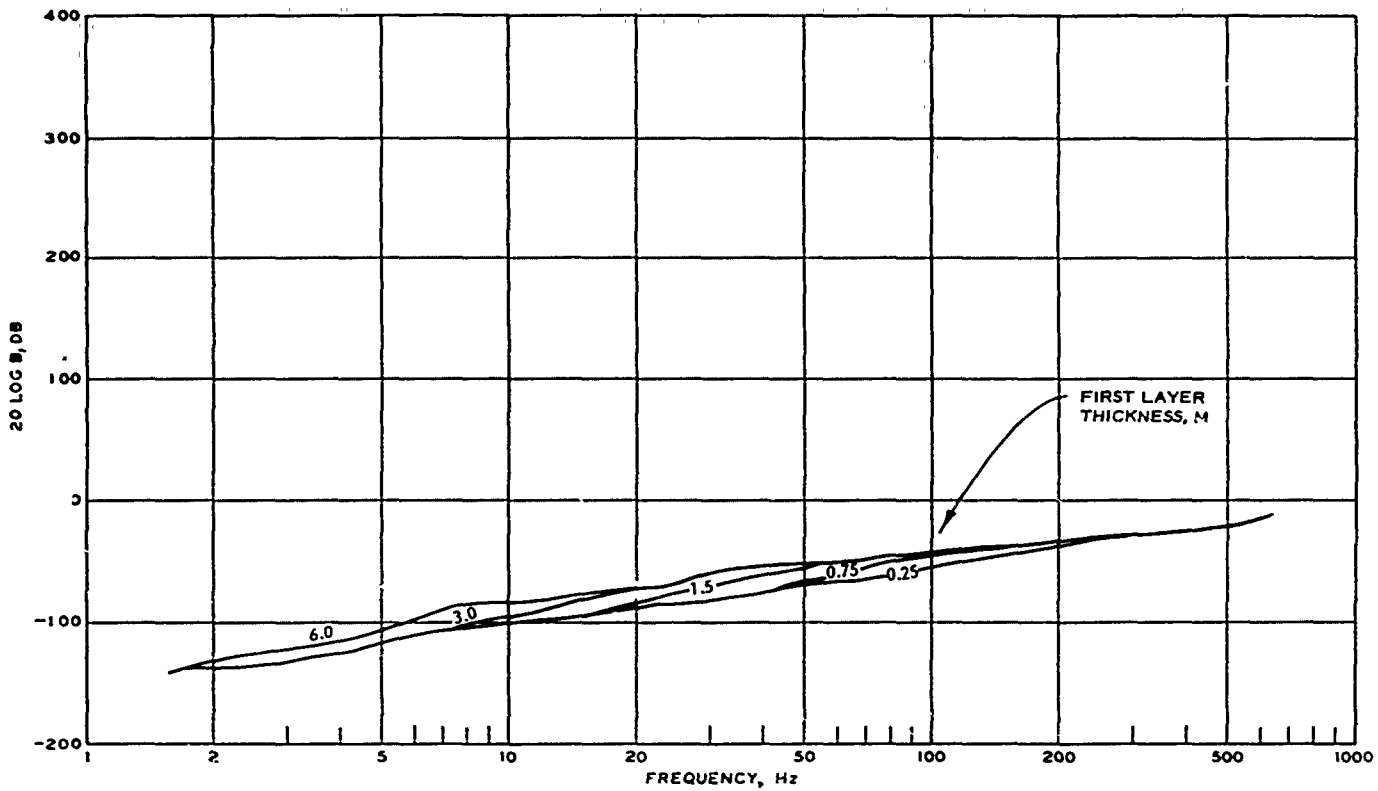

SOURCE COUPLING COEFFICIENT, B

RADIAL COMPONENT, ξ = 0.03

TOP LAYER MATERIAL – B
BASE MATERIAL – D

PLATE 13

PLATE 14

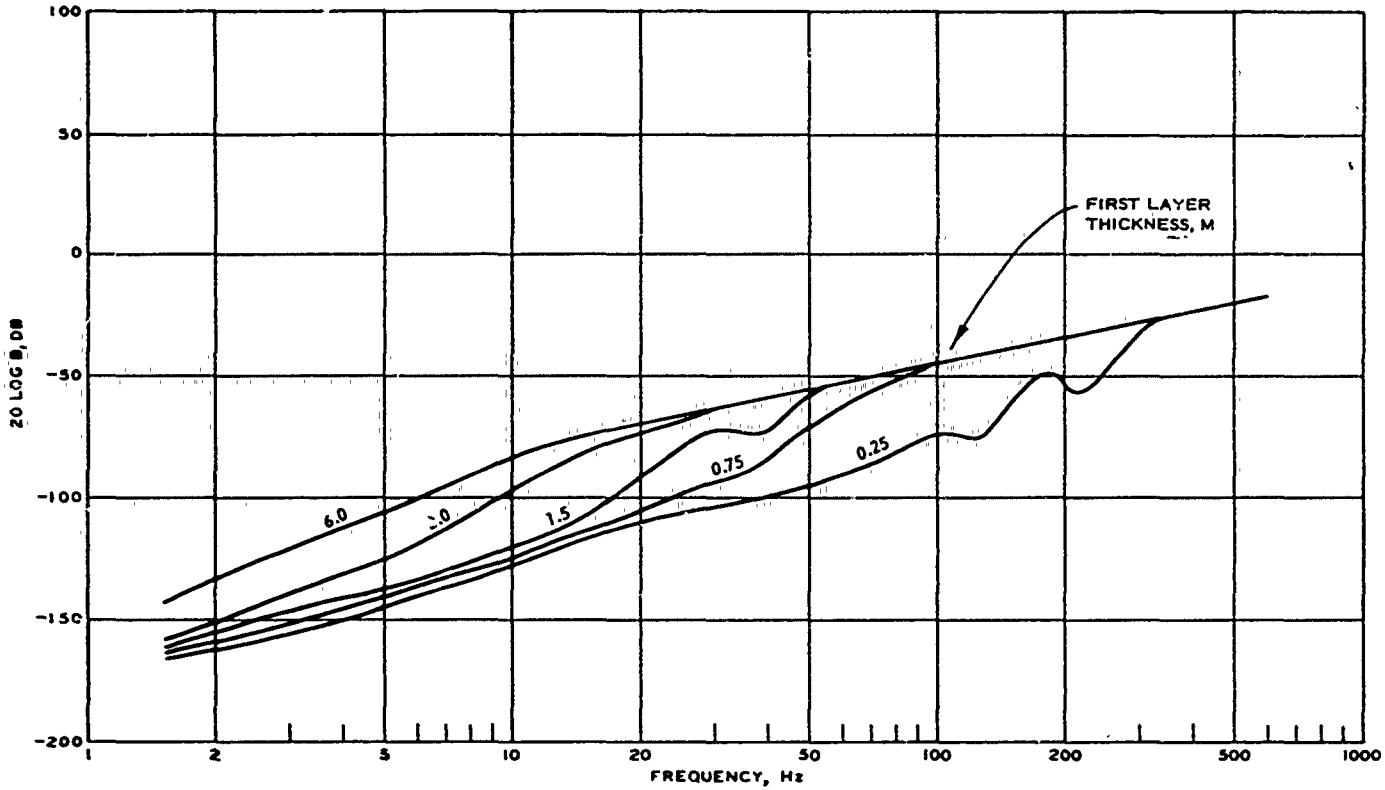

SOURCE COUPLING COEFFICIENT, B

RADIAL COMPONENT, $\xi = 0.03$

TOP LAYER MATERIAL – B
BASE MATERIAL – E

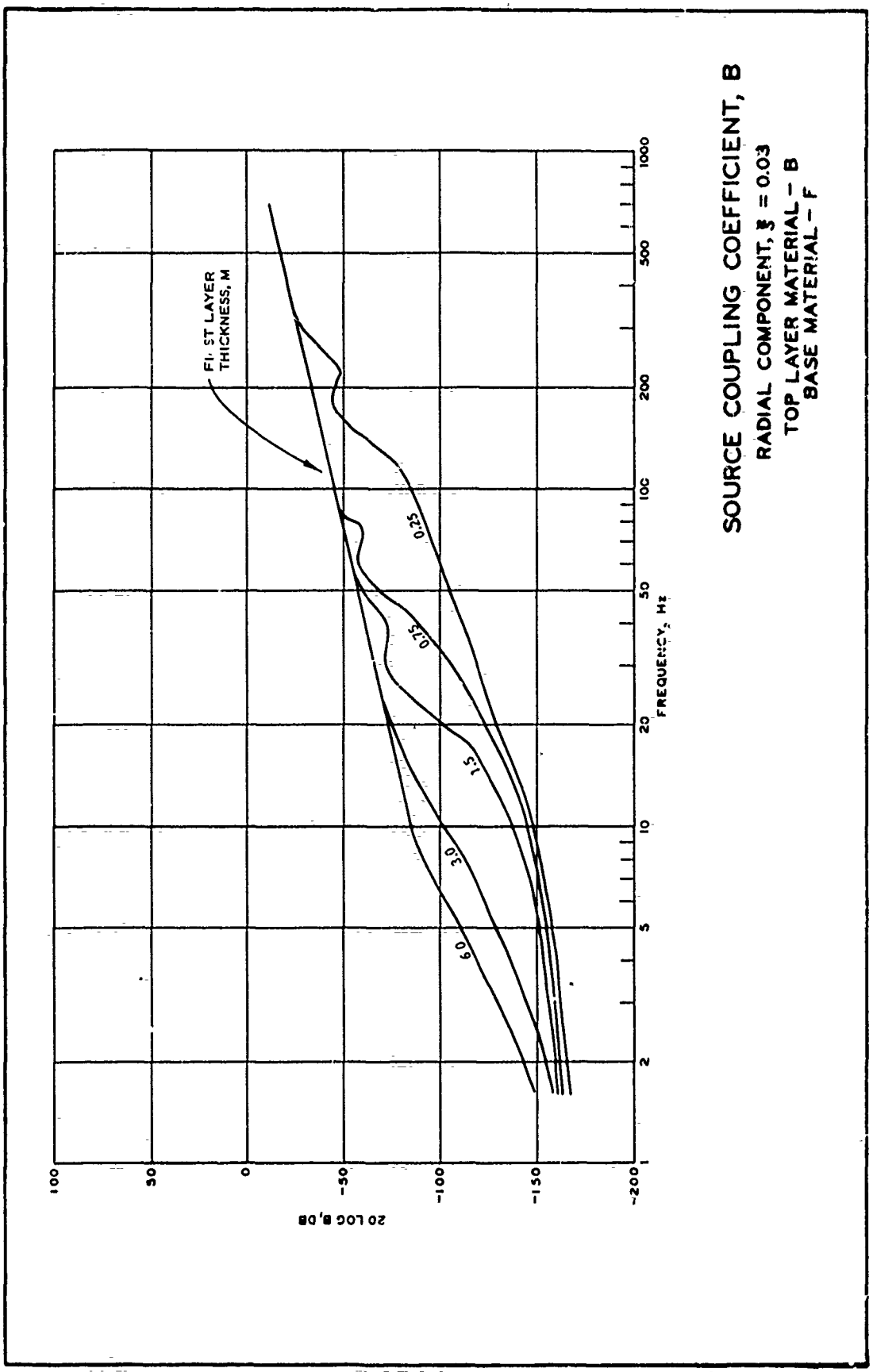
SOURCE COUPLING COEFFICIENT, B
RADIAL COMPONENT, ϑ = 0.03
TOP LAYER MATERIAL – B
BASE MATERIAL – F
FIRST LAYER THICKNESS, M
0.25
0.75
1.5
3.0
6.0
20 LOG B, DB
FREQUENCY, Hz
100
50
0
-50
-100
-150
-200
1
2
5
10
20
50
100
200
500
1000

PLATE 15

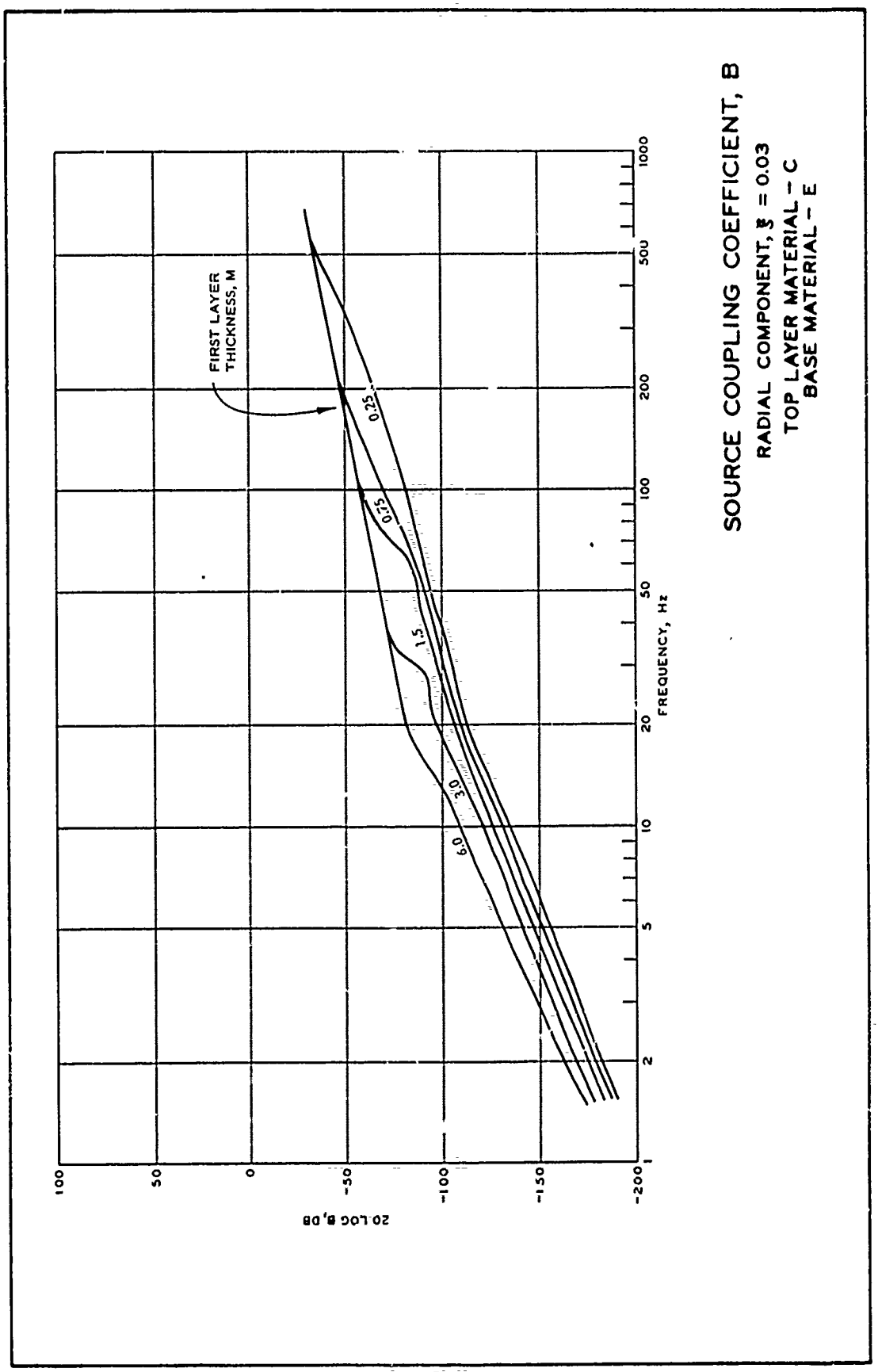
SOURCE COUPLING COEFFICIENT, B
RADIAL COMPONENT, ξ = 0.03
TOP LAYER MATERIAL – C
BASE MATERIAL – E
FIRST LAYER THICKNESS, M
0.25
0.75
1.5
3.0
6.0
FREQUENCY, Hz
1000
500
200
100
50
20
10
5
2
1
100
50
0
-50
-100
-150
-200
20 LOG B, DB

PLATE 16

SOURCE COUPLING COEFFICIENT, B
RADIAL COMPONENT, ξ = 0.03
TOP LAYER MATERIAL – C
BASE MATERIAL – F
FIRST LAYER THICKNESS, M
0.25
0.75
1.5
3.0
6.0
20 LOG B, DB
100
50
0
-50
-100
-150
-200
FREQUENCY, Hz
1
2
5
10
20
50
100
200
500
1,000

PLATE 17

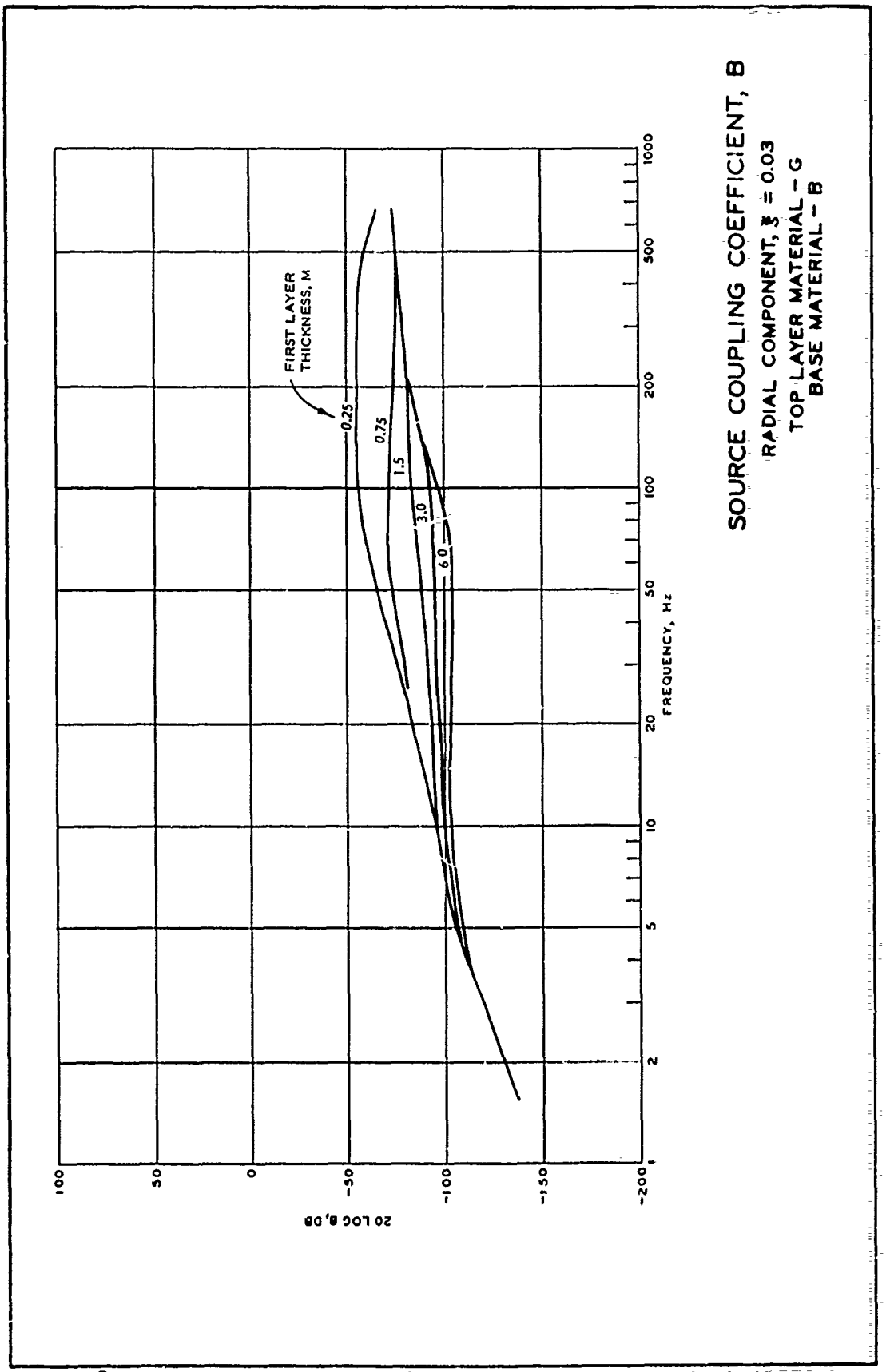
SOURCE COUPLING COEFFICIENT, B
RADIAL COMPONENT, ξ = 0.03
TOP LAYER MATERIAL - G
BASE MATERIAL - B
FIRST LAYER THICKNESS, M
0.25
0.75
1.5
3.0
6.0
FREQUENCY, Hz
20 LOG B, DB
100
50
0
-50
-100
-150
-200
1000
500
200
100
50
20
10
5
2
1

PLATE 18

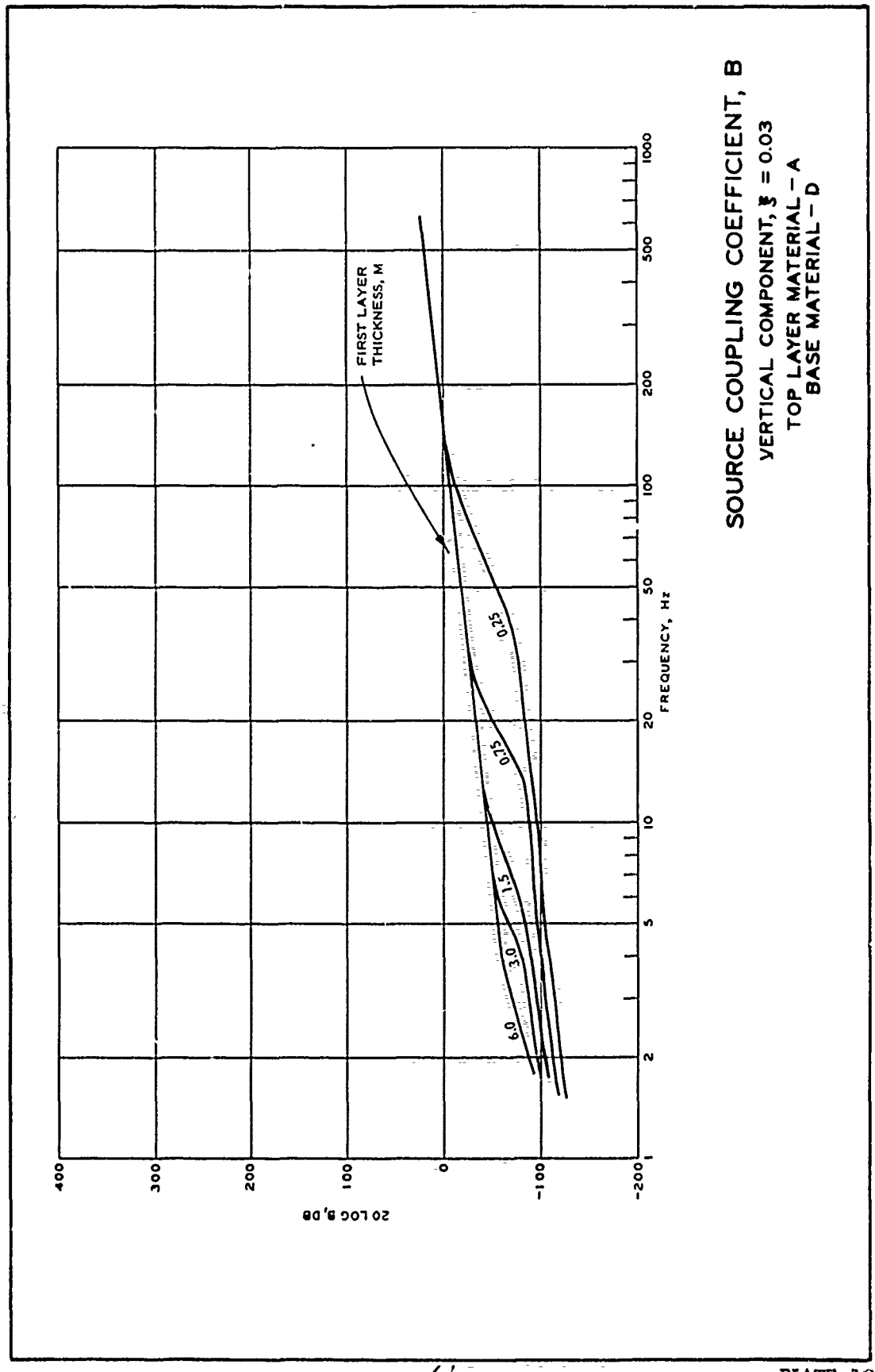
SOURCE COUPLING COEFFICIENT, B
VERTICAL COMPONENT, ξ = 0.03
TOP LAYER MATERIAL – A
BASE MATERIAL – D
FIRST LAYER THICKNESS, M
0.25
0.75
1.5
3.0
6.0
FREQUENCY, Hz
1
2
5
10
20
50
100
200
500
1000
20 LOG B, DB
400
300
200
100
0
-100
-200

PLATE 19

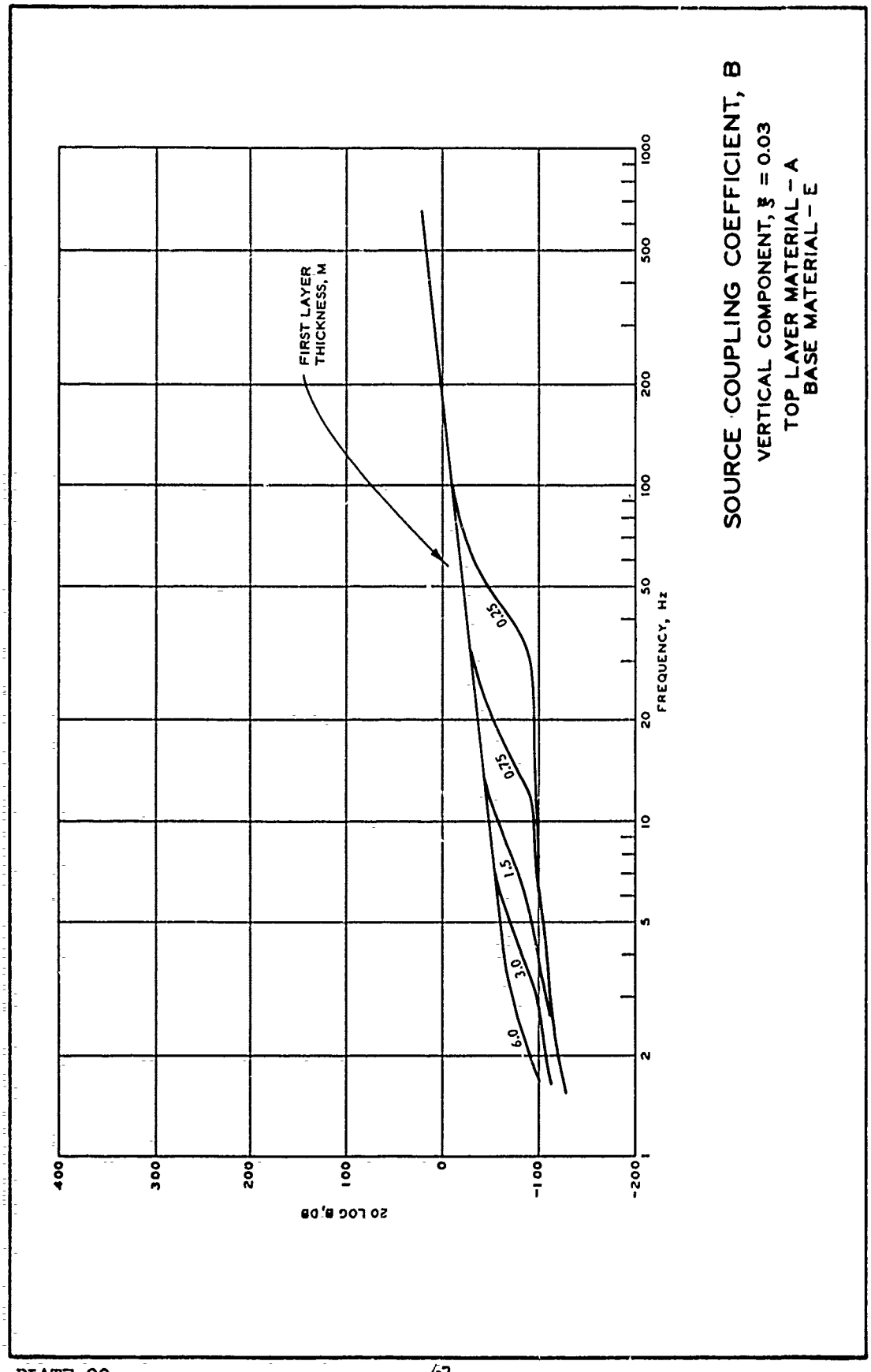
SOURCE COUPLING COEFFICIENT, B
VERTICAL COMPONENT, ξ = 0.03
TOP LAYER MATERIAL – A
BASE MATERIAL – E
FIRST LAYER THICKNESS, M
0.25
0.75
1.5
3.0
6.0
FREQUENCY, Hz
1
2
5
10
20
50
100
200
500
1000
20 LOG B, DB
400
300
200
100
0
-100
-200

PLATE 20

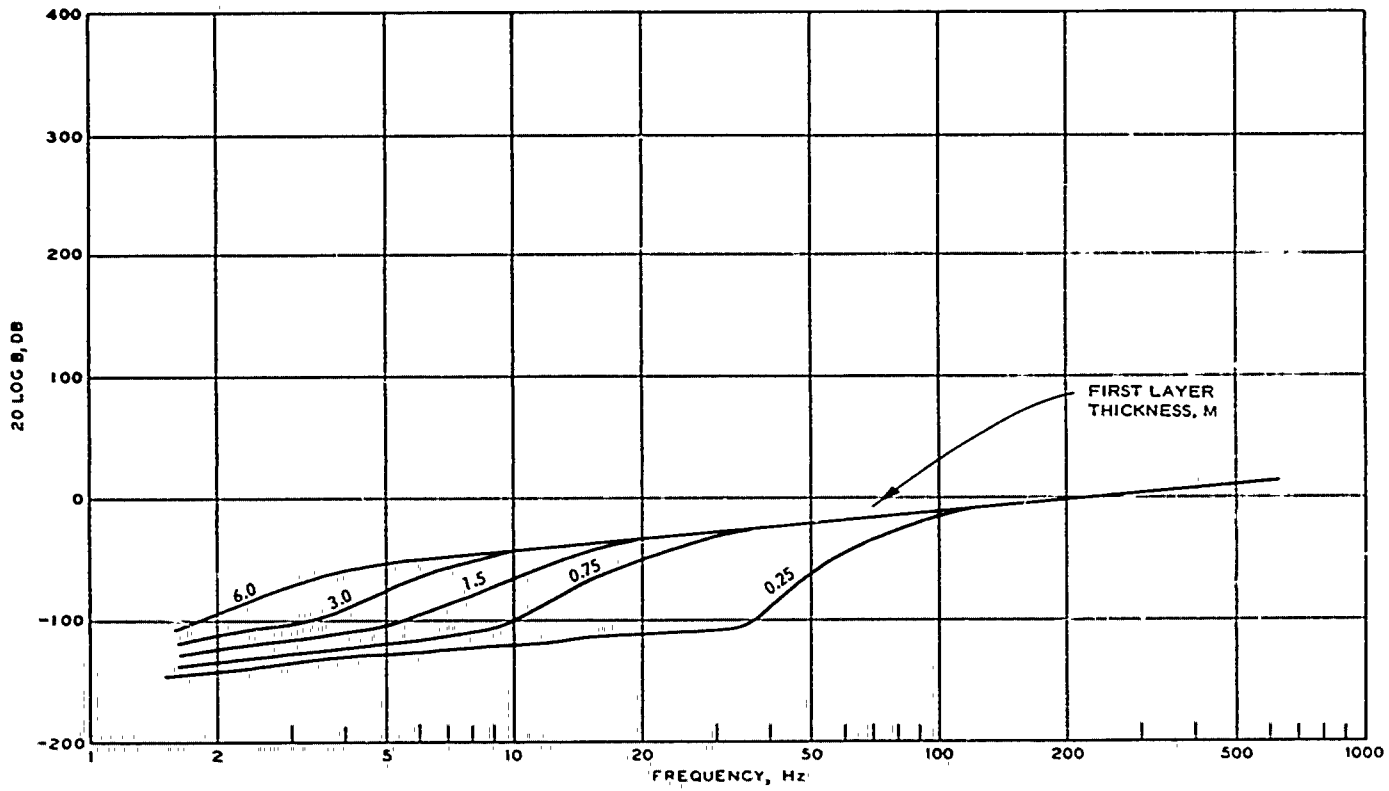

SOURCE COUPLING COEFFICIENT, B

VERTICAL COMPONENT, $\xi = 0.03$

TOP LAYER MATERIAL – A
BASE MATERIAL – F

PLATE 21

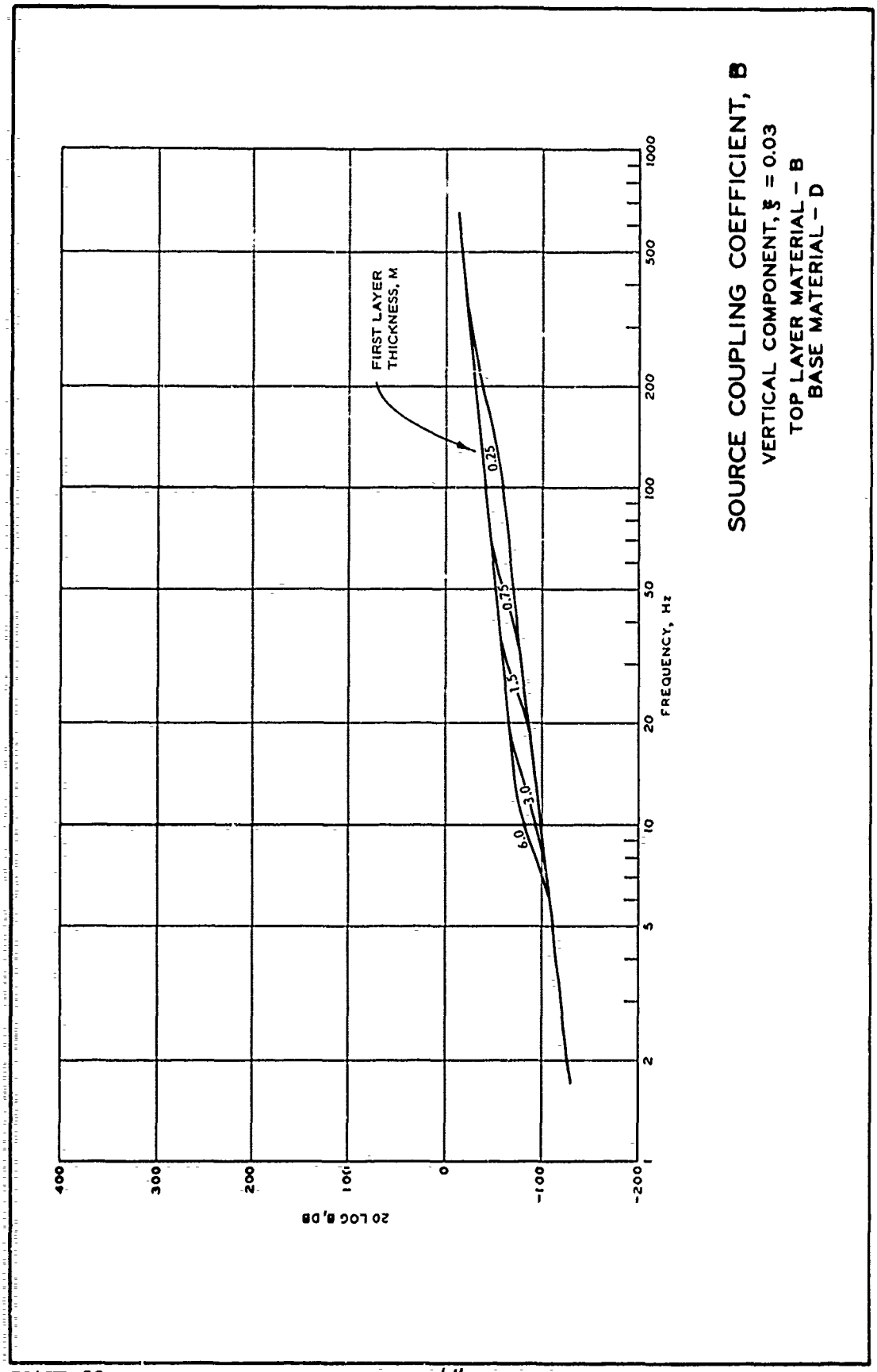
SOURCE COUPLING COEFFICIENT, B
VERTICAL COMPONENT, ξ = 0.03
TOP LAYER MATERIAL – B
BASE MATERIAL – D
FIRST LAYER THICKNESS, M
0.25
0.75
1.5
3.0
6.0
FREQUENCY, Hz
1
2
5
10
20
50
100
200
500
1000
20 LOG B, DB
400
300
200
100
0
-100
-200

PLATE 22

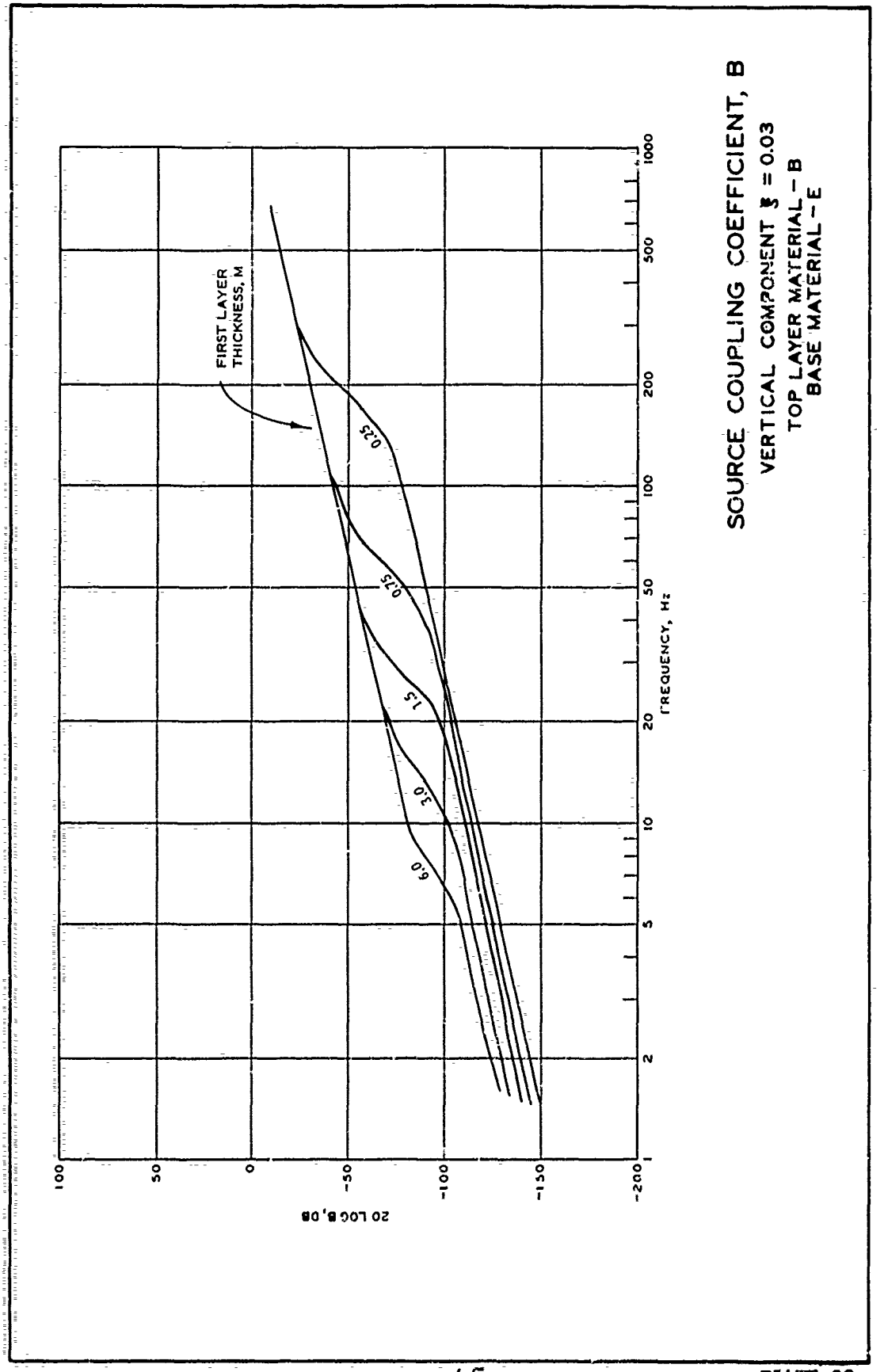
SOURCE COUPLING COEFFICIENT, B
VERTICAL COMPONENT ⅄ = 0.03
TOP LAYER MATERIAL - B
BASE MATERIAL - E
FIRST LAYER THICKNESS, M
0.25
0.75
1.5
3.0
6.0
20 LOG B, DB
FREQUENCY, Hz
100
50
0
-50
-100
-150
-200
1
2
5
10
20
50
100
200
500
1000

PLATE 23

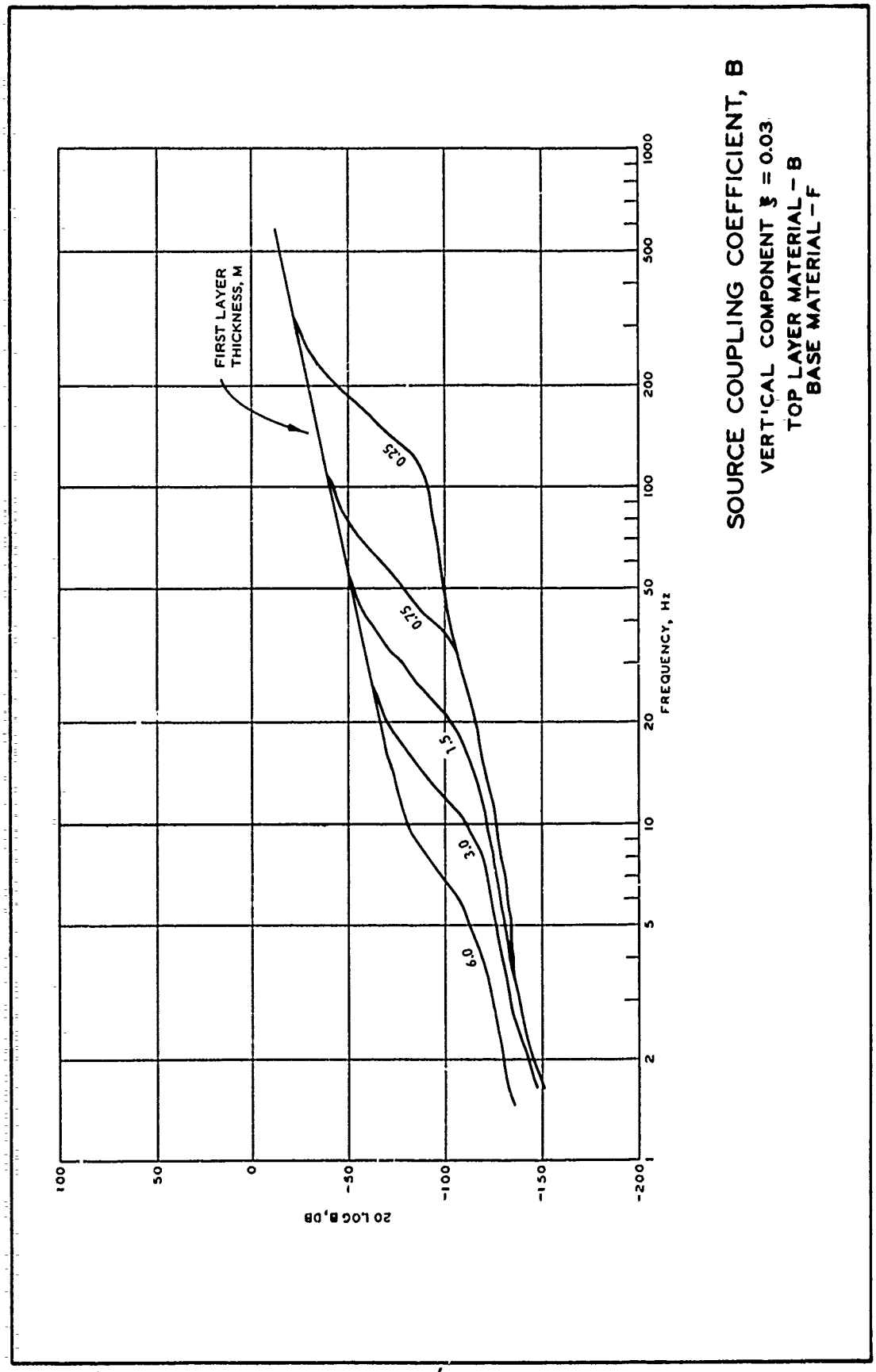
SOURCE COUPLING COEFFICIENT, B
VERTICAL COMPONENT ϑ = 0.03
TOP LAYER MATERIAL - B
BASE MATERIAL - F
FIRST LAYER THICKNESS, M
0.25
0.75
1.5
3.0
6.0
20 LOG B, DB
100
50
0
-50
-100
-150
-200
1
2
5
10
20
50
100
200
500
1000
FREQUENCY, Hz

PLATE 24

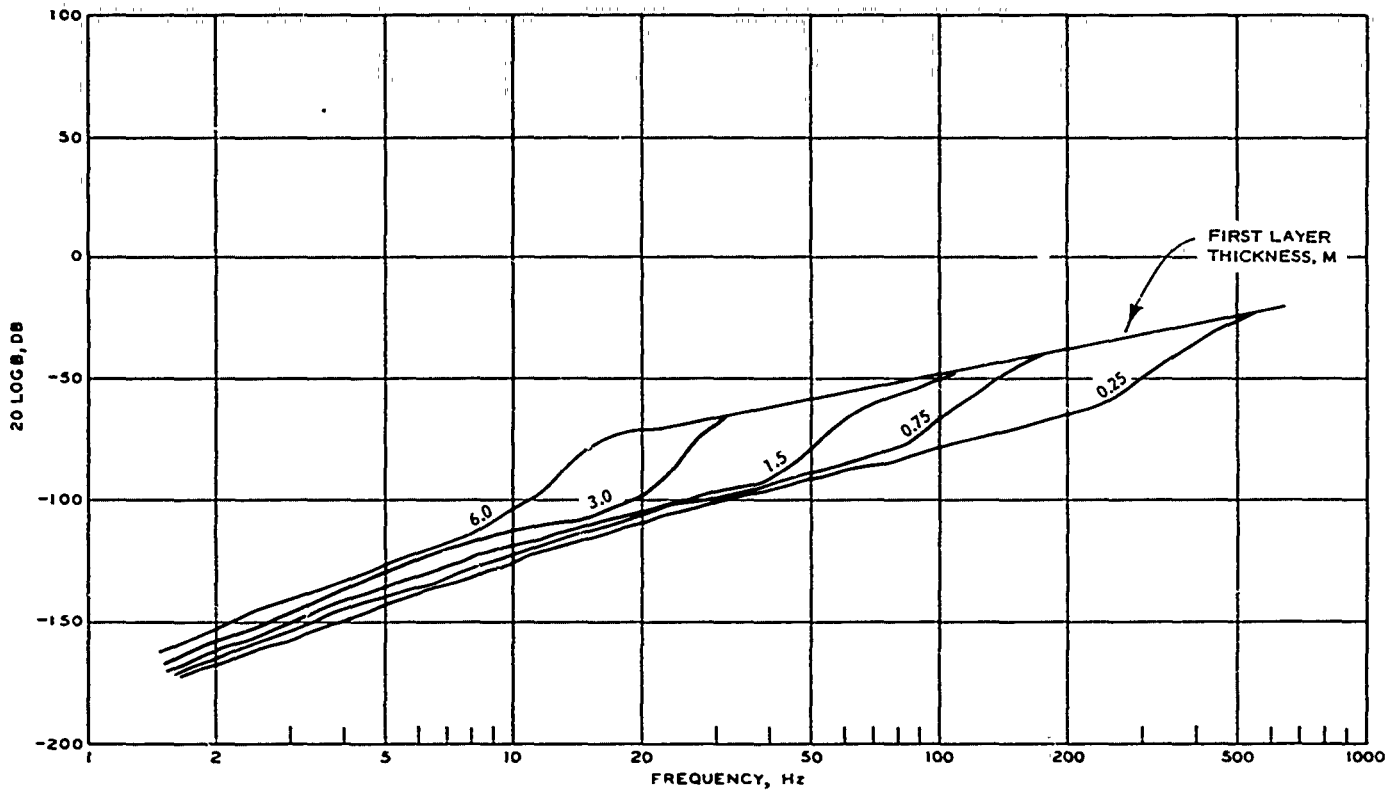

SOURCE COUPLING COEFFICIENT, B

VERTICAL COMPONENT, β = 0.03

TOP LAYER MATERIAL – C
BASE MATERIAL – E

PLATE 25

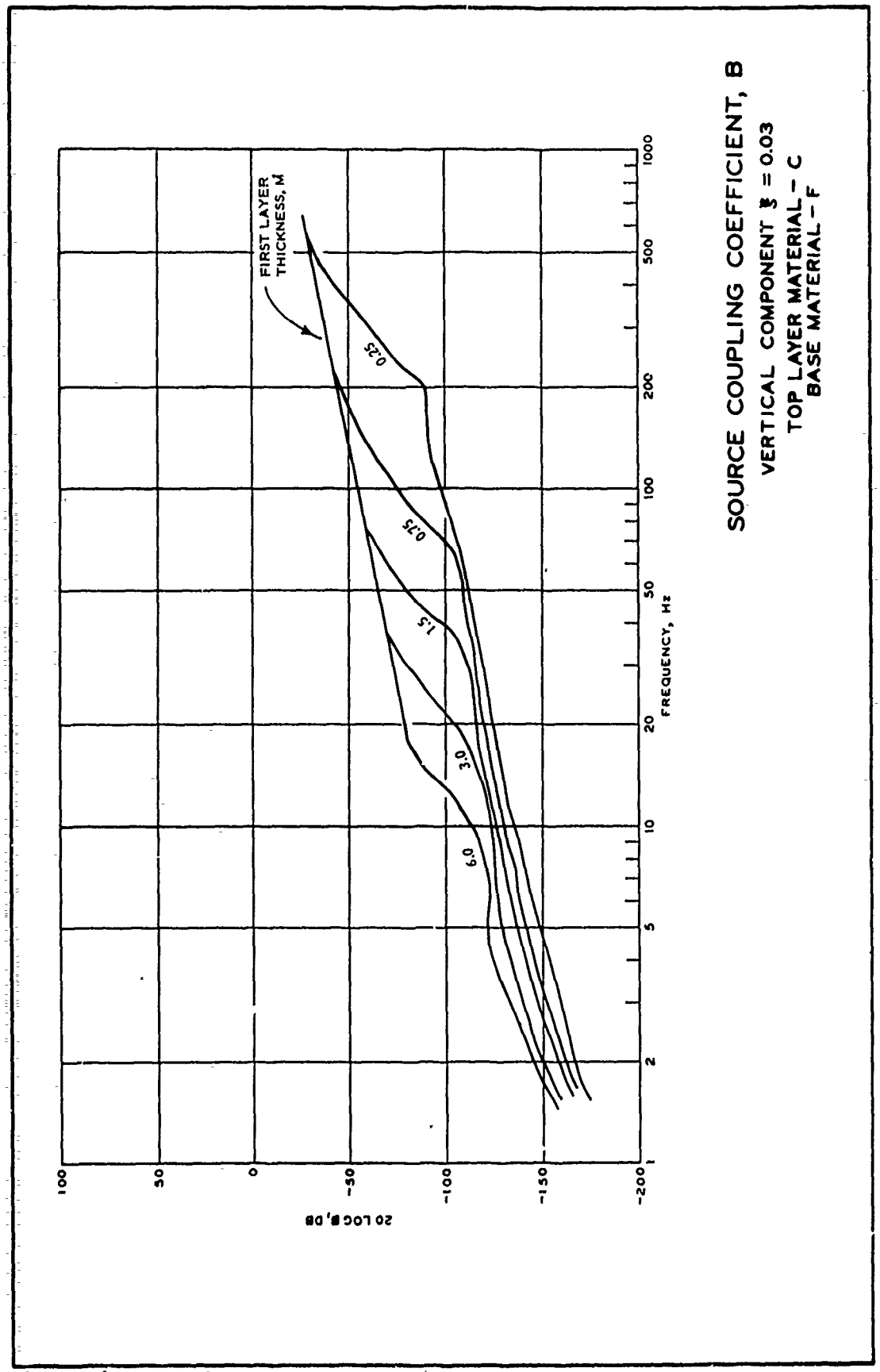
SOURCE COUPLING COEFFICIENT, B
VERTICAL COMPONENT ⅄ = 0.03
TOP LAYER MATERIAL – C
BASE MATERIAL – F
FIRST LAYER THICKNESS, M
0.25
0.75
1.5
3.0
6.0
FREQUENCY, Hz
1
2
5
10
20
50
100
200
500
1000
20 LOG B, DB
100
50
0
-50
-100
-150
-200

PLATE 26

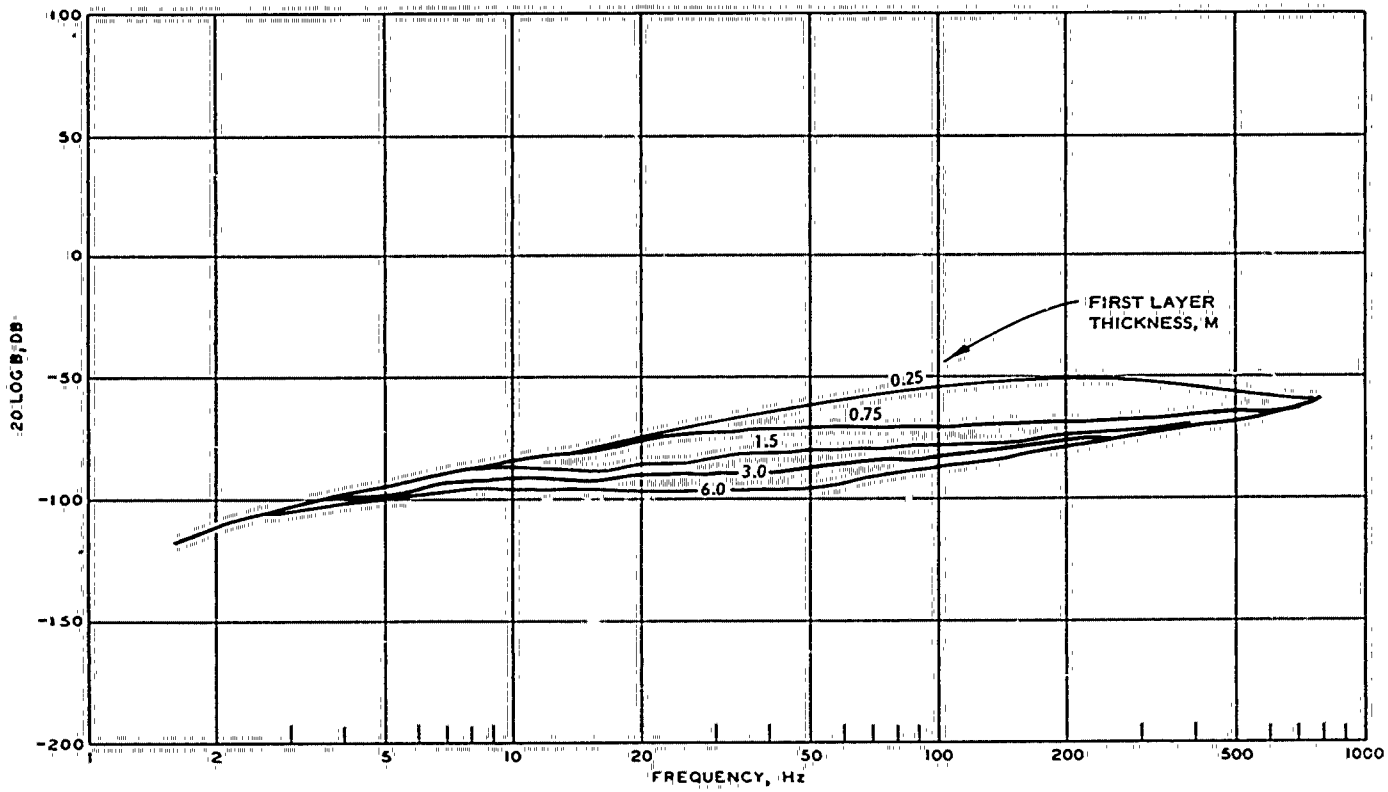

SOURCE COUPLING COEFFICIENT, B

VERTICAL COMPONENT $\xi = 0.03$

TOP LAYER MATERIAL – G
BASE MATERIAL – B

PLATE 27

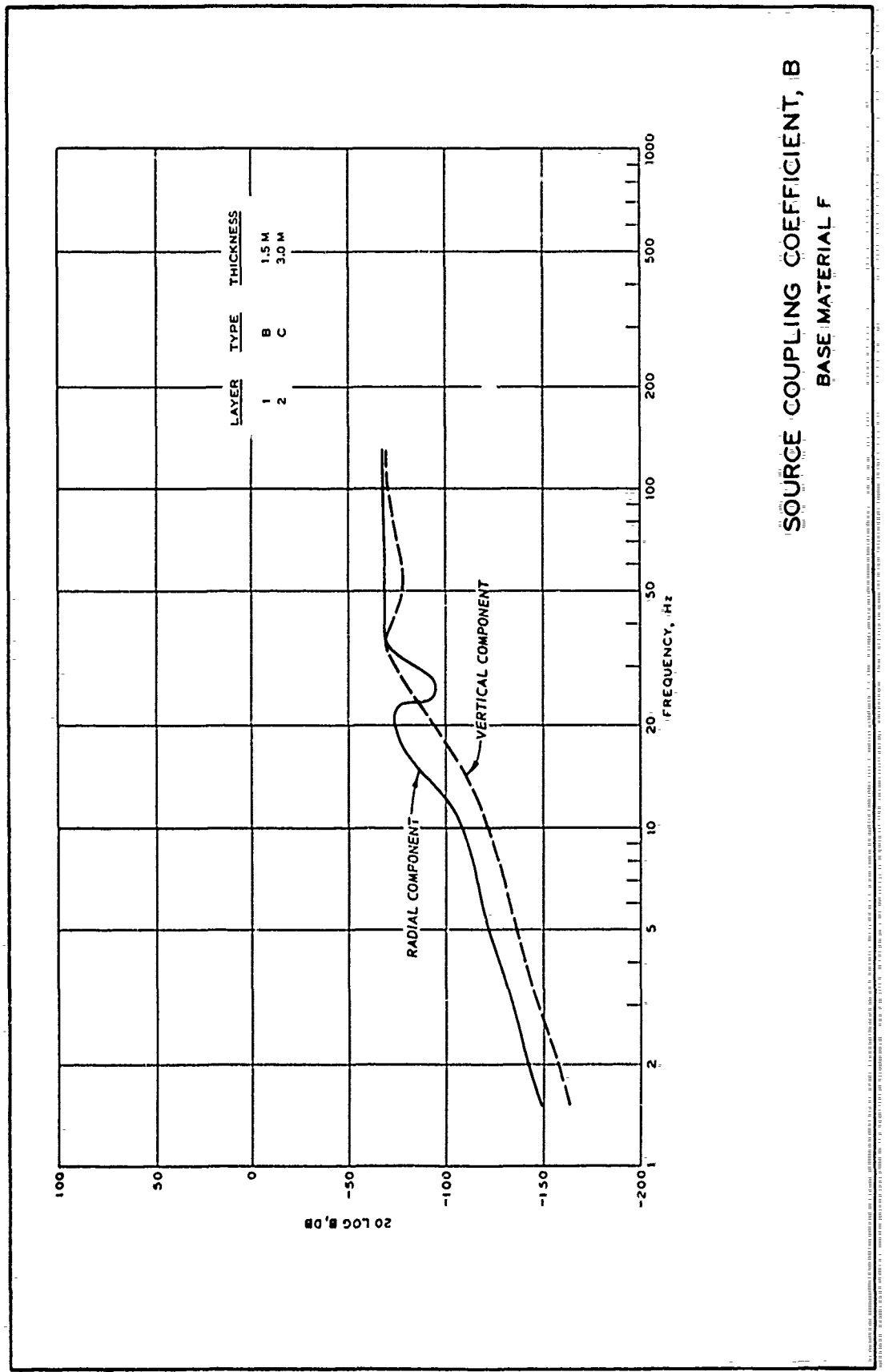
SOURCE COUPLING COEFFICIENT, B
BASE MATERIAL F
LAYER TYPE THICKNESS
1 B 1.5 M
2 C 3.0 M
RADIAL COMPONENT
VERTICAL COMPONENT
FREQUENCY, Hz
20 LOG B, DB
100
50
0
-50
-100
-150
-200
1
2
5
10
20
50
100
200
500
1000

PLATE 28

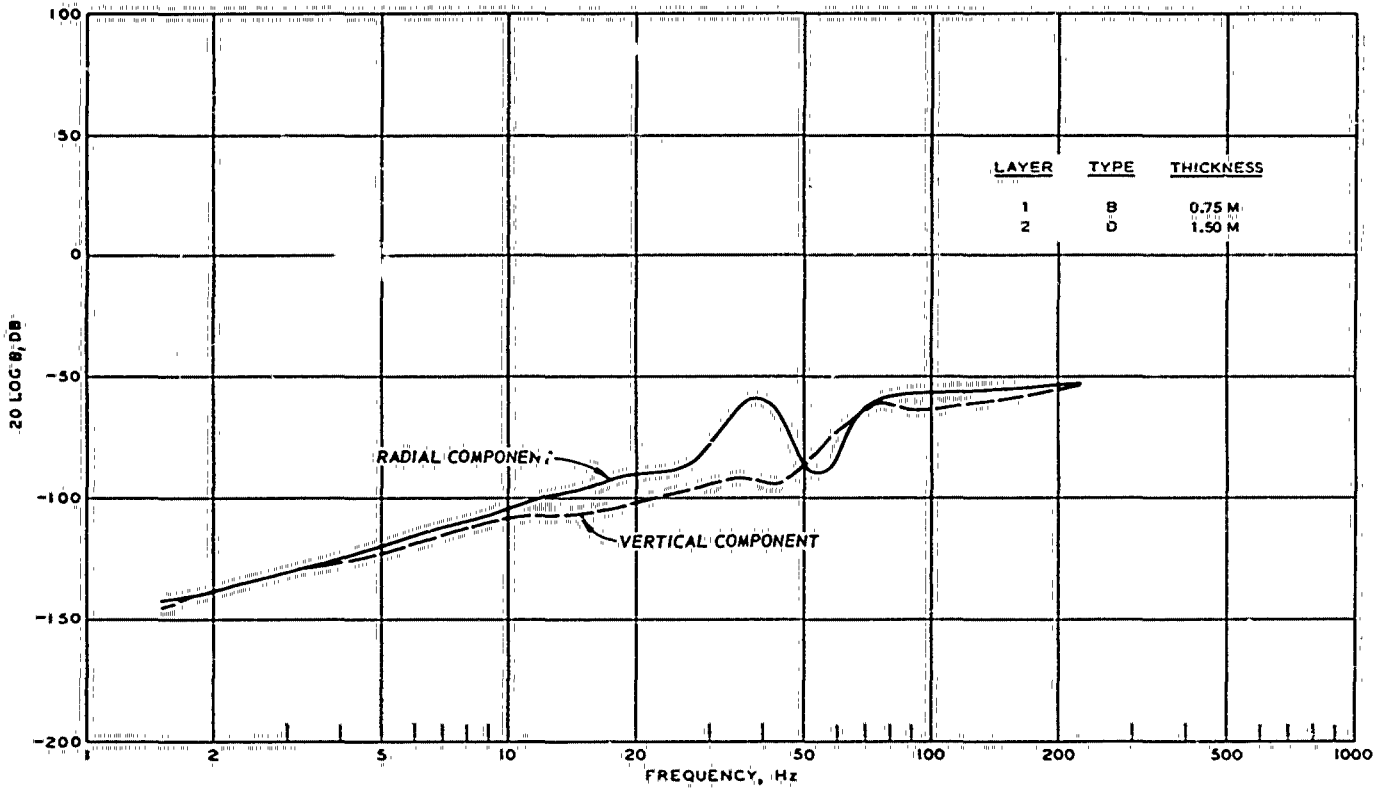

SOURCE COUPLING COEFFICIENT, B

BASE MATERIAL E

PLATE 29

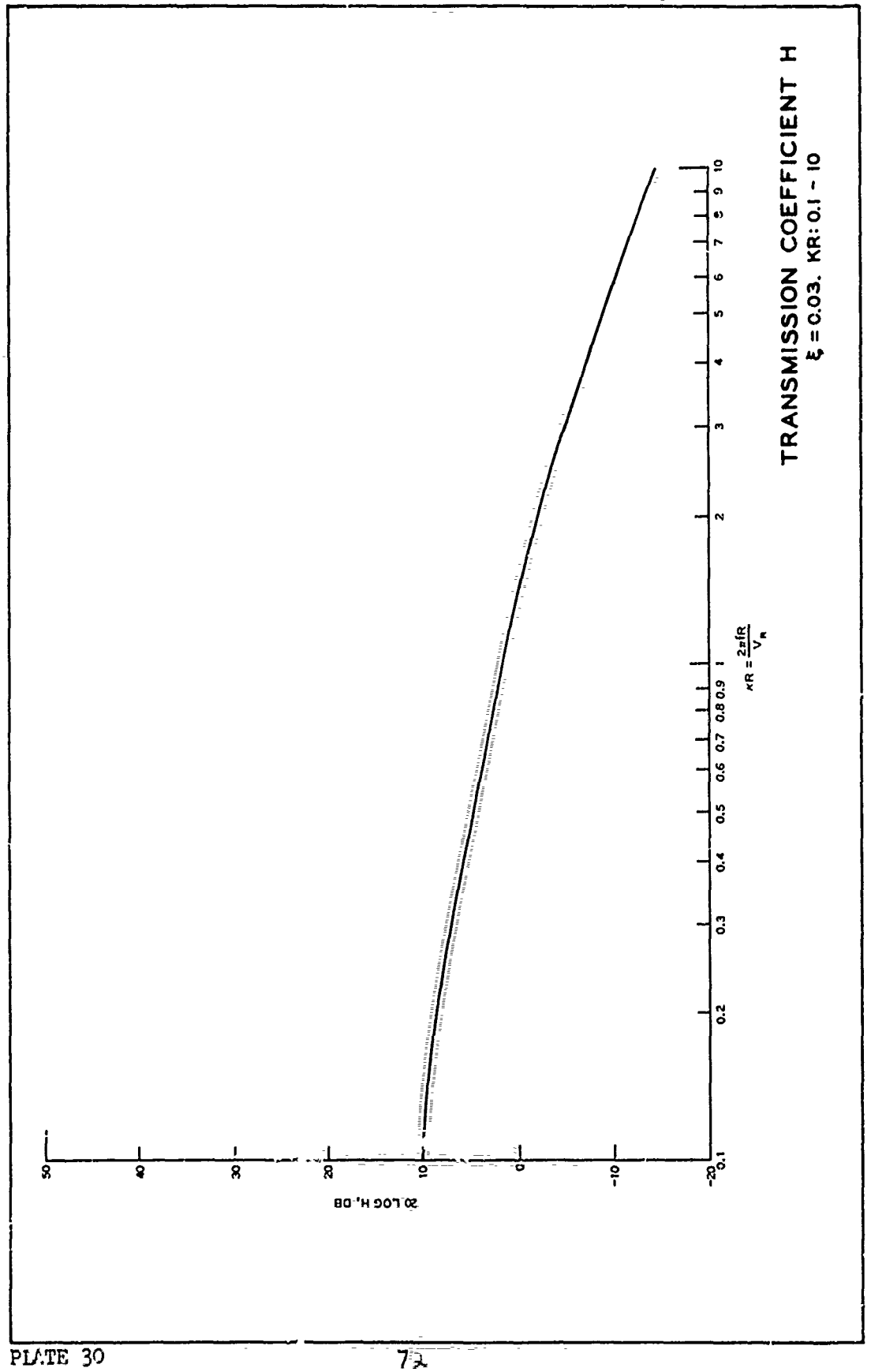
TRANSMISSION COEFFICIENT H
ξ = 0.03. KR: 0.1 - 10
20 LOG H, DB
50
40
30
20
10
0
-10
-20
0.1
0.2
0.3
0.4
0.5
0.6
0.7
0.8
0.9
1
2
3
4
5
6
7
8
9
10
$\kappa R = \frac{2\pi fR}{V_R}$

PLATE 30

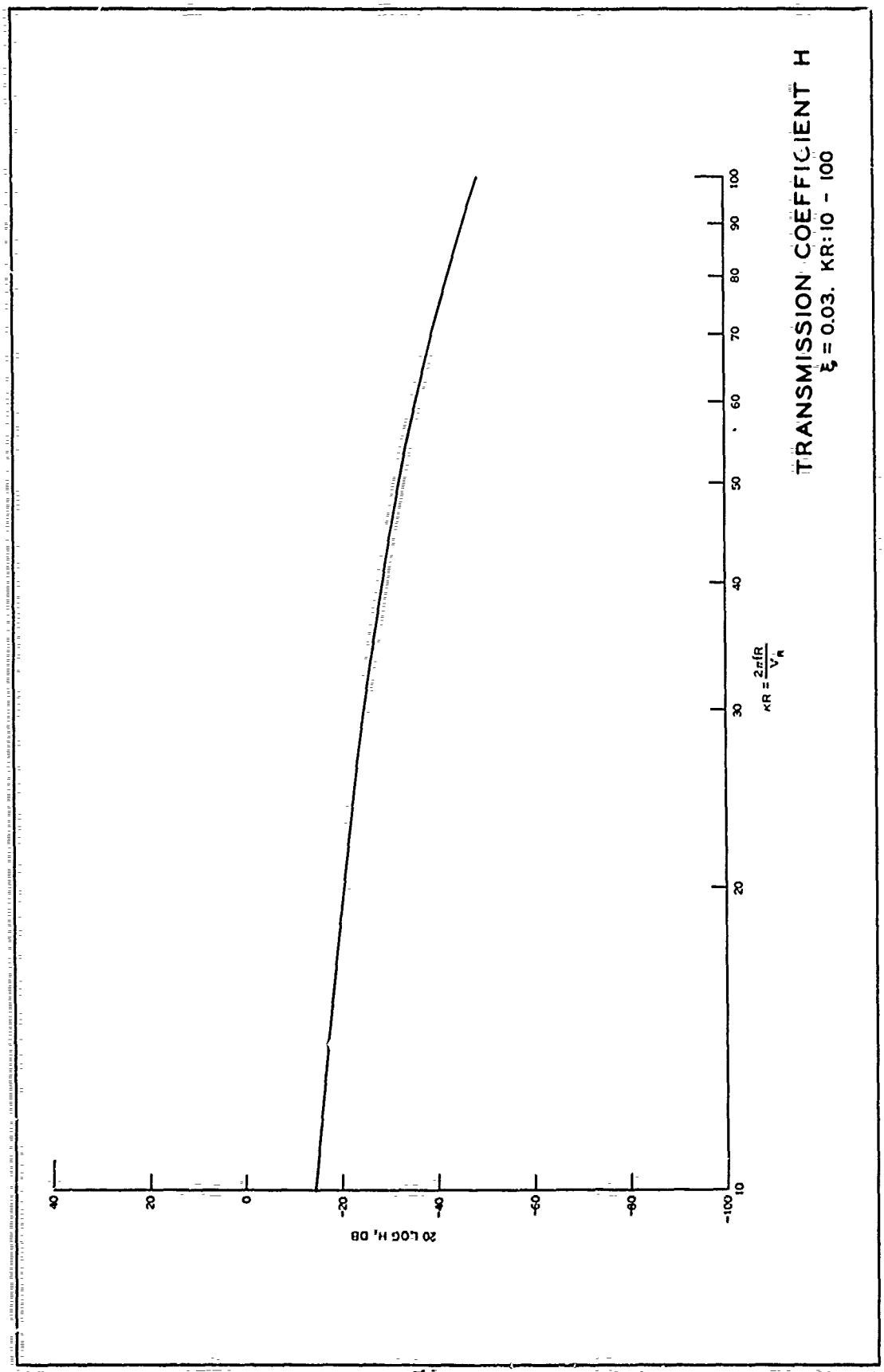
TRANSMISSION COEFFICIENT H
ξ = 0.03. KR: 10 - 100
$\kappa R = \frac{2\pi fR}{V_R}$
20 LOG H, DB
10
20
30
40
50
60
70
80
90
100
-100
-80
-60
-40
-20
0
20
40

PLATE 31

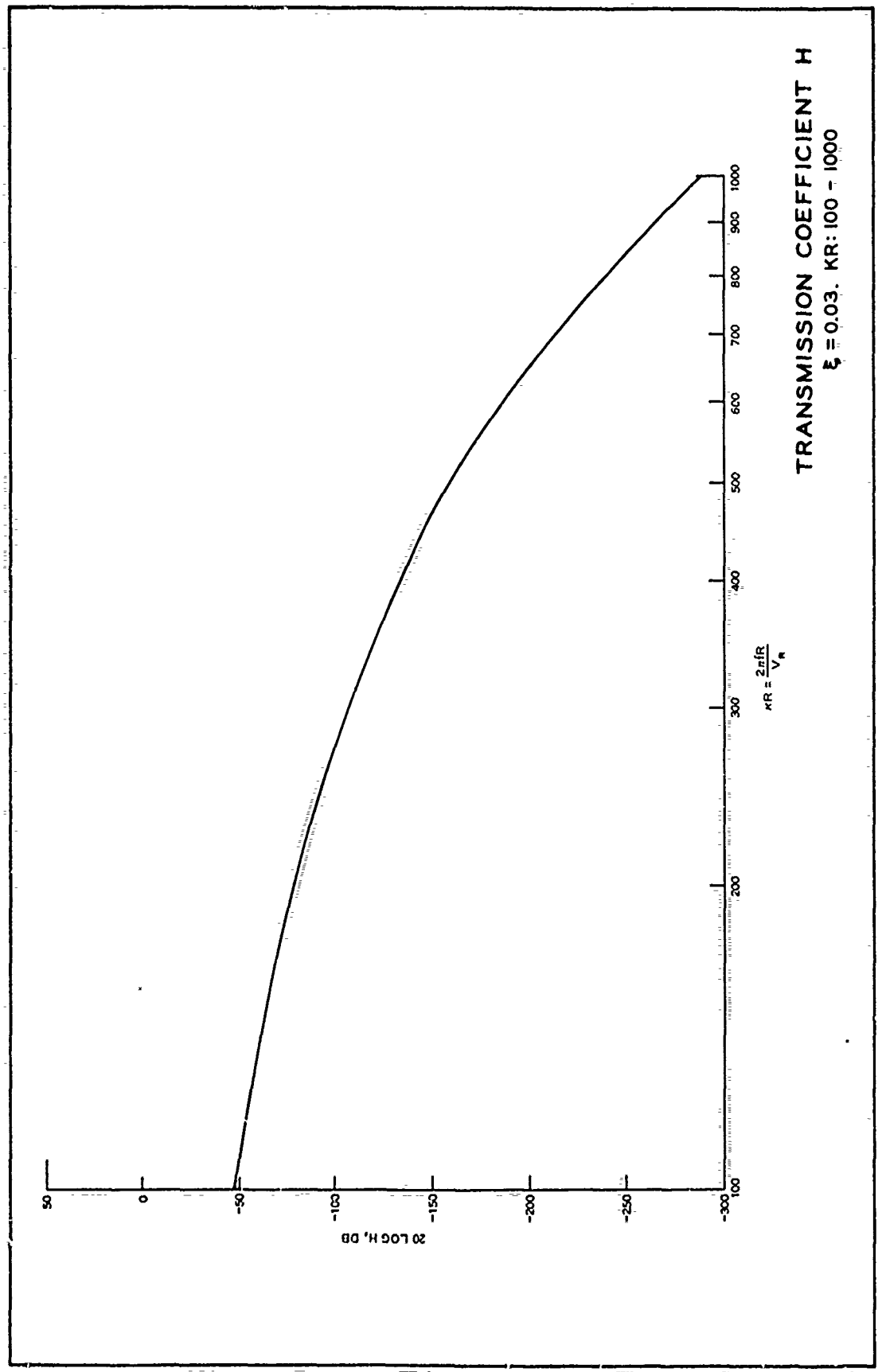
TRANSMISSION COEFFICIENT H
ξ = 0.03. KR: 100 - 1000
$KR = \frac{2\pi fR}{V_R}$
20 LOG H, DB
100
200
300
400
500
600
700
800
900
1000
-300
-250
-200
-150
-100
-50
0
50

PLATE 32

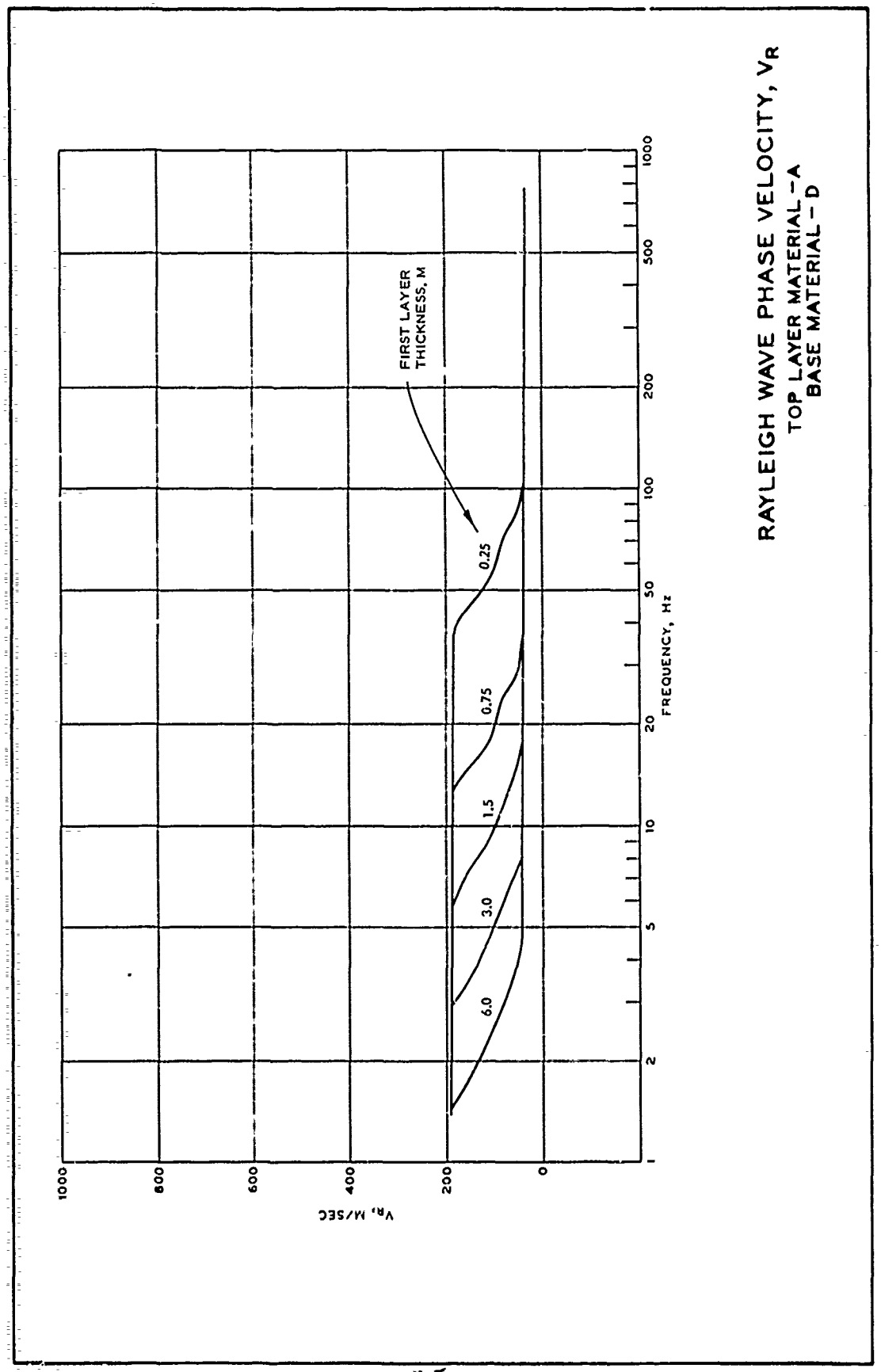
RAYLEIGH WAVE PHASE VELOCITY, V_R
TOP LAYER MATERIAL – A
BASE MATERIAL – D
FIRST LAYER THICKNESS, M
0.25
0.75
1.5
3.0
6.0
FREQUENCY, Hz
1
2
5
10
20
50
100
200
500
1000
V_R, M/SEC
0
200
400
600
800
1000

PLATE 33

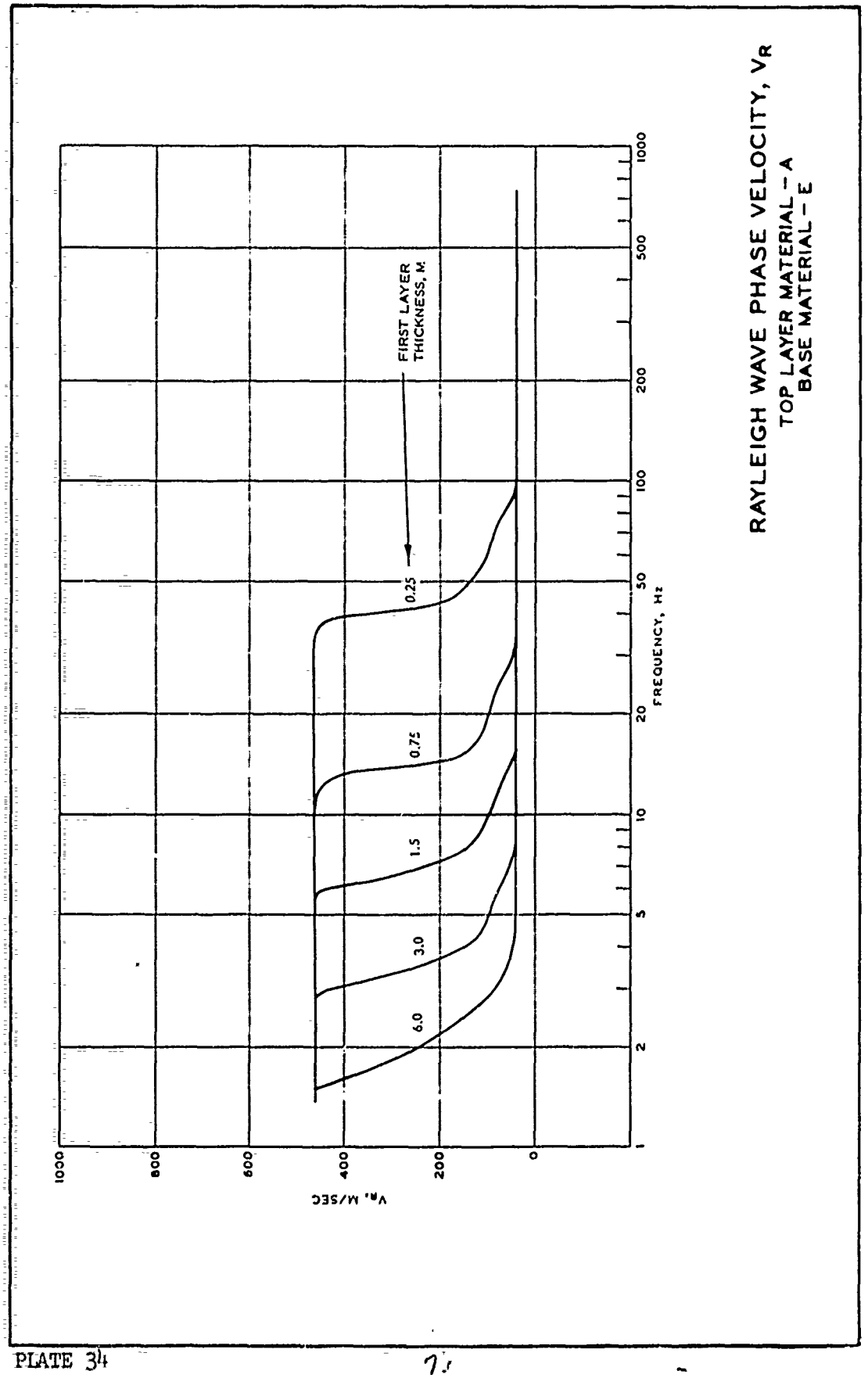
RAYLEIGH WAVE PHASE VELOCITY, V_R
TOP LAYER MATERIAL – A
BASE MATERIAL – E
FIRST LAYER THICKNESS, M
0.25
0.75
1.5
3.0
6.0
FREQUENCY, Hz
V_R, M/SEC
1000
800
600
400
200
0
1
2
5
10
20
50
100
200
500
1000

PLATE 34

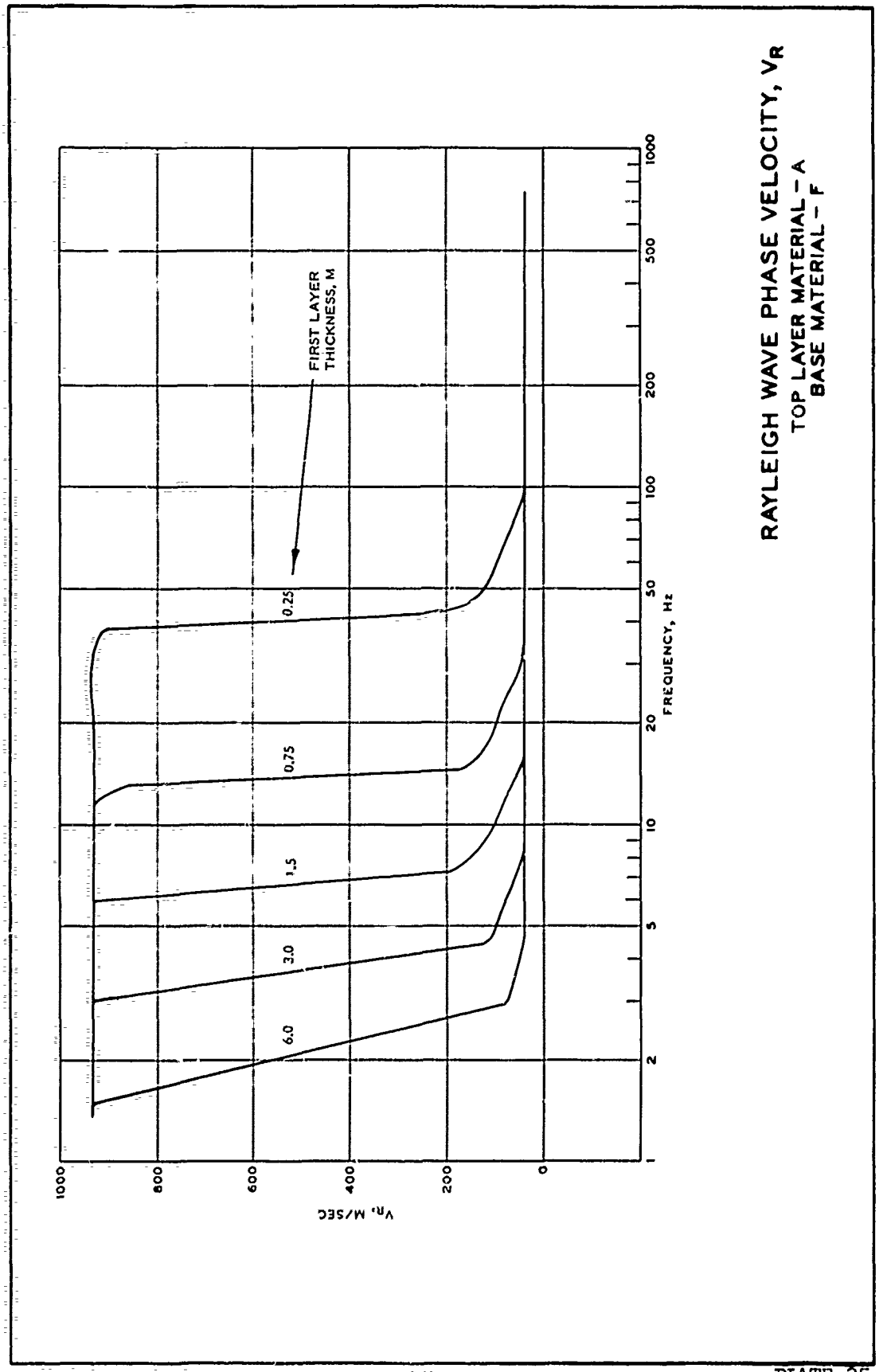
RAYLEIGH WAVE PHASE VELOCITY, V_R
TOP LAYER MATERIAL - A
BASE MATERIAL - F
FIRST LAYER THICKNESS, M
0.25
0.75
1.5
3.0
6.0
FREQUENCY, Hz
1
2
5
10
20
50
100
200
500
1000
V_R, M/SEC
1000
800
600
400
200
0

PLATE 35

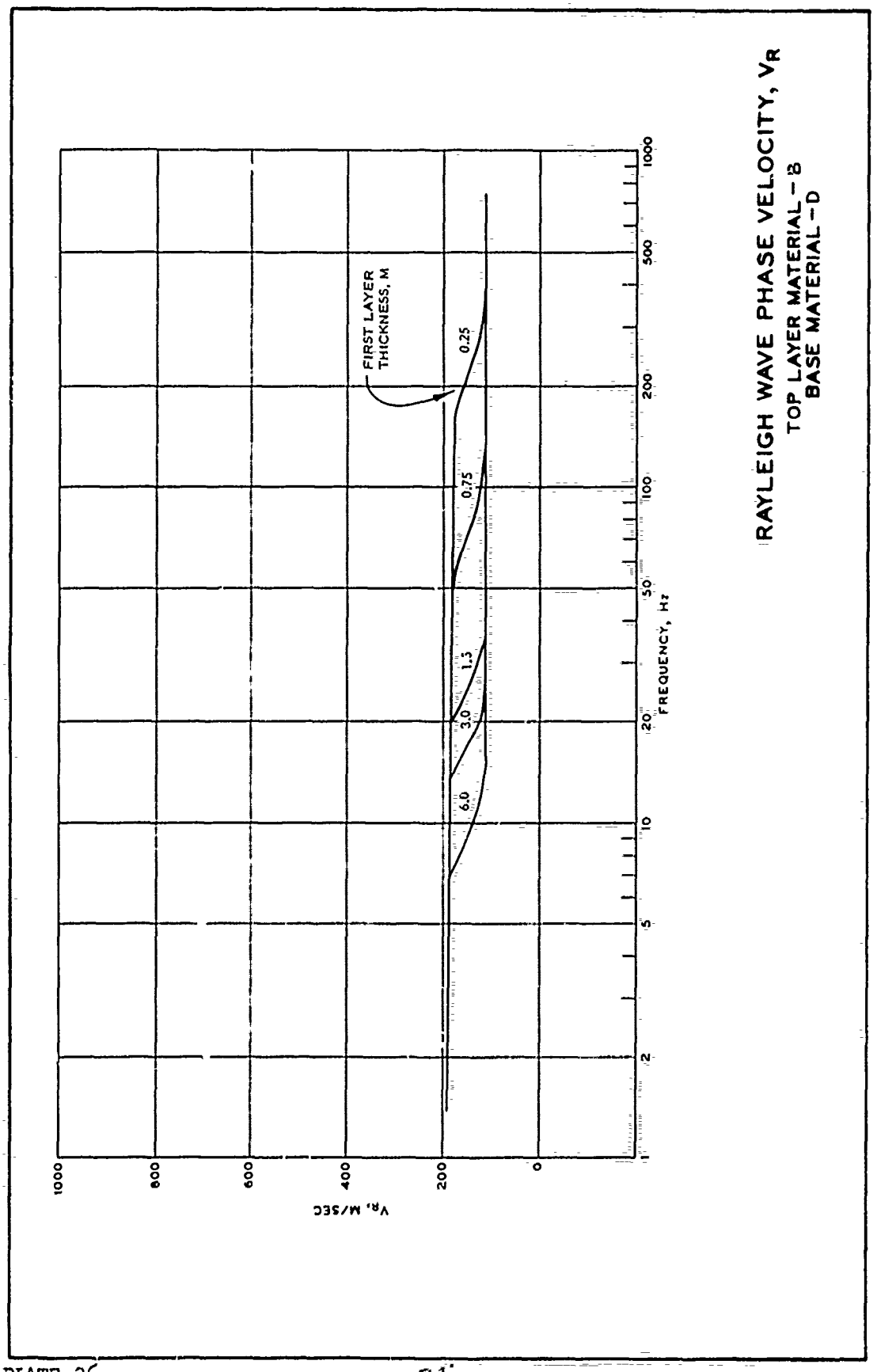
RAYLEIGH WAVE PHASE VELOCITY, V_R
TOP LAYER MATERIAL - B
BASE MATERIAL - D
FIRST LAYER THICKNESS, M
0.25
0.75
1.5
3.0
6.0
FREQUENCY, Hz
1000
500
200
100
50
20
10
5
2
1
V_R, M/SEC
1000
800
600
400
200
0

PLATE 36

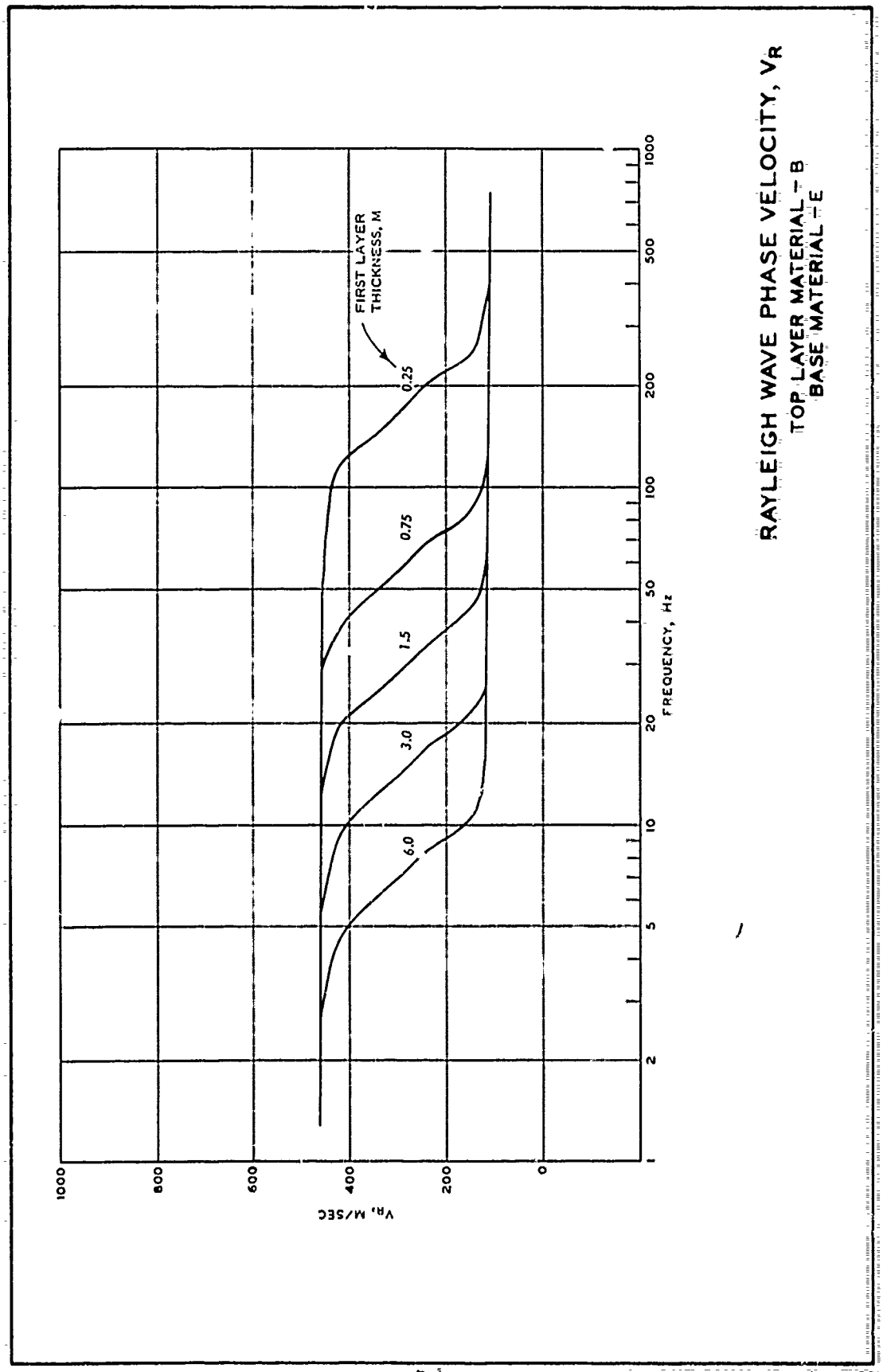
RAYLEIGH WAVE PHASE VELOCITY, V_R
TOP LAYER MATERIAL – B
BASE MATERIAL – E
FIRST LAYER THICKNESS, M
0.25
0.75
1.5
3.0
6.0
FREQUENCY, Hz
1
2
5
10
20
50
100
200
500
1000
V_R, M/SEC
0
200
400
600
800
1000

PLATE 37

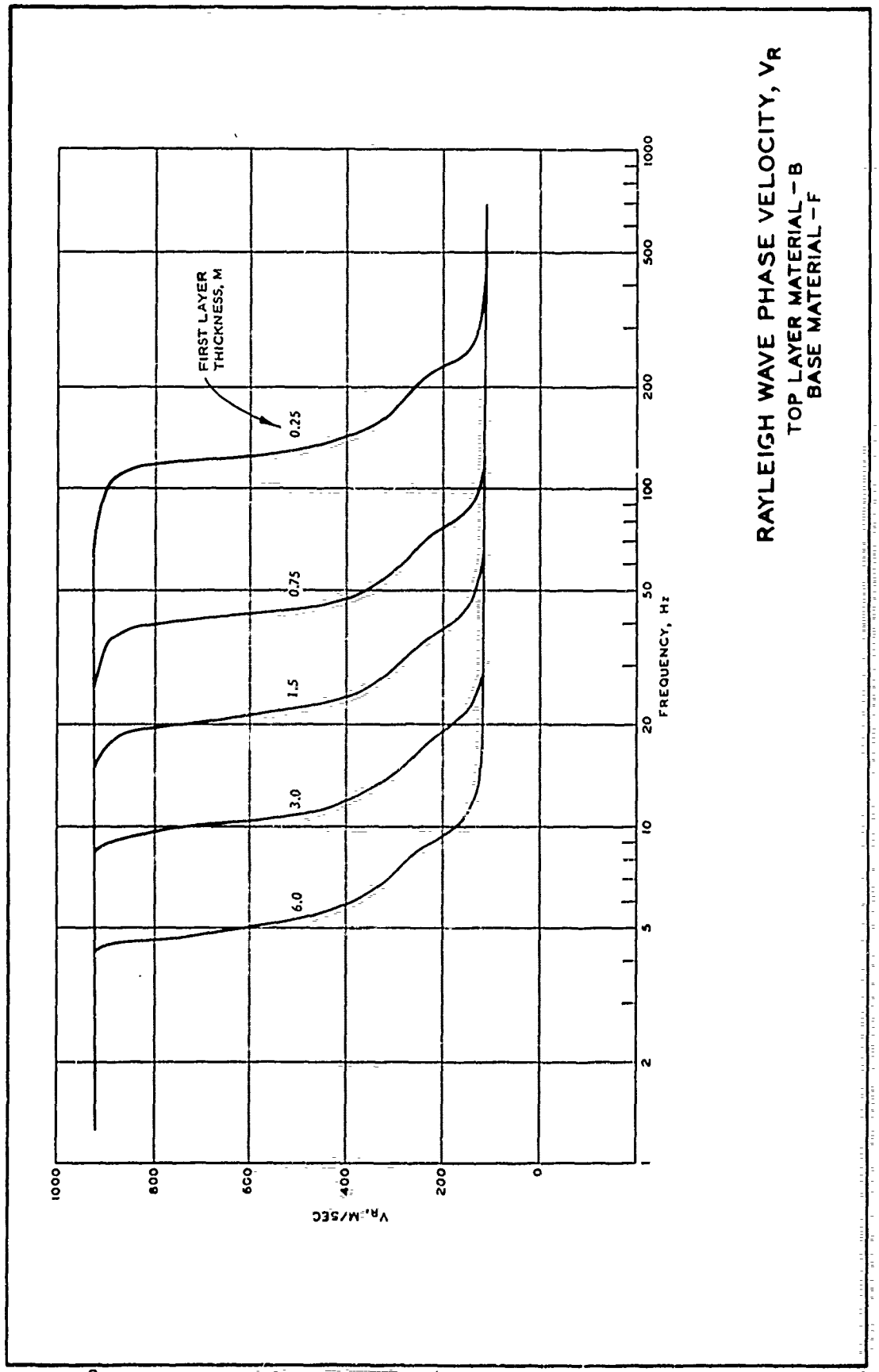
RAYLEIGH WAVE PHASE VELOCITY, V_R
TOP LAYER MATERIAL – B
BASE MATERIAL – F
FIRST LAYER THICKNESS, M
0.25
0.75
1.5
3.0
6.0
FREQUENCY, Hz
1
2
5
10
20
50
100
200
500
1000
V_R, M/SEC
0
200
400
600
800
1000

PLATE 38

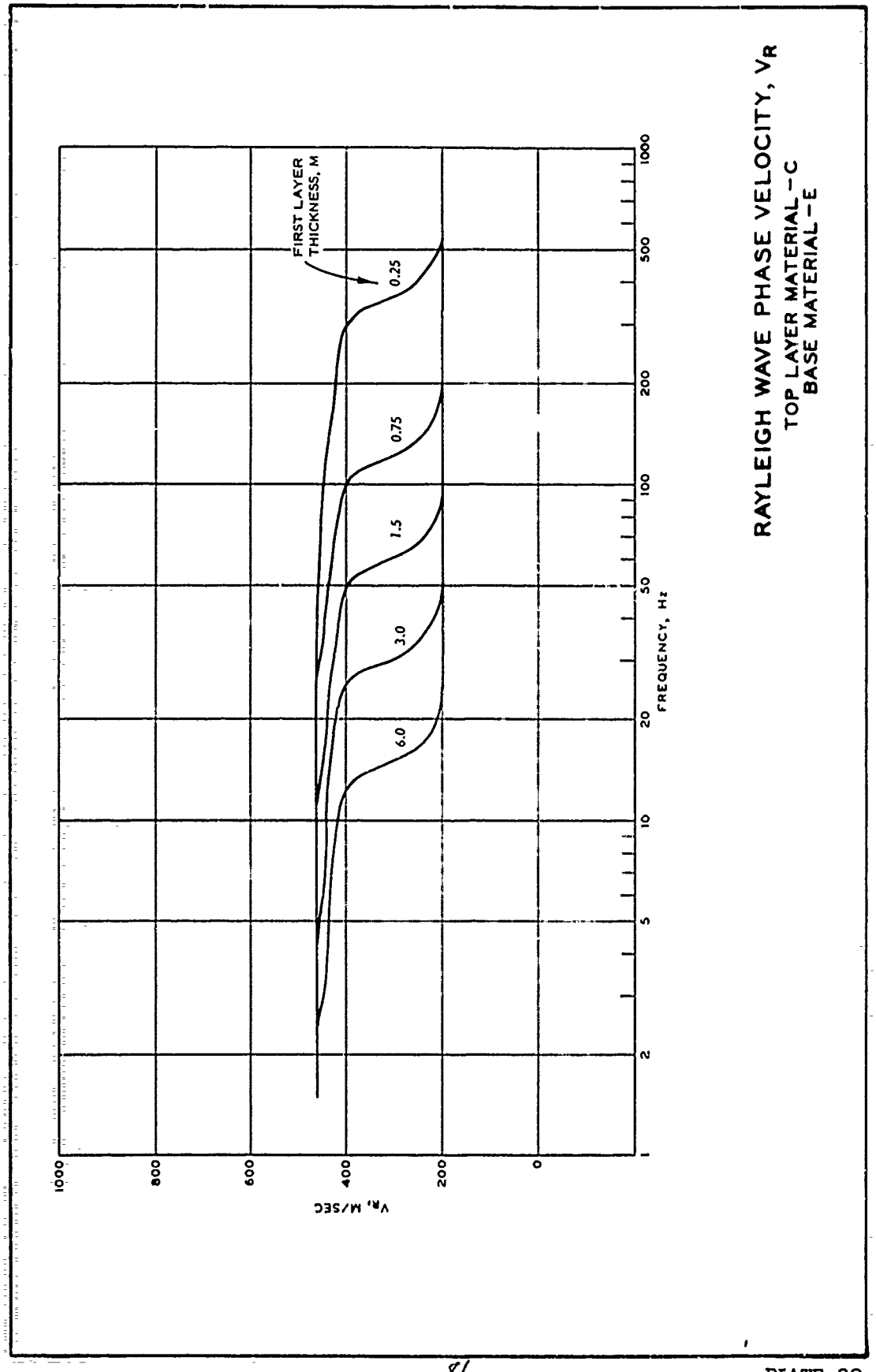
RAYLEIGH WAVE PHASE VELOCITY, V_R
TOP LAYER MATERIAL – C
BASE MATERIAL – E
FIRST LAYER THICKNESS, M
0.25
0.75
1.5
3.0
6.0
FREQUENCY, Hz
1
2
5
10
20
50
100
200
500
1000
V_R, M/SEC
0
200
400
600
800
1000

PLATE 39

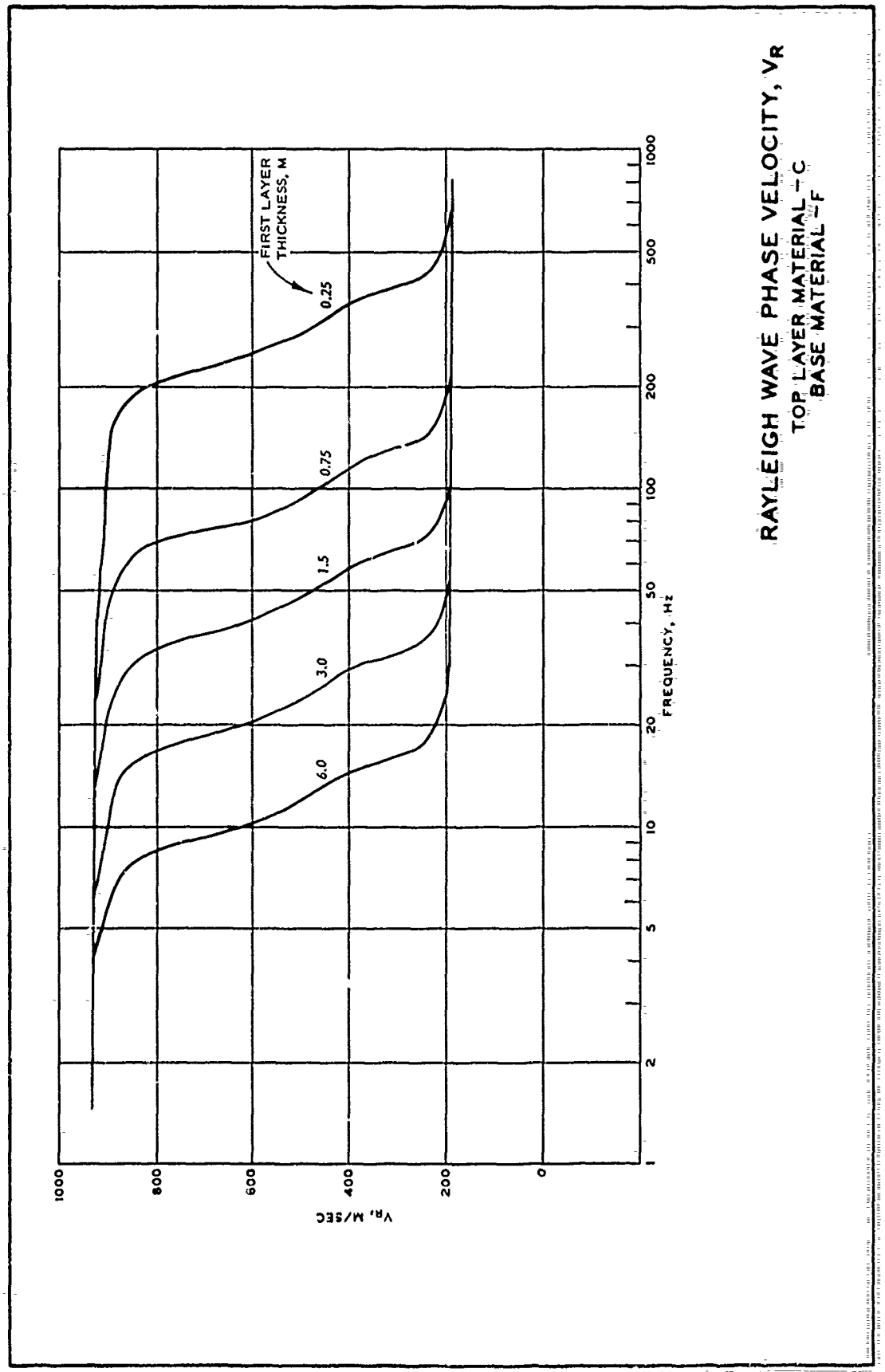
RAYLEIGH WAVE PHASE VELOCITY, V_R
TOP LAYER MATERIAL – C
BASE MATERIAL – F
FIRST LAYER THICKNESS, M
0.25
0.75
1.5
3.0
6.0
FREQUENCY, Hz
1
2
5
10
20
50
100
200
500
1000
V_R, M/SEC
0
200
400
600
800
1000

PLATE 40

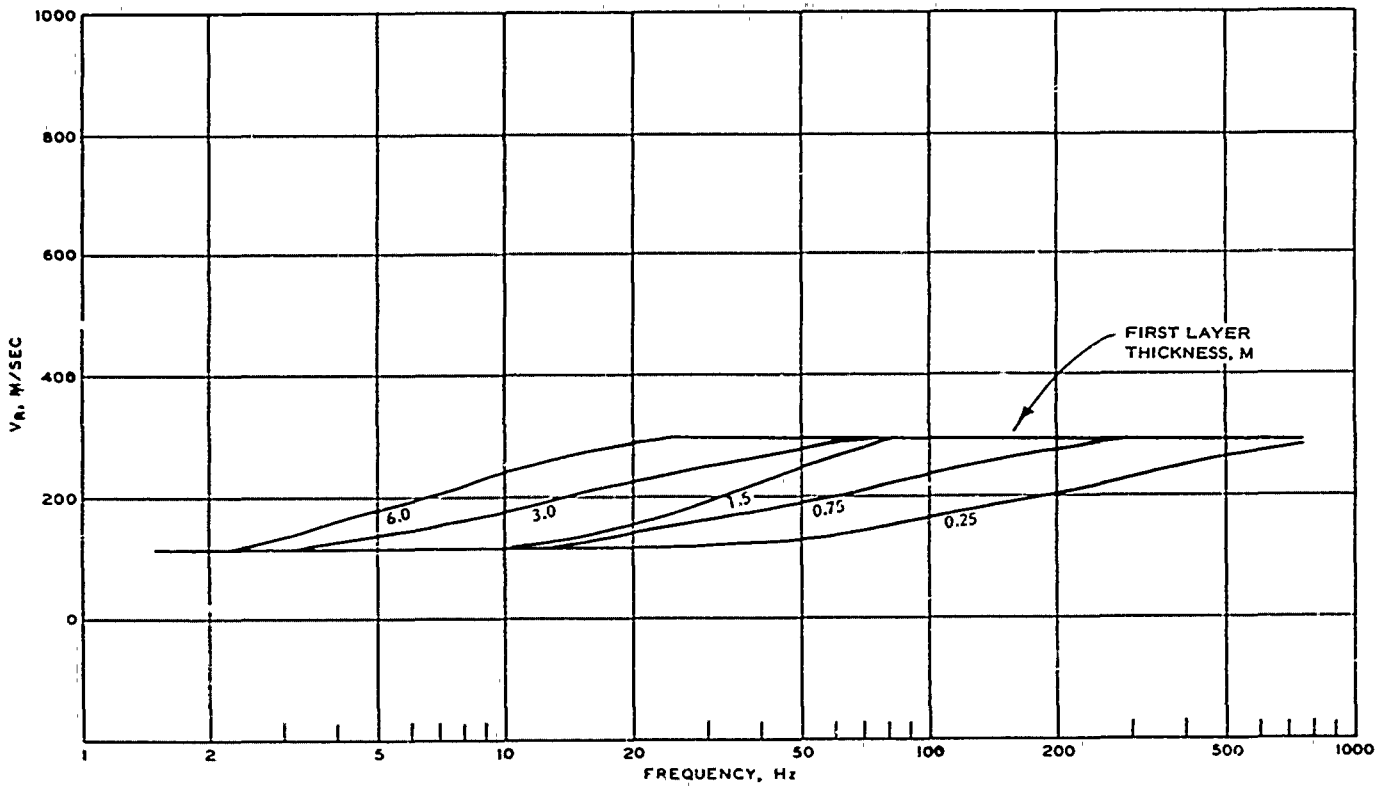

RAYLEIGH WAVE PHASE VELOCITY, V_R

TOP LAYER MATERIAL – G
BASE MATERIAL – B

PLATE 42

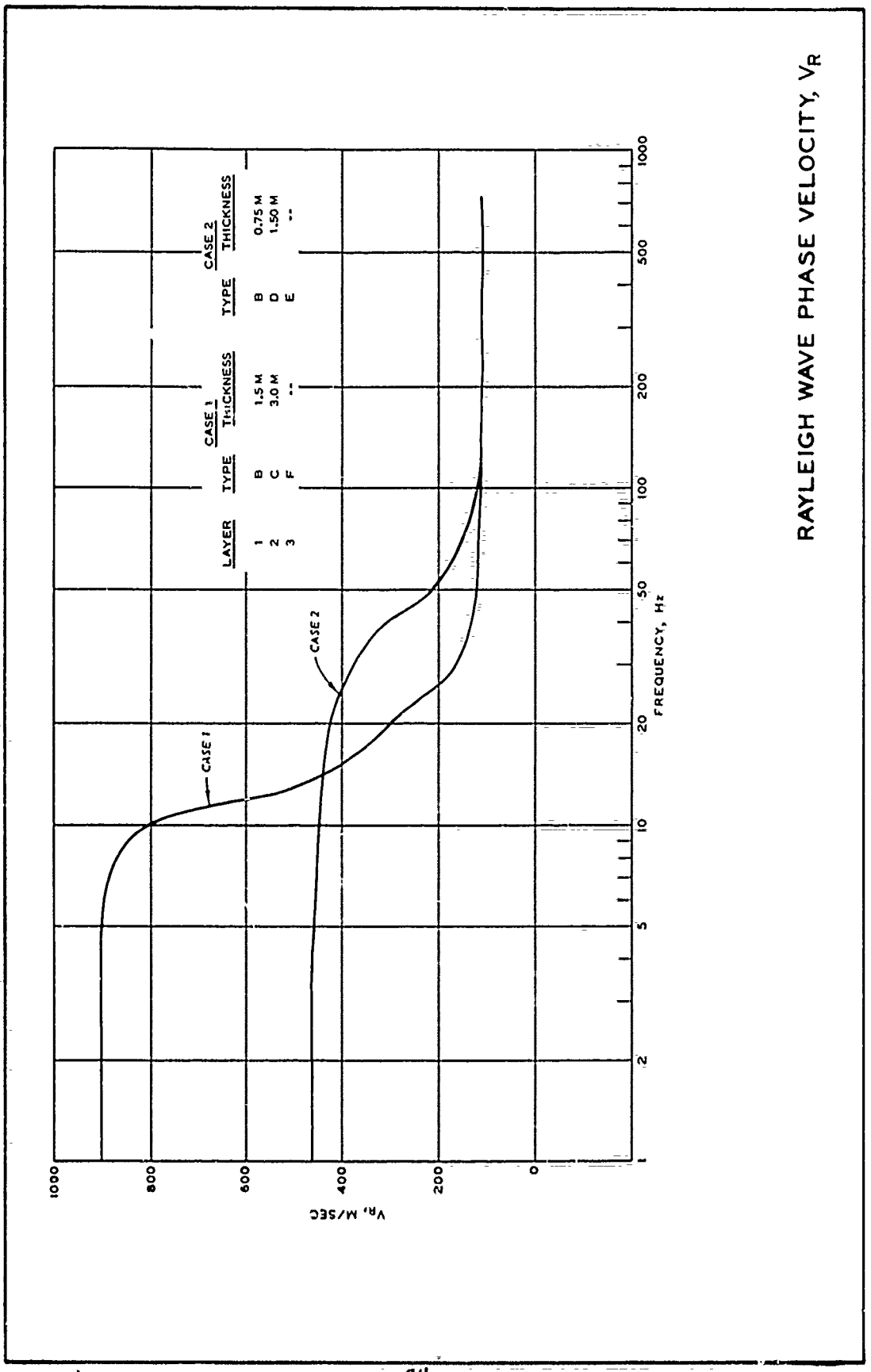
RAYLEIGH WAVE PHASE VELOCITY, V_R
CASE 1
LAYER TYPE THICKNESS
1 B 1.5 M
2 C 3.0 M
3 F --
CASE 2
TYPE THICKNESS
B 0.75 M
D 1.50 M
E --
CASE 1
CASE 2
V_R, M/SEC
FREQUENCY, Hz
1000
800
600
400
200
0
1
2
5
10
20
50
100
200
500
1000

PLATE 42

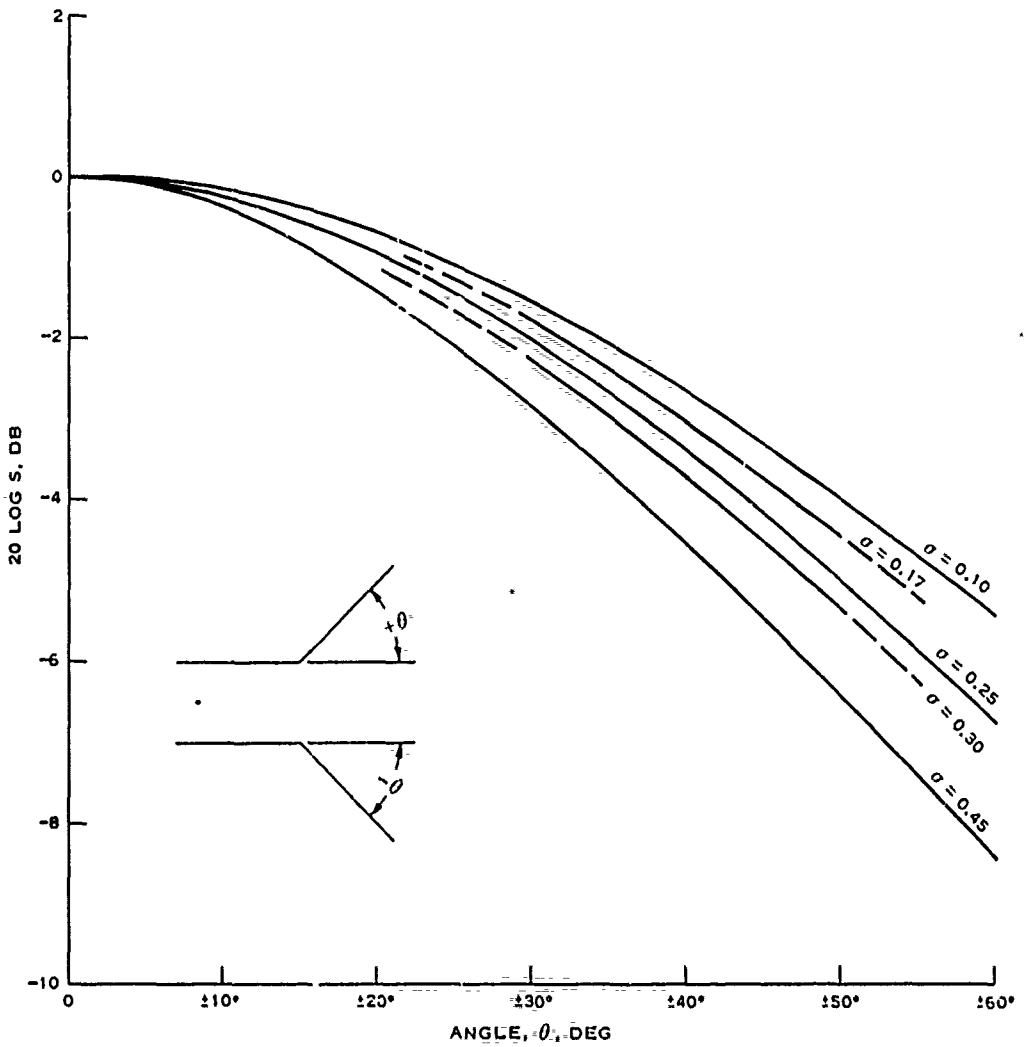

SURFACE MACROGEOMETRY
(TRANSMISSION) COEFFICIENT, S, FOR
A WEDGE (σ = POISSON'S RATIO)

PLATE 43

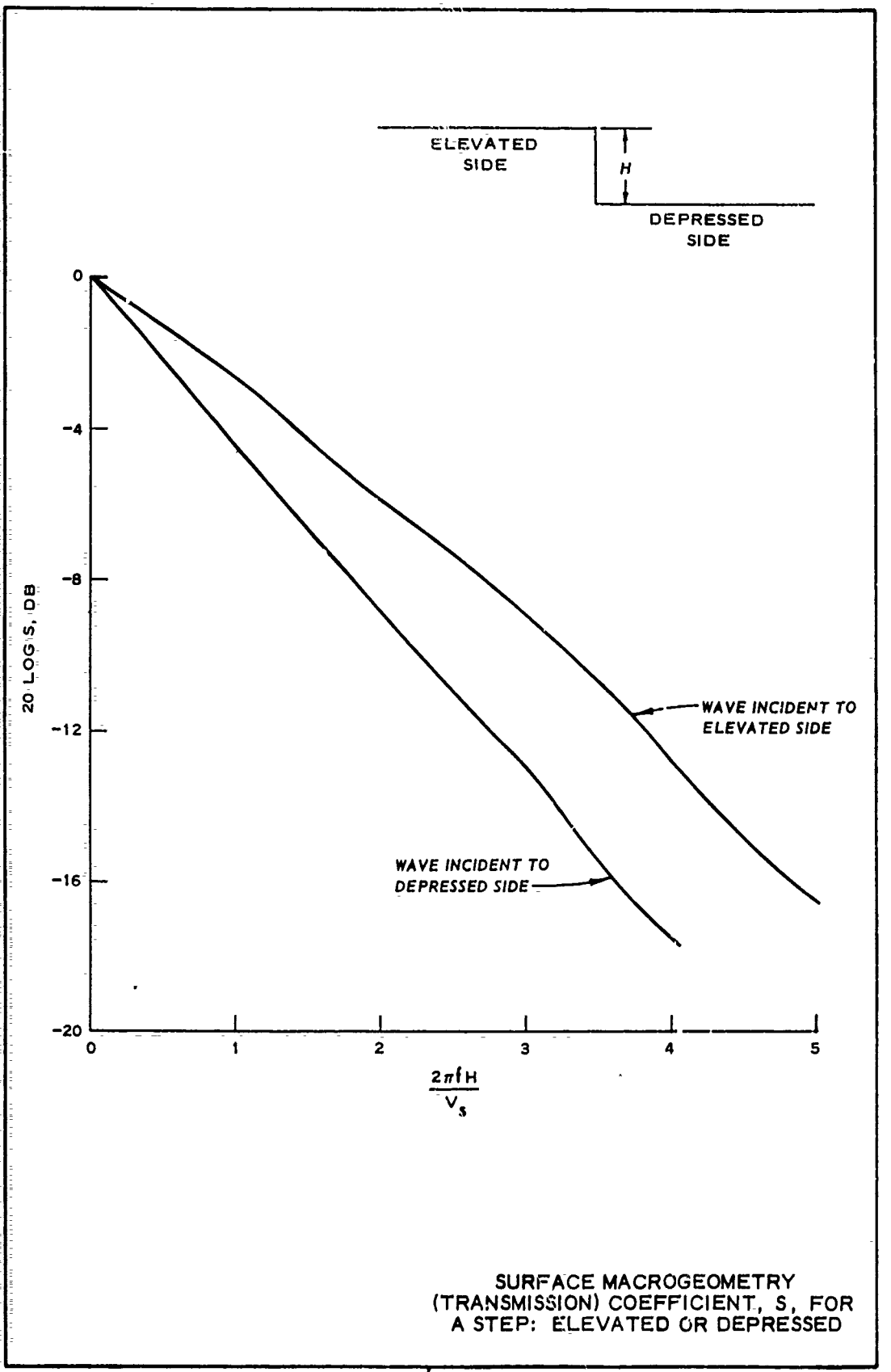

SURFACE MACROGEOMETRY (TRANSMISSION) COEFFICIENT, S, FOR A STEP: ELEVATED OR DEPRESSED

PLATE 44

In accordance with ER 70-2-3, paragraph 6c(1)(b), dated 15 February 1973, a facsimile catalog card in Library of Congress format is reproduced below:

Lundien, Jerry R.
Generation and propagation of microseismic signals from footsteps, by J. R. Lundien [and] B. O. Benn. Vicksburg, Miss., U. S. Army Engineer Waterways Experiment Station, 1973.
1 v. (various pagings) illus. 27 cm. (U. S. Waterways Experiment Station. Miscellaneous paper M-73-12)
Sponsored by Project Manager, Remotely Monitored Battlefield Surveillance System, U. S. Army Materiel Command, Fort Monmouth, N. J., Project No. 1X663719DK73.
Includes bibliography.
1. Footsteps. 2. Microseismic waves. 3. Rayleigh waves. 4. Terrain factors. 5. Terrain models. 6. Wave propagation. I. Benn, Bob O., joint author. II. U. S. Army Materiel Command. (Series: U. S. Waterways Experiment Station, Vicksburg, Miss. Miscellaneous paper M-73-12)
TA7.W34m no.M-73-12